

LV-2019-004



Landsvirkjun



ABI IMAGE PROCESSING AND  
INTERPRETATION OF WELL ÞG-18  
ÞEISTAREYKIR FIELD, ÞINGEYJARSVEIT,  
ICELAND

ABI Image Processing and  
Interpretation of Well ÞG-18,  
Þeistareykir Field, Þingeyjarsveit,  
Iceland

LV report no: LV-2019-004 Date: 31 January 2019

Number of pages: 132 Copies: 01 Distribution:  Open  
 Limited until

Title: ABI Image Processing and Interpretation of Well ÞG-18, Peistareykir Field, Þingeyjarsveit, Iceland

Authors / Company: Tito Satria Putra Perdana

Project manager: Anette K. Mortensen (LV) Tito Satria Putra Perdana (GeothermEx)

Prepared for: Landsvirkjun

Co-operators: \_\_\_\_\_

**Abstract:** Production well ÞG-18 was logged on behalf of Landsvirkjun on 26 August 2017, using an ABI tool deployed by ÍSOR. The subject well is in the Peistareykir Field in northeastern Iceland. The ABI logging was conducted in the 8.5-inch diameter of the well (2,494-1,748 m MD), which passes through volcanic formations. The ABI logging was conducted in 3 runs: 1,748-2,313.5 m MD, 2,309-2,393 m MD, and 2,392-2,494 m MD.

Fractures are well developed over almost the entire logged interval, with a total of 3,850 open fractures identified. Discontinuous open fracture is the predominant fracture type. A total of 2,840 such fractures were identified in the interval; they show a dominant strike orientation of NNE-SSW, with WNW and ESE azimuths, with dip magnitudes vary from horizontal to vertical, but are mainly >70°. A total of 202 large discontinuous open fractures were identified, they show a dominant strike orientation of NNE-SSW, with WNW and ESE azimuths, and dip magnitudes vary from 10° to vertical, but are mainly >70°. A total of 81 continuous open fractures were identified; they show a dominant strike orientation of NNE-SSW with WNW and ESE azimuths, and dip magnitudes from nearly horizontal to vertical but are mainly >65°. A total of 117 large open fractures were identified; they show a dominant strike orientation of NNE-SSW, with WNW, E, and ESE azimuths, and dip magnitudes vary from 15° to vertical, but are mainly >65°. Only 56 litho-bound open fractures were recognized in the entire logged interval; they demonstrate dominant strike orientations of NNE-SSW, NW-SE, and ENE-WSW, with ESE, WNW, NE, and SSE azimuths; and dip magnitudes are highly variable, from nearly horizontal to vertical. A total of 554 possible open fractures were recognized, they demonstrate dominant strike orientations of NNW-SSE, NNE-SSW, and NE-SW, with westward (WNW, W, WSW) azimuth, and dip magnitudes that vary from nearly horizontal to vertical, but are mainly >45°. A total of 28 possible open faults were identified, they have a dominant strike orientation of NNE-SSW, with ESE and WNW azimuths, and dip magnitudes vary from 38° to vertical, but mainly >70°. A total of 2 drilling-induced fractures were identified, with a dominant strike orientation of N-S. A total of 13 borehole breakouts were identified, with a dominant strike of E-W/ENE-WSW.

Four fracture zones were determined, based mainly on fracture strike orientation, dip magnitude, and lithology. Fracture Zone 1 (2,491-2,357 m MD) has the highest rates of lost circulation. The open fractures in this fracture zone demonstrate a dominant NNE-SSW strike with WNW and ESE azimuths, and dip magnitudes from nearly horizontal to vertical. One feed zone was identified within this fracture zone from temperature log and the circulation losses. Zones of lost circulation and feed zones are mainly associated with zones of large continuous and discontinuous open fractures, and possible open faults.

**Keywords:** Well ÞG-18, Acoustic Borehole Imager, 8.5-inch, ABI, Peistareykir Field, Þingeyjarsveit, Iceland, fracture analysis, fracture classification, fracture orientation, fracture density, fracture zone, open fracture, possible open fault, feed zone, lost circulation, intrusion, basalt, Landsvirkjun, GeothermEx, Schlumberger, Techlog.

\_\_\_\_\_  
Project Manager Approval

Rev. No.	Effective Date	Description	Prepared by	Reviewed by	Approved by
A	06 JAN 2019	First release	TP	AR-T	TP
B	31 JAN 2019	Final	TP	AR-T	TP

## Disclaimer

Any interpretation, research, analysis, data, results, estimates, or recommendation furnished with the services or otherwise communicated by GeothermEx to its customers at any time in connection with the services are opinions based on inferences from measurements, empirical relationships and/or assumptions. These inferences, empirical relationships and/or assumptions are not infallible, and professionals in the industry may differ with respect to such inferences, empirical relationships and/or assumptions. Accordingly, GeothermEx cannot and does not warrant the accuracy, correctness or completeness of any such interpretation, research, analysis, data, results, estimates or recommendation.

Customer acknowledges that it is accepting the services "as is," that GeothermEx makes no representation or warranty, express or implied, of any kind or description in respect thereto. Specifically, Customer acknowledges that GeothermEx does not warrant that any interpretation, research, analysis, data, results, estimates, or recommendation is fit for a particular purpose, including but not limited to compliance with any government request or regulatory requirement. Customer further acknowledges that such services are delivered with the explicit understanding and agreement that any action taken based on the services received shall be at its own risk and responsibility, and no claim shall be made against GeothermEx as a consequence thereof.

## CONTENTS

EXECUTIVE SUMMARY .....	vi
1. INTRODUCTION .....	1-1
1.1 Background .....	1-1
1.2 Objectives .....	1-5
1.3 Database .....	1-5
2. RESULTS OF ABI PROCESSING AND INTERPRETATION .....	2-1
2.1 ABI Log Quality and Borehole Conditions .....	2-1
2.2 Manual Dip Classification .....	2-2
2.3 Structural Interpretation .....	2-4
3. FRACTURE ZONATION .....	3-1
4. CONCLUSIONS .....	4-1
5. REFERENCES .....	5-1

## ILLUSTRATIONS

### Table

- 1.1 Wellbore parameters of well PG-18 and ABI tool service details
- 2.2 Dip classification and interpretation scheme
- 3.1 Summary of fracture zonation

### Figure

- 2.1.1 ABI Borehole Shape Analysis and Calipers (X and Y) Depth Plot Interval 1,748-2,494 m MD, Well PG-18
- 2.1.2 Examples of “Good” and “poor” ABI Image Quality, Well PG-18
- 2.1.3 Well Deviation and Well Azimuth Data from ABI and Gyro Surveys, Well PG-18
- 2.1.4 Simple (Bulk/Block) Depth Shifts of the ABI Images
- 2.3.1 ABI Image Examples of Discontinuous, Large Discontinuous, Continuous, and Large Continuous Open Fractures
- 2.3.2 ABI Image Examples of Discontinuous, Large Discontinuous, Continuous, and Large Continuous Open Fractures
- 2.3.3 Dip Statistics of Discontinuous Open Fractures, Interval 1,748-2,494 m MD
- 2.3.4 Dip Statistics of Discontinuous Open Fractures ( $\geq 70^\circ$  Dip Magnitudes and  $< 70^\circ$  Dip Magnitudes), Interval 1,748-2,494 m MD
- 2.3.5 Dip Statistics of Large Discontinuous Open Fractures, Interval 1,748-2,494 m MD
- 2.3.6 Dip Statistics of Large Discontinuous Open Fractures ( $\geq 70^\circ$  Dip Magnitudes and  $< 70^\circ$  Dip Magnitudes), Interval 1,748-2,494 m MD
- 2.3.7 Dip Statistics of Continuous Open Fractures, Interval 1,748-2,494 m MD
- 2.3.8 Dip Statistics of Continuous Open Fractures ( $\geq 65^\circ$  Dip Magnitudes and  $< 65^\circ$  Dip Magnitudes), Interval 1,748-2,494 m MD
- 2.3.9 Dip Statistics of Large Continuous Open Fractures, Interval 1,748-2,494 m MD
- 2.3.10 Dip Statistics of Large Continuous Open Fractures ( $\geq 65^\circ$  Dip Magnitudes and  $< 65^\circ$  Dip Magnitudes), Interval 1,748-2,494 m MD
- 2.3.11 ABI Image Examples of Litho-bound Open Fractures
- 2.3.12 Dip Statistics of Litho-bound Open Fractures, Interval 1,748-2,494 m MD

- 2.3.13 Dip Statistics of Litho-bound Open Fractures ( $\geq 70^\circ$  Dip Magnitudes and  $< 70^\circ$  Dip Magnitudes), Interval 1,748-2,494 m MD
- 2.3.14 ABI Image Examples of Possible Open Fractures
- 2.3.15 Dip Statistics of Possible Open Fractures, Interval 1,748-2,494 m MD
- 2.3.16 Dip Statistics of Possible Open Fractures ( $\geq 70^\circ$  Dip Magnitudes and  $< 70^\circ$  Dip Magnitudes), Interval 800-2, 679 m MD
- 2.3.17 ABI Image Examples of Possible Open Faults
- 2.3.18 ABI Image Examples of Possible Open Faults
- 2.3.19 Dip Statistics of Possible Open Faults, Interval 1,748-2,494 m MD
- 2.3.20 Dip Statistics of Possible Open Fault ( $\geq 70^\circ$  Dip Magnitudes and  $< 70^\circ$  Dip Magnitudes), Interval 1,748-2,494 m MD
- 2.3.21 ABI Image Examples of Drilling Induced Fractures and Borehole Breakouts
- 2.3.22 Dip Statistics of Borehole Breakouts and Drilling Induced Fractures, Interval 1,748-2,494 m MD
- 2.3.23 ABI Image Examples of Lithologic Boundaries
- 2.3.24 Dip Statistics of Lithologic Boundaries, Interval 1,748-2,494 m MD
- 3.1 Fracture Zonation, Interval 1,748-2,494 m MD, Well PG-18
- 3.2 Zones of Lost Circulation and Feed Zone, Fracture Zone 1 (2,494-2,357 m MD)
- 3.3 Examples of Feed Zone, Fracture Zone 1 (2,494-2,357 m MD)
- 3.4 Examples of Feed Zone, Fracture Zone 1 (2,494-2,357 m MD)
- 3.5 Examples of Large Continuous Open Fractures, Large Discontinuous Open Fractures, and Possible Open Faults in Fracture Zone 2 (2,357-2,252 m MD)
- 3.6 Examples of Large Continuous Open Fractures, Large Discontinuous Open Fractures, and Possible Open Faults in Fracture Zone 2 (2,357-2,252 m MD)
- 3.7 Examples of Large Continuous Open Fractures and Large Discontinuous Open Fractures in Fracture Zone 3 (2,252-1,956 m MD)
- 3.8 Examples of Large Continuous Open Fractures, Large Discontinuous Open Fractures, and Possible Open Faults in Fracture Zone 3 (2,252-1,956 m MD)
- 3.9 Examples of Large Continuous Open Fractures and Large Discontinuous Open Fractures in Fracture Zone 4 (1,956-1,748 m MD)

## EXECUTIVE SUMMARY

Production well PG-18 was logged on behalf of Landsvirkjun on 26 August 2017, using an ABI tool deployed by ÍSOR. The subject well is in the Peistareykir Field in northeastern Iceland. The ABI logging was conducted in the 8.5-inch diameter of the well (2,494-1,748 m MD), which passes through volcanic formations. The ABI logging was conducted in 3 runs: 1,748-2,313.5 m MD, 2,309-2,393 m MD, and 2,392-2,494 m MD.

GeothermEx has been contracted by Landsvirkjun to provide ABI image processing and interpretation services for the logged intervals of well PG-18. The main objective of the study is to provide detailed fracture analysis, including fracture classification and determination of the orientation and density of fractures.

Borehole conditions are good in the interval of 2,494-2,200 m MD, with only a few large and minor washouts, and the image quality in this interval is generally good. Borehole washouts that are evident in the interval of 2,200-1,748 m MD adversely affected ABI Image quality, but fractures and faults could still be identified and analyzed. The inclinometry data from the ABI tool were found to be in good agreement with the deviation data from gyro surveys, indicating that the tool was correctly oriented in the borehole and that the calculated dips are correct. The GR logs from GR-ABI logging runs 9 and 10 are off-depth relative to GR log from NN-GR logging run 6; simple (bulk / block) depth shifts were performed during the ABI processing for run numbers 9 and 10 using single offset values of 5.8 m and 5.4 m respectively. ABI logging from run 11 is off-depth relative to “processed” and “depth-matched” ABI image from run 10; a bulk / block depth shift was performed during the ABI processing for run 11 using a single offset value of 5.7 m.

Fractures are well developed over almost the entire logged interval, with a total of 3,850 open fractures identified. Discontinuous open fracture is the predominant fracture type. A total of 2,840 such fractures were identified in the interval; they show a dominant strike orientation of NNE-SSW, with WNW and ESE azimuths. Dip magnitudes for this fracture type are highly variable, from horizontal to vertical, but are mainly steeper than 70°.

The discontinuous open fractures with large low amplitude events are classified as large discontinuous open fracture. A total of 202 large discontinuous open fractures were identified in the interval, they show a dominant strike orientation of NNE-SSW, with WNW and ESE azimuths. Dip magnitudes for this fracture type are highly variable, from 10° to vertical, but are mainly steeper than 70°.

Continuous open fractures are rare compared to the discontinuous conductive fractures. A total of 81 such fractures were identified in the logged interval; they show a dominant strike orientation of NNE-SSW with WNW and ESE azimuths, and dip magnitudes from nearly horizontal to vertical but are mainly steeper than 65°.

The continuous open fractures with large low amplitude events are classified as large continuous open fracture. A total of 117 such fractures were identified in the logged interval; they show a dominant strike orientation of NNE-SSW, with WNW, E, and ESE azimuths, and dip magnitudes vary from 15° to vertical, but are mainly steeper than 65°.

Only 56 litho-bound open fractures were recognized in the entire logged interval. Dips of litho-bound fractures demonstrate dominant strike orientations of NNE-SSW, NW-SE, and ENE-WSW, with ESE, WNW, NE, and SSE azimuths; and dip magnitudes are highly variable, from nearly horizontal to vertical.

A total of 554 possible open fractures were recognized in the logged interval. Dips of possible open fractures demonstrate dominant strike orientations of NNW-SSE, NNE-SSW, and NE-SW, with westward (WNW, W, WSW) azimuth, and dip magnitudes that vary from nearly horizontal to vertical, but are mainly >45°.

The facies changes seen on the ABI image are marked as lithologic boundaries. A total of 95 lithologic boundaries were recognized over the entire logged interval. Lithologic-boundary dip statistics in the interval show a dominant azimuth orientation of westerly (WSW, W, and WNW). Dip magnitudes are also highly variable, from nearly horizontal to vertical.

The density of discontinuous open fractures varies from 0 to 13 per meter; the density is greatest at 2,406-2,407 m MD. The density of large discontinuous open fractures varies from 0 to 6 per meter, with the highest density occurring at 2,418.5-2,420 m MD and 2,357-2,358 m MD. The density of continuous open fractures varies from 0 to 3 per meter, with the highest densities observed at 1,794.5-1,796.5 m MD, 1,834-1,835 m MD, 1,838-1,839 m MD, and 2,017-2,018 m MD. The density of large continuous open fractures varies from 0 to 8 per meter, and is highest at 2,420-2,421.5 m MD. Litho-bound open fractures are more localized and are developed mainly in association with intrusion and/or possible intrusive rocks, their density varies from 0 to 6 per meter (with a peak at 2,061-2,062.5 m MD). The fracture density of possible open fracture varies from 0 to 11 per meter, with the highest densities observed at 2,463-2,464.5 m MD.

A total of 28 possible open faults were identified in the logged interval. They have a dominant strike orientation of NNE-SSW, with ESE and WNW azimuths. Possible-open-fault dip magnitudes are highly variable (from 38° to vertical), but mainly >70°.

A total of 2 drilling-induced fractures were identified, with a dominant strike orientation of N-S. A total of 13 borehole breakouts were identified, with a dominant strike of E-W/ENE-WSW (perpendicular to the strike orientation of the drilling-induced fractures). Well PG-18 has a deviation of approximately 33° to 40.6° from vertical, so the strikes of drilling induced fractures and borehole breakouts may not align with the trends of maximum and minimum horizontal stress (respectively).

Four fracture zones were identified, based mainly on fracture strike orientation. They are:

- **Fracture Zone 1 (2,494-2,357 m MD):** Comprised mainly of intensely-altered fine-medium-grained and medium-coarse-grained basalt lavas, intermediate fine-medium-grained rock, and basaltic breccia. Open fractures are well developed and are mainly discontinuous, but continuous open fractures, large continuous open fractures, large discontinuous open fractures, litho-bound open fractures and possible open fractures are also observed. Open fractures demonstrate a dominant NNE-SSW strike with WNW and ESE azimuths, and dip magnitudes from nearly horizontal to vertical, but are mainly >70°.

Circulation losses were reported at 6 depths in this interval, with loss rates between 4 L/s and 8 L/s. They may be associated with possible open faults and zones of large continuous and discontinuous open fractures.

One feed zone was identified from temperature logs and the circulation losses. The “size 2” feed zone at 2,420-2,485 m MD may be associated with a high angle (68°) NNE-SSW possible open fault at 2,420.4 m MD, a high angle (86°) NNE-SSW possible open fault at 2,428 m MD, a high angle (70°) NNW-SSE possible open fault at 2,436.1 m MD, a high angle (87°) N-S possible open fault at 2,436.4 m MD, a high angle (79°) NNE-SSW possible open fault at 2,443.4 m MD, a lower angle (47°) NW-SE possible open fault at 2,444.8 m MD, a lower angle (37°) NNE-SSW possible open fault at 2,453.2 m MD, a high angle (83°) NNE-SSW possible open fault at 2,458 m MD, a high angle (89°) NNE-SSW possible open fault at 2,485.6 m MD, a high angle (71°) possible open fault at 2,485.8 m MD, and some large continuous and discontinuous open fractures at 2,417-2,491 m MD which demonstrate a dominant strike orientation of NNE-SSW, with WNW azimuth, and dip magnitudes that vary from 20° to vertical but are mainly >70°. ÍSOR (2017) considers this feed zone to be one of the most permeable the entire logged interval.

- **Fracture Zone 2 (2,357-2,252 m MD):** Comprised mainly of intensely-altered fine-medium-grained and medium-coarse-grained basalt lavas, and glassy basalt. Open fractures are well developed and are mainly discontinuous, though continuous open fractures, large continuous open fractures, large discontinuous open fractures, litho-bound open fractures and possible open fractures are also observed. The dip statistics of the open fractures demonstrate dominant high degree of scatter (NE-SW, NNE-SSW, N-S, and ENE-WSW strikes with WNW, NW, E, ESE, ENE, and SSE and NNW azimuths), and dip magnitudes from nearly horizontal to vertical, but are mainly >65°.

No losses of circulation occurred within this fracture zone, and no feed zones were recognized in this fracture zone.

- **Fracture Zone 3 (2,252-1,956 m MD):** Comprised mainly intensely-altered of fine-medium-grained, medium-coarse-grained, to coarse-grained basalt lavas, glassy basalt, and basaltic breccia. Open fractures are well developed and are mainly discontinuous, but continuous open fractures, large continuous open fractures, large discontinuous

open fractures, litho-bound open fractures and possible open fractures are also observed. These fractures have a dominant strike orientation of NNE-SSW, with WNW and ESE azimuths, and dip magnitudes vary from nearly horizontal to vertical but are mainly  $>70^\circ$ .

No losses of circulation occurred within this fracture zone, and no feed zones were recognized in this fracture zone.

- Fracture Zone 4 (1,956-1,748 m MD): Comprised mainly of intensely-altered fine-medium-grained, medium-coarse-grained, to coarse-grained basalt lavas, glassy basalt, intermediate coarse-grained rock, and basaltic breccia. Open fractures are well developed, and are mainly discontinuous, but continuous open fractures, large continuous open fractures, large discontinuous open fractures, and possible open fractures are also observed. These open fractures demonstrate dominant strike orientations of NNE-SSW, N-S, and ENE-WSW with WNW, ESE, W, E, and NW azimuths, and dip magnitudes vary from nearly horizontal to vertical but are mainly  $>55^\circ$ .

No losses of circulation occurred within this fracture zone, and no feed zones were recognized in this fracture zone.

## 1. INTRODUCTION

### 1.1 Background

Acoustic Borehole Imager (“ABI”) logging yields an image of the inside of a borehole generated by the transmission and reception of ultrasonic pulses. Two types of information are gathered by this technique: the travel time of the sonic wave, which is dependent on the shape and diameter of the well, and the returning amplitude of the wave, which relates to the acoustic impedance of the borehole wall (Massiot *et al.*, 2016 [citing Davatzes and Hickman, 2010]).

The ABI images with 100% coverage allow analysis of fractures, the stress regime, and borehole stability. The sensitivity of the measurement in combination with 100% circumferential coverage makes acoustic borehole images useful for detecting drilling-induced fractures, improving fracture analysis, determining borehole stability, diagnosing the severity and orientation of keyhole wear, identifying borehole breakouts and shear sliding, determining horizontal stresses, and analyzing hole shape.

Production well ÞG-18, located in the Þeistareykir Field, in the County of Þingeyjarsveit, northeastern Iceland (X= 592972.687, Y= 599923.916, at elevation of 343 m asl) was logged on behalf of Landsvirkjun (hereinafter “Landsvirkjun” or “Client”) on 26 August 2017, using an ABI tool deployed by Íslenskar Orkurannsóknir (hereinafter “ÍSOR”). The ABI logging was conducted from 1750 m to 2,494 m depth in the 8.5-inch-diameter section of the well, which passes through volcanic formations. The logging was conducted in 3 runs: 1,748-2,313.5 m measured depth (MD), 2,309-2,393 m MD, and 2,392-2,494 m MD. Wellbore parameters and service details are listed in Table 1.1 below.

GeothermEx, Inc., a Schlumberger Company (hereinafter “GeothermEx”) has been contracted by Landsvirkjun to provide ABI image processing and interpretation services for the logged intervals of well ÞG-18. ABI image processing and data interpretation were carried out using

the Techlog\* wellbore software platform (version 2017.2). Techlog is Schlumberger's integrated reservoir characterization system, which provides support for project management, data preparation, and log analysis.

Tool Type	ABI
Intervals (m MD)	2,392-2,494 (Run 9); 2,309-2,393 (Run 10); and 1,748-2,313.5 (Run 11)
Date Logged	26 August 2017
Bit Size (inch)	8.5
Borehole Coverage (%)	100
Well Deviation (degrees)	33 to 40.6
Well Azimuth (degrees)	80.5 to 83 (WNW/W)
Drilling Fluid Type	Mud / Water

**Table 1.1: Wellbore parameters of well bG-18 and ABI tool service details**

For each interval where ABI data have been provided by Landsvirkjun, GeothermEx has performed:

- ABI image processing: The primary purpose of computer processing of raw acoustic image data is to convert the raw data into the best visual representation of the borehole. Proper conditioning of the data is achieved using certain correction algorithms, prominent examples of which are:
  - Image Correction / Equalization:

---

\* Mark of Schlumberger

- a. Amplitude and transit / travel time processing: eccentric correction, convert transit time to radius, output uncorrected radius, azimuth equalization, resampling correction
  - b. Filtering: noise filter, correct sampling bias
  - c. Hole shape analysis
- Image Orientation: image is oriented with respect to the north side of the borehole.
  - Image Depth Shift / Depth Match: when logging tools are run in sequence, differences always occur in depth from tool to tool and from run to run due to differential cable stretch. Stretch can be pronounced when the logging string sticks or temporarily hangs up in the hole. All logging measurements must be adjusted to a common depth reference before data processing can continue. All depths should be referenced to a base log. The base log is selected from a logging tool where strong or forceful tool positioning is not used (e.g., GR log from run 6 using tool numbers GO-NG1 and GOLind1). Free-moving tools travel through the borehole more smoothly than tools that are pushed with great force against the borehole wall. For this reason, strongly centralized tools (e.g., ABI tool) are not selected as the base log.  
  
GR logs are available from the ABI tools (tool numbers: ABI-073603, ABI-000703, and GR-144701) and the NN-GR tools (tool numbers: GO-NG1 and GOLind1). GR log from NN-GR tools was selected as the base log. The GR from the ABI tools and all curves recorded with the ABI tools were then shifted to match the NN-GR log depths.
  - Image Normalization:
    - a. One single color scale (static image)
    - b. Sliding window (1 m) color scale (dynamic image): dynamic normalization was applied to both images (amplitude and transit / travel (radius)) to highlight the

features of the borehole. Dark colors represent low amplitude and large radii, indicating borehole rugosity, enlargements, and attenuative material.

- ABI image interpretation: The processing of ABI images was followed by interactive dip picking and feature classification using normalized images. The dip picking enabled computation of the dip angle of lithological boundary, fracture, fault, and/or any other planar features. Drilling-induced fractures and borehole breakouts were also easily recognizable in most situations with these acoustic images. Interactive dip picking was performed manually using a sine wave, with its amplitude and azimuth fitted to planar features on the image.
- Presentation of results: A presentation based on the preliminary results of ABI image processing and interpretation was prepared and presented to Landsvirkjun's management and technical teams on 9 January 2019. It included:
  - A description and discussion of the data reviewed, including data quality.
  - A description of the data processing and interpretation workflows and manual dip classification.
  - Discussion of the structural interpretation, including fracture and fault interpretation.
  - Discussion of the present-day geo-stress analysis (maximum and minimum stress orientations) from drilling induced fractures and borehole breakouts interpretation.
  - Discussion of the fracture zonation.
  - Discussion of the relationship between open fractures and/or faults and zones of lost circulation.
  - Discussion of the relationship between open fractures and/or faults and feed zones.

- Discussion of the comparison of the results of ABI structural interpretation, present-day geo-stress analysis, and fracture zonation of wells PG-15, PG-17, PG-12, and PG-18.

The presentation provided by GeothermEx to Landsvirkjun’s management and technical team, is included as Appendix A to this report.

This “ABI Image Processing and Interpretation of Well PG-18, Peistareykir Field, Pingeyjarsveit, Iceland” report has been prepared by GeothermEx in its capacity as Landsvirkjun’s contractor per the term of the contract between Landsvirkjun and GeothermEx dated 22 November 2018 (Landsvirkjun Contract Agreement Number: LV 2371).

## 1.2 Objectives

The main objective of this study is to provide detailed fracture analysis of well PG-18, including fracture classification and determination of the orientation and density of fractures.

## 1.3 Database

For this evaluation, GeothermEx has relied primarily on data provided by Landsvirkjun, and secondarily on information in the public domain. Landsvirkjun delivered:

- ABI image logs.
- Temperature and pressure logs.
- Caliper logs.
- Gyro logs.
- Standard open-hole logs, which include:
  - Gamma ray (GR)
  - Resistivity (16” and 64”)
  - Neutron-porosity

- Spinner logs.
- Lithological log plots from cutting analysis.
- Intrusion log plot.
- Alteration log plot.
- Lost circulation intervals.
- Feed zone intervals.
- A report from ÍSOR (dated December 2017, written in English), titled “Þeistareykir – Well ÞG-18. Phase 3: Drilling for a 7” Perforated Liner down to 2644 m” (report number: LV-2017-105). The report discusses: the location, planned design, planned trajectory, and drilling operation of well ÞG-18; lithology, alteration, and intrusion interpretation from cutting analysis; lost circulation during phase 3 drilling (8.5-inch section); wireline logging operation, results, and interpretation (for spinner logs); multirate injection test; and stimulation. The report also contains: location map of production wells and well pads in the Þeistareykir area; map view of ÞG-18 and nearby wells; a graphic of drilling progress, phases 0-3; BHA setup for drilling of phase 3 from 997 to 1,754 m; BHA graphical reports; casing information report; casing tally run report; description and interpretation of lithology and alteration from 998 m MD to 2,644 m MD; lithology and drilling data from 998 m MD to 2,644 m MD; lithology, alteration, and geophysical logging from 998 m MD to 2,644 m MD in well ÞG-18 (including lithologic column, alteration, intrusion, feed points, caliper logs, resistivity logs, neutron-porosity log, and gamma ray log); a summary of alteration minerals; some graphics related to temperature logs; an overview of geophysical logs conducted in the production part (drilling phase 3) of well ÞG-18 (including temperature log, caliper logs, resistivity logs, neutron log, and gamma ray log); a graphic related to caliper logs and calculated eccentricity; some graphics related to spinner logs; some graphics related to

the multirate injection test; some graphics related to stimulation; a plot of well azimuth and inclination versus depth of well PG-18 (from surface down to 2,630 m); results of gyro logs; and some graphics displaying geophysical logs (caliper logs, resistivity logs, SP log, neutron log, and gamma ray log).

All data listed above have been delivered in a format that allow the contents to be evaluated and used for analysis. Full references for the data sources introduced herein are provided at the end of this report, and the sources are cited as appropriate in the text.

## 2. RESULTS OF ABI PROCESSING AND INTERPRETATION

### 2.1 ABI Log Quality and Borehole Conditions

The ABI logging was conducted from 1,748-2,494 m MD in the 8.5-inch-diameter interval of the well, which passes through volcanic formations. The logging was performed in 3 runs: 2,392-2,494 m MD (run 9), 2,309-2,393 m MD (run 10), and 1,748-2,313.5 m MD (run 11).

The borehole conditions from 2,494-2,200 m MD are good, with only few large and minor washouts, and the image quality in this interval is generally good (Figures 2.1.1 and 2.1.2). Evident borehole washouts in the interval of 2,200-1,748 m MD adversely affected ABI Image quality (Figures 2.1.1 and 2.1.2), but fractures and faults could still be identified and analyzed.

In general, the inclinometry data from the ABI tool agreed with the well deviation and well azimuth data from gyro surveys, indicating that the tool was correctly oriented in the borehole and that the calculated dips are correct (Figure 2.1.3).

The GR logs from GR-ABI logging runs 9 and 10 (tool numbers: ABI-073603, ABI-000703, and GR-144701) are off-depth relative to GR log from NN-GR logging run 6 (tool numbers: GO-NG1 and GOLind1). The aforementioned GR logs are offset by the same amount throughout the log (fixed distance between the measure points and the depth reference is 5.8 m for run 9 and 5.4 m for run 10); thus simple (bulk / block) depth shifts were performed during the ABI processing, in which the ABI logs were shifted/moved up by 5.8 m (for run number 9) and 5.4 m (for run number 10) (Figure 2.1.4).

ABI logging from run 11 (tool numbers: ABI-073603, ABI-000703) was not complemented by GR log, thus the depth matching was performed solely using “processed” and “depth-matched” ABI image from run 10. The ABI image from run 11 is off-depth relative to “processed” and “depth-matched” ABI image from run 10, and fixed distance between the measure points and the depth of reference is 5.7 m. A bulk / block depth shift was performed during the ABI processing, in which the ABI log was moved/shifted up by 5.7 m (Figure 2.1.4).

## 2.2 Manual Dip Classification

Structural features were picked manually using sine waves, with their amplitudes and azimuths fitted to planar features on the borehole image. The lowest point of the sinusoid troughs defines the dip azimuths, and the amplitude of the sinusoids define the dip magnitudes.

All dip interpretations have been made using a combination of static and dynamic normalized images, along with gamma-ray, resistivity, and neutron-porosity logs, results of cutting analysis, interpreted intrusion log plot, lost circulation intervals from drilling reports, and interpreted feed zone intervals from spinner logs. The dip classification scheme is summarized in Table 2.2.

In acoustic images, the fractures that have low amplitude traces are termed open fractures. Their low amplitudes result from the density variation between the open section (filled with drilling mud) and the surrounding rock. The fractures are further classified into continuous open fractures and discontinuous open fractures, based on their appearance and continuity across the borehole diameter. The continuous and discontinuous open fractures with large low amplitude events are termed large continuous open fractures and large discontinuous open fractures respectively.

Fractures that appear to be of low amplitude and compartmentalized within an individual lithologic unit bounded and/or terminated by lithologic boundaries are classified as litho-bound open fractures. Places where potential low-amplitude-fracture traces are present have been classified as possible open fractures.

Fractures with high amplitude traces are termed closed fractures. The high amplitudes are due to the density difference between the open section (filled with calcite, quartz or other minerals) and the surrounding rock. These fractures are further classified into continuous closed fractures and discontinuous closed fractures, based on their appearance and continuity across the borehole diameter. No closed fractures were observed in well PG-18.

Possible faults are similar in appearance to fractures, but they show indications of displacement and/or truncation.

Drilling-induced tensile fractures and borehole breakouts were oriented by fitting sinusoids to these features where they occur on directly opposite sides of the borehole wall. Although these features do not have a dip direction or dip magnitude, their strikes can be defined and used to indicate the maximum and minimum horizontal stress directions.

Sedimentary dips generally reflect depositional processes and attitudes, but the interval logged in well PG-18 is entirely volcanic, and bedding is not observed anywhere. The lithologies (as defined by cutting analysis) are mainly basalt lava (varying from glassy basalt, fine-medium grained basalt, medium-coarse grained basalt, to coarse grained basalt), with some sections of intermediate fine-medium grained rock, intermediate tuff, and basaltic breccia. The facies changes seen on the ABI image are marked as lithologic boundaries (Figure 2.3.23). A total of 95 lithologic boundaries were recognized over the entire logged interval (2,494-1,748 m MD). Lithologic-boundary dip statistics in the interval show a dominant azimuth orientation of westerly (WSW, W, and WNW). Dip magnitudes are also highly variable, from nearly horizontal to vertical (Figure 2.3.24).

Feature Name	Description	Symbol
<b>Lithologic Dips:</b>		
Litho-Boundary	Apparently non-erosional boundary / contact between different lithologies / facies. Solid brown circle.	
<b>Structural Dips:</b>		
Continuous Open Fracture	Fracture with low-amplitude image, continuous across borehole diameter. Solid blue square.	
Large Continuous Open Fracture	Fracture with large low-amplitude event, continuous across borehole diameter. Blue square.	
Discontinuous Open Fracture	Fracture with low-amplitude image, discontinuous across borehole diameter. Solid blue triangle.	
Large Discontinuous Open Fracture	Fracture with large low-amplitude event, discontinuous across borehole diameter. Blue triangle.	
Litho-bound Open Fracture	Fracture with low amplitude, compartmentalized within individual lithologic unit bounded and/or terminated by lithologic boundaries. Solid dark blue diamond.	
Possible Open Fracture	Fracture with low-amplitude image, discontinuous across borehole diameter (not seen across borehole diameter due to the poor-quality image caused by bad hole or artifact). Solid light pink triangle.	
Possible Open Fault	Continuous low-amplitude planar features cutting bedding and/or fracture with a tentative evidence for movement. Solid red square.	
Drilling-Induced Fracture	Fractures that track vertically down but do not cross the borehole, or appear as discontinuous "gashes" on opposing sides of the borehole. These features appear with high amplitude on images. Red strike.	
Borehole Breakout	Vertical irregular low amplitude areas on opposing sides of the borehole wall. Black strike.	

**Table 2.2: Dip classification and interpretation scheme**

## 2.3 Structural Interpretation

Structural interpretation includes identifying and determining the orientation of features with a tectonic origin (including fractures and faults), and determining the present-day tectonic stress field orientation from drilling-induced features and borehole breakouts. Detailed fracture

analysis, consisting of fracture classification, fracture orientation, and fracture density analysis, was requested for the interval of 2,494-1,748 m MD.

### *Fracture Types, Morphology, and Orientation*

Fractures are well developed over almost the entire interval logged. They could not, however, be confidently identified in some intervals (e.g., 1,781-1,783 m MD, 1,792.5-1,794 m MD, 1,797.5-1,800 m MD, 1,824.5-1,833 m MD, 1,859.5-1,862.5 m MD, 1,881-1,883 m MD, 1,902-1,903.5 m MD, 1,906.5-1,912 m MD, 1,915-1,916.3 m MD, 1,934.5-1,936.5 m MD, 1,947-1,948.5 m MD, 1,949.5-1,952.5 m MD, 1,958.5-1,965.5 m MD, 1,975-1,977 m MD, 1,983.5-1,986.5 m MD, 2,018.5-2,023.5 m MD, 2,030-2,031.5 m MD, 2,068-2,071.5 m MD, 2,080-2,083 m MD, 2,101.5-2,102.5 m MD, 2,103.2-2,105 m MD, 2,115-2,117 m MD, 2,130-2,132.5 m MD, 2,150-2,151 m MD, 2,225-2,228.5 m MD, 2,242-2,244 m MD, 2,249-2,251.5 m MD, 2,270-2,273 m MD, 2,450-2,451 m MD, 2,460-2,461 m MD, 2,463-2,464.5 m MD, 2,467.5-2,468.5 m MD, and 2,471.1-2,473.2 m MD), because of reduced image quality caused by borehole rugosity. The fractures in these intervals are classified as “possible open fractures”.

The fractures identified are almost exclusively low-amplitude (considered to be open). No high-amplitude (considered to be closed) fractures were recognized. As discussed in Section 2.2, open and closed fractures are further classified as either continuous or discontinuous; respectively they can be seen to be continuous around the borehole on the image, or discontinuous around the borehole. The continuous and discontinuous open fractures with large low amplitude events are termed large continuous open fractures and large discontinuous open fractures respectively. Fracture types, morphology, and orientation are described below:

- **Discontinuous Open Fractures**: The predominant fracture type, they appear as linear fractures that do not completely transect the borehole (Figures 2.3.1 and 2.3.2). Even though discontinuous, where the open section includes the peak and/or trough of the trace, the fracture can safely be considered to be of natural origin. Where the fracture is discontinuous, and the trace only follows the sinewave limbs, but does not describe

the sinewave peak or trough, then it might be drilling-induced, or, possibly, a closed fracture that has been partly opened by the drilling process.

A total of 2,840 discontinuous open fractures were identified over the entire logged interval (2,494-1,748 m MD). Discontinuous-open-fracture dip statistics over the interval demonstrate a dominant strike orientation of NNE-SSW, with WNW and ESE azimuths (Figure 2.3.3). Dip magnitudes for this fracture type are highly variable, from horizontal to vertical, but mainly steeper than 70° (Figure 2.3.3). Discontinuous open fractures with dip magnitudes  $\geq 70^\circ$  show a dominant strike orientation of NNE-SSW, with WNW and ESE azimuths. Discontinuous open fractures with dip magnitudes  $< 70^\circ$  show a dominant strike orientation of ENE-WSW, with NNW and SSE azimuths (Figure 2.3.4).

- Large Discontinuous Open Fractures: The discontinuous open fractures with large low amplitude events are classified as large discontinuous open fractures. A total of 202 large discontinuous open fractures were identified over the entire logged interval (2,494-1,748 m MD). Large-discontinuous-open-fracture dip statistics over the interval demonstrate a dominant strike orientation of NNE-SSW, with WNW and ESE azimuths (Figure 2.3.4). Dip magnitudes for this fracture type are highly variable, from 10° to vertical, but mainly steeper than 70° (Figure 2.3.5). Large discontinuous open fractures with dip magnitudes  $\geq 70^\circ$  show a dominant strike orientation of NNE-SSW, with WNW, ESE azimuths. Large discontinuous open fractures with dip magnitudes  $< 70^\circ$  show a high degree of scatter but E-W strike with Northerly azimuth predominate (Figure 2.3.6).
- Continuous Open Fractures: Relatively rare compared to the discontinuous conductive fractures, they completely transect the borehole without a break in the fracture trace on the ABI image (Figures 2.3.1 and 2.3.2). These fractures may also represent discontinuous fractures that have been cut by the borehole in a continuous section. Away from the borehole they might be discontinuous.

A total of 81 continuous open fractures were identified over the entire logged interval (2,494-1,748 m MD). Continuous-open-fracture dip statistics in the interval indicate a dominant strike orientation of NNE-SSW with WNW and ESE azimuths (Figure 2.3.7). The dip magnitudes of the continuous open fractures vary from nearly horizontal (approximately 8°) to vertical, but they are mainly steeper than 65° (Figure 2.3.7). Continuous open fractures with dip magnitudes  $\geq 65^\circ$  show dominant strike orientation of NNE-SSW with WNW and ESE dips (Figure 2.3.8). Continuous open fractures with dip magnitudes of  $< 65^\circ$  indicate dominant strike orientations of NNE-SSW, NE-SW, and E-W with WNW, NW, SW, SSW, SSE, and SW azimuths (Figure 2.3.8).

- **Large Continuous Open Fractures:** The continuous open fractures with large low amplitude events are classified as large continuous open fractures. A total of 117 large continuous open fractures were identified over the entire logged interval (2,494-1,748 m MD). Large-continuous-open-fracture dip statistics over the interval demonstrate a dominant strike orientation of NNE-SSW, with WNW, E, and ESE azimuths (Figure 2.3.9). Dip magnitudes for this fracture type are highly variable, from 15° to vertical, but mainly steeper than 65° (Figure 2.3.9). Large discontinuous open fractures with dip magnitudes  $\geq 65^\circ$  show a dominant strike orientation of NNE-SSW, with WNW, E, and ESE azimuths (Figure 2.3.10). Discontinuous open fractures with dip magnitudes  $< 65^\circ$  show a high degree of scatter but a NE-SW strike with NW azimuth predominates (Figure 2.3.10).
- **Litho-bound Open Fractures:** Only 56 litho-bound open fractures were recognized in the entire logged interval (2,494-1,748 m MD). This fracture type has a low amplitude and is compartmentalized within individual lithologic units bounded and/or terminated by lithologic boundaries (Figure 2.3.11). The development of this fracture type is mainly associated with intrusion and/or possible intrusive rocks.

Litho-bound-open-fracture dip statistics over the interval demonstrate dominant strike orientations of NNE-SSW, NW-SE, and ENE-WSW, with ESE, WNW, NE, and SSE azimuths

(Figure 2.3.12). Dip magnitudes for this fracture type are highly variable, from nearly horizontal to vertical (Figure 2.3.12). Litho-bound open fractures with dip magnitudes  $\geq 70^\circ$  show a dominant strike orientation of NNE-SSW, with ESE and WNW azimuths (Figure 2.3.13). Discontinuous open fractures with dip magnitudes  $< 70^\circ$  show a high degree of scatter but NW-SE and ENE-WSW strikes with NE and SSE azimuths predominate (Figure 2.3.13).

- Possible Open Fractures: This fracture type has a low amplitude and is discontinuous across the borehole diameter, due to poor image quality caused by bad hole condition or logging artifacts (Figure 2.3.14). As previously discussed, in some intervals there are possible low-amplitude fracture traces which could not be confidently identified because of reduced image quality caused by borehole rugosity. All such traces in these intervals are classified as “possible open fractures.”

A total of 554 possible open fractures were recognized over the entire logged interval (2,494-1,748 m MD). Possible-open-fracture dip statistics in the interval demonstrate dominant strike orientations of NNW-SSE, NNE-SSW, and NE-SW, with westward (WNW, W, WSW) azimuth, and dip magnitudes that vary from nearly horizontal to vertical, but mainly  $> 45^\circ$  (Figure 2.3.15). Possible open fractures with dip magnitudes of  $\geq 70^\circ$  show dominant strike orientations of NNW-SSE, with WSW and ENE azimuths (Figure 2.3.16). Possible open fractures with dip magnitudes of  $< 70^\circ$  demonstrate dominant strike orientations of NNE-SSW and NE-SW, with WNW and NW azimuths (Figure 2.3.16).

### *Fracture Density*

Fracture density is computed in Techlog using the “Dip Feature Counting” method. The fracture density can be computed as total (using all fracture types), per fracture type, or for a combination of fracture types. GeothermEx has provided Landsvirkjun with a fracture density log of each open fracture type (i.e., the density of continuous open fractures, density of discontinuous open fractures, and density of possible open fractures). Fracture-density logs are

computed as continuous curves and presented as the number of fractures per meter selected along a line perpendicular to the fracture plane.

Fractures are well developed over almost the entire logged intervals (2,494-1,748 m MD), with a total of 3,850 open fractures identified. GeothermEx's ABI interpretation plots titled "Landsvirkjun PG-18 ABI Interpretation\_2314-1753 m MD\_Scale 240", "Landsvirkjun PG-18 ABI Interpretation\_2393-2315 m MD\_Scale 240", and "Landsvirkjun PG-18 ABI Interpretation\_2494-2398 m MD\_Scale 240", presented and delivered to Landsvirkjun on 31 December 2018, show the variations in fracture densities over the intervals studied.

Discontinuous open fractures are the dominant fracture type; they are well developed throughout the logged interval, with a density of 0 to 13 per meter (the highest being at 2,406-2,407 m MD).

Discontinuous open fractures with large low amplitude events are classified as large discontinuous open fractures. Their density varies from 0 to 6 per meter, and is highest at 2,418.5-2,420 m MD and 2,357-2,358 m MD.

Continuous open fractures are rare compared to the discontinuous conductive fractures. Their density varies from 0 to 3 per meter, and the highest densities observed at 1,794.5-1,796.5 m MD, 1,834-1,835 m MD, 1,838-1,839 m MD, and 2,017-2,018 m MD.

Continuous open fractures with large low amplitude events are classified as large continuous open fractures. Their density varies from 0 to 8 per meter, and is highest at 2,420-2,421.5 m MD.

Litho-bound open fractures are more localized and are developed mainly in association with intrusion and/or possible intrusive rocks. Their density varies from 0 to 6 per meter (with a peak at 2,061-2,062.5 m MD).

Possible open fractures are identified where potential low-amplitude-fracture traces are present, and appear discontinuous across the borehole due to poor image quality. These

fractures were observed throughout the logged intervals. Their fracture density varies from 0 to 11 per meter, with the highest density observed at 2,463-2,464.5 m MD.

### *Possible Faults*

The factors generally considered for locating possible faults on the borehole images are:

- abrupt changes in bedding dip attitude (either magnitude or azimuth) across the plane of the feature;
- large high-angle, high-amplitude or low-amplitude events developed across the wellbore;
- enlarged hole at the fault / borehole intersection;
- shift in the trend of in-situ stress;
- abrupt termination of layers and/or fractures on the plane of the feature;
- changing thickness of the fault bounded layer across the wellbore;
- occurrence of fractures around the fault intersection; and
- abrupt changes in log response across the feature interpreted as a fault.

Several faults were identified based on the above criteria, with diagnostic features including (but not restricted to): indications of large low-amplitude events developed across the wellbore, enlarged hole at possible faults, abrupt termination of fractures on the possible fault plane, and occurrence of fractures around the possible fault intersection (Figures 2.3.17 and 2.3.18).

A total of 28 possible open faults were identified in the logged interval. Possible-open-fault dip statistics demonstrate a dominant strike orientation of NNE-SSW, with ESE and WNW azimuths (Figure 2.3.19). Dip magnitudes vary from 38° to vertical, but are mainly >70° (Figure 2.3.19). The features with dip magnitudes  $\geq 70^\circ$  show dominant strike orientations of NNE-SSW with ESE

and WNW azimuth; those with dip magnitudes  $<70^\circ$  have dominant strike orientations of NNE-SSW and NNW-SSE with ESE and ENE azimuths (Figure 2.3.20).

### *Geo-Stress Analysis*

The subsurface of the Earth's crust rarely stays in a lithostatic stress condition (with stresses equal in all directions; that is,  $\sigma_1 = \sigma_2 = \sigma_3$ ). The equilibrium of the stress state is generally disturbed by movements of tectonic plates, leading to the formation of a regional stress system, which may itself be partially or completely overprinted by localized stresses associated with faults, folding, diapirism, volcanism and so forth. The orientation of such local stresses may change abruptly over short distances in any area.

Wells drilled in areas subjected to unbalanced stresses often exhibit two types of borehole failures (shear failure and tensile failure) when the rocks they penetrate are replaced by drilling fluid. The rocks can bear both compressive and shear stresses, but the fluid filling the borehole can bear only compressive stress. Consequently, concentration of stresses takes place around the borehole in the form of hoop stress or tangential stress. When the mud weight is too low (i.e., radial stress = mud weight minus pore pressure), the maximum hoop stress becomes much higher than the radial stress. Consequently, a shear failure of rocks exposed to the borehole takes place; this appears as borehole elongation on the orthogonal calipers and as long dark regions on the ABI images that are 180 degrees apart.

Conversely, when the mud weight is too high, the radial stress increases and the hoop stress decreases; consequently, the rock around the borehole comes under tension and fails in tension. The fractures thus created are called drilling-induced fractures, which appear as fractures seen in the ABI images oriented at 180 degrees from each other.

Generally, in vertical to near-vertical wells, the axis of borehole elongation is aligned with the trend of minimum horizontal stress, and the strike of drilling-induced fractures is aligned with the trend of maximum horizontal stress. However, this may not be the case for deviated wells,

particularly those that are not aligned with either of the two horizontal stresses. In such wells, the orientations of borehole breakouts and drilling-induced fractures may not represent the true orientation of the two horizontal stresses, because all three principal stresses (vertical and two horizontal) act obliquely to the borehole.

Both drilling-induced fractures and borehole breakouts are developed in the interval logged in well PG-18 (2,494-1,748 m MD; Figure 2.3.21). A total of 2 drilling-induced fractures were identified, both of the two drilling induced fractures have a strike orientation of N-S (Figure 2.3.22). A total of 13 borehole breakouts were identified, with dip statistics showing a dominant strike of E-W/ENE-WSW (perpendicular to the strike orientation of the drilling-induced fractures) (Figure 2.3.22).

Well PG-18 has a deviation of approximately  $33^{\circ}$  to  $40.6^{\circ}$  from vertical, so (as previously discussed) the strikes of drilling induced fractures and borehole breakouts may not align with the trends of maximum and minimum horizontal stress (respectively).

### 3. FRACTURE ZONATION

The logged interval in well PG-18 can be subdivided into several discrete zones characterized mainly by fracture strike orientation, dip magnitude, and type of lithology (Figure 3.1). These are discussed below and summarized in Table 3.1.

#### *Fracture Zone 1 (2,494-2,357 m MD)*

Cuttings analysis shows this interval to be comprised of fine-medium-grained and medium-coarse-grained basalt lavas, intermediate fine-medium-grained rock, and basaltic breccia. The majority of these lithologies are described as “intensely-altered” (ÍSOR, 2017).

Based on the ABI images, open fractures are well developed in this zone, and are mainly discontinuous open fractures. Continuous open fractures, large continuous open fractures, large discontinuous open fractures, litho-bound open fractures and possible open fractures are also observed. These demonstrate a dominant NNE-SSW strike with WNW and ESE azimuths, and dip magnitudes from nearly horizontal to vertical but are mainly  $>70^\circ$  (Figure 3.1).

Circulation losses occurred within this fracture zone at 2,438 m MD (4 L/s), 2,450 m MD (5.5 L/s), 2,462 m MD (7 L/s), 2,474 m MD (8 L/s), and 2,485 m MD (6 L/s) (Figure 3.2).

The rate of circulation loss increased from 4 L/s to 8 L/s between 2,438 m MD to 2,474 m MD. This could be associated with a high angle ( $79^\circ$ ) NNE-SSW possible open fault at 2,443.4 m MD, a lower angle ( $47^\circ$ ) NW-SE possible open fault at 2,444.8 m MD, a lower angle ( $37^\circ$ ) NNE-SSW possible open fault at 2,453.2 m MD, a high angle ( $83^\circ$ ) NNE-SSW possible open fault at 2,458 m MD, and zone of large continuous and discontinuous open fractures at 2,439-2,478 m MD, which demonstrate dominant strike orientations of N-S, NNE-SSE, and NE-SW with NNW, ESE, E, W, and NW azimuths, and dip magnitudes that vary from approximately  $20^\circ$  to vertical, but are mainly  $>70^\circ$ .

ÍSOR (2017) identified feed zones in the well based on the circulation losses and temperature, classifying them by magnitude on a scale of 1 to 2. These are discussed below.

One feed zone (at 2,420-2,485 m MD) was identified within this fracture zone based on temperature logs and the circulation losses (Figure 3.2). Based on the ABI image, this “size 2” feed zone is possibly associated with a high angle (68°) NNE-SSW possible open fault at 2,420.4 m MD, a high angle (86°) NNE-SSW possible open fault at 2,428 m MD, a high angle (70°) NNW-SSE possible open fault at 2,436.1 m MD, a high angle (87°) N-S possible open fault at 2,436.4 m MD, a high angle (79°) NNE-SSW possible open fault at 2,443.4 m MD, a lower angle (47°) NW-SE possible open fault at 2,444.8 m MD, a lower angle (37°) NNE-SSW possible open fault at 2,453.2 m MD, a high angle (83°) NNE-SSW possible open fault at 2,458 m MD, a high angle (89°) NNE-SSW possible open fault at 2,485.6 m MD, a high angle (71°) possible open fault at 2,485.8 m MD, and some large continuous and discontinuous open fractures at 2,417-2,491 m MD which demonstrate a dominant strike orientation of NNE-SSW, with WNW azimuth, and dip magnitudes that vary from 20° to vertical but are mainly >70° (Figures 3.3 and 3.4). ÍSOR (2017) considers this feed zone to be one of the most permeable the entire logged interval.

### *Fracture Zone 2 (2,357-2,252 m MD)*

Cuttings analysis shows this interval to be comprised of fine-medium-grained and medium-coarse-grained basalt lavas, and glassy basalt. The majority of these lithologies are described by ÍSOR (2017) as “intensely-altered” (Figure 3.1).

Based on the ABI images, open fractures are well developed in this fracture zone, and are mainly discontinuous open fractures, though continuous open fractures, large continuous open fractures, large discontinuous open fractures, litho-bound open fractures and possible open fractures are also observed. The dip statistics of the open fractures in this zone demonstrate high degree of scatter (NE-SW, NNE-SSW, N-S, and ENE-WSW strikes with WNW, NW, E, ESE, ENE, and SSE and NNW azimuths), and dip magnitudes vary from nearly horizontal to vertical, but are mainly >65° (Figure 3.1).

Large continuous and discontinuous open fractures are observed at 2,344-2,357 m MD, 2,338-2,340 m MD, 2,311.5-2,313 m MD, 2,277-2,285 m MD, 2,263-2,267 m MD, 2,253-2,255 m MD, 2,333-2,335 m MD, and 2,326-2,330 m MD, which demonstrate a dominant strike orientation of NNE-SSW with WNW and ESE azimuths, and dip magnitudes that vary from approximately 20° to vertical, but are mainly >75° (Figures 3.5 and 3.6).

Possible open faults were recognized at 2,357 m MD, 2,356.8 m MD, 2,346.8 m MD, 2,340 m MD, 2,339.7 m MD, 2,319.5 m MD, 2,303.4 m MD, and 2,277.1 m MD, which demonstrate a dominant strike orientation of NNE-SSW with ESE and WNW azimuths, and dip magnitudes range from 70° to nearly vertical (85°) (Figures 3.5 and 3.6).

No losses of circulation occurred within this fracture zone, and no feed zones were recognized in this fracture zone.

### *Fracture Zone 3 (2,252-1,956 m MD)*

According to cuttings analysis, this interval is comprised of fine-medium-grained, medium-coarse-grained, to coarse-grained basalt lavas, glassy basalt, and basaltic breccia. These lithologies are described by ÍSOR (2017) as “intensely altered”.

Based on the ABI images, open fractures are well developed in this fracture zone, and are mainly discontinuous open fractures. Continuous open fractures, large continuous open fractures, large discontinuous open fractures, litho-bound open fractures and possible open fractures are also observed. Dip statistics indicate a dominant strike orientation of NNE-SSW, with WNW and ESE azimuths. Dip magnitudes vary from nearly horizontal to vertical but are mainly >70° (Figure 3.1).

Large continuous and discontinuous open fractures are observed at 2,230-2,233 m MD, 2,223-2,224 m MD, 2,220-2,221 m MD, 2,215 m MD, 2,213.7 m MD, 2,205-2,206 m MD, 2,201.8 m MD, 2,197.5-2,199 m MD, 2,193-2,197 m MD, 2,185-2,190 m MD, 2,177-2,179 m MD, 2,170-2,174 m MD, 2,167-2,168 m MD, 2,156.5-2,161 m MD, 2,152-2,154 m MD, 2,139-2,141 m MD,

2,132.5 m MD, 2,128 m MD, 2,116-2,122 m MD, 2,111-2,115 m MD, 2,103 m MD, 2,100 m MD, 2,094-2,096 m MD, 2,087-2,089 m MD, 2,072-2,074 m MD, 2,036-2,043 m MD, 2,033-2,034 m MD, 1,990.5 m MD, and 1,978-1,983 m MD, which demonstrate a dominant strike orientation of NNE-SSW with WNW and ESE azimuths, and dip magnitudes that vary from approximately 15° to vertical, but are mainly >80° (Figures 3.7 and 3.8).

Possible open faults were recognized at 2,156.5 m MD and 2,154 m MD, which demonstrate a dominant strike orientation of NNE-SSW with ESE azimuth, and dip magnitudes range from 67° to 75° (Figures 3.8).

No losses of circulation occurred within this fracture zone, and no feed zones were recognized in this fracture zone.

#### *Fracture Zone 4 (1,956-1,748 m MD)*

Cuttings analysis shows this interval to be comprised of fine-medium-grained, medium-coarse-grained, to coarse-grained basalt lavas, glassy basalt, intermediate coarse-grained rock, and basaltic breccia. These lithologies are described by ÍSOR (2017) as “intensely altered”.

Based on the ABI images, open fractures are well developed in this fracture zone, and are mainly discontinuous open fractures. Continuous open fractures, large continuous open fractures, large discontinuous open fractures, and possible open fractures are also observed. Dip statistics indicate dominant strike orientations of NNE-SSW, N-S, and ENE-WSW with WNW, ESE, W, E, and NW azimuths. Dips magnitudes vary from nearly horizontal to vertical but are mainly >55° (Figure 3.1).

Large continuous and discontinuous open fractures are observed at 1,928-1,937 m MD, 1,898-1,902 m MD, 1,887-1,891.5 m MD, 1,851-1,855 m MD, 1,819.8 m MD, 1,788-1,797.5 m MD, and 1,784-1,787 m MD, which demonstrate dominant strike orientations of N-S, NNE-SSW, and NNW-SSE with ESE, W, WNW, ENE, and WSW azimuths, and dip magnitudes that vary from approximately 20° to vertical, but are mainly >75° (Figure 3.9).

No possible open faults were recognized in this fracture zone.

No losses of circulation occurred within this fracture zone, and no feed zones were recognized in this fracture zone.

Fracture Zone (Interval)	Strike and Azimuth Orientations of Open Fractures	Dip Magnitude of Open Fractures
FZ 1 (2,494-2,357 m MD)	NNE-SSW strike with WNW and ESE azimuths	Nearly horizontal to vertical, but mainly >70°
FZ 2 (2,357-2,252 m MD)	High degree of scatter (NE-SW, NNE-SSW, N-S, and ENE-WSW strikes with WNW, NW, E, ESE, ENE, and SSE and NNW azimuths)	Nearly horizontal to vertical, but mainly >65°
FZ 3 (2,252-1,956 m MD)	NNE-SSW strike with WNW and ESE azimuths	nearly horizontal to vertical, but mainly >70°.
FZ 4 (1,956-1,748 m MD)	NNE-SSW, N-S, and ENE-WSW strikes with WNW, ESE, W, E, and NW azimuths.	nearly horizontal to vertical, but mainly >55°

**Table 3.1: Summary of fracture zonation**

## 4. CONCLUSIONS

- The ABI logging was conducted in the 8.5-inch-diameter (2,494-1,748 m MD) interval of the well, which passes through volcanic formations. The ABI logging was conducted in 3 runs: 1,748-2,313.5 m MD, 2,309-2,393 m MD, and 2,392-2,494 m MD.
- Borehole conditions are good in the interval of 2,494-2,200 m MD, with only a few large and minor washouts, and the image quality in this interval is generally good. Borehole washouts that are evident in the interval of 2,200-1,748 m MD adversely affected ABI Image quality, but fractures and faults could still be identified and analyzed.
- The inclinometry data from the ABI tool were found to be in good agreement with the deviation data from gyro surveys, indicating that the tool was correctly oriented in the borehole and that the calculated dips are correct.
- The GR logs from GR-ABI logging runs 9 and 10 are off-depth relative to GR log from NN-GR logging run 6; simple (bulk / block) depth shifts were performed during the ABI processing for run numbers 9 and 10 using single offset values of 5.8 m and 5.4 m respectively. ABI logging from run 11 is off-depth relative to “processed” and “depth-matched” ABI image from run 10; a bulk / block depth shift was performed during the ABI processing for run 11 using a single offset value of 5.7 m.
- Fractures are well developed over almost the entire logged interval, with a total of 3,850 open fractures identified.
- Discontinuous open fracture is the predominant fracture type. A total of 2,840 such fractures were identified in the interval; they show a dominant strike orientation of NNE-SSW, with WNW and ESE azimuths. Dip magnitudes for this fracture type are highly variable, from horizontal to vertical, but are mainly steeper than 70°.
- The discontinuous open fractures with large low amplitude events are classified as large discontinuous open fracture. A total of 202 large discontinuous open fractures were

identified in the interval, they show a dominant strike orientation of NNE-SSW, with WNW and ESE azimuths. Dip magnitudes for this fracture type are highly variable, from 10° to vertical, but are mainly steeper than 70°.

- Continuous open fractures are rare compared to the discontinuous conductive fractures. A total of 81 such fractures were identified in the logged interval; they show a dominant strike orientation of NNE-SSW with WNW and ESE azimuths, and dip magnitudes from nearly horizontal to vertical but are mainly steeper than 65°.
- The continuous open fractures with large low amplitude events are classified as large continuous open fracture. A total of 117 such fractures were identified in the logged interval; they show a dominant strike orientation of NNE-SSW, with WNW, E, and ESE azimuths, and dip magnitudes vary from 15° to vertical, but are mainly steeper than 65°.
- Only 56 litho-bound open fractures were recognized in the entire logged interval. Dips of litho-bound fractures demonstrate dominant strike orientations of NNE-SSW, NW-SE, and ENE-WSW, with ESE, WNW, NE, and SSE azimuths; and dip magnitudes are highly variable, from nearly horizontal to vertical.
- A total of 554 possible open fractures were recognized in the logged interval. Dips of possible open fractures demonstrate dominant strike orientations of NNW-SSE, NNE-SSW, and NE-SW, with westward (WNW, W, WSW) azimuth, and dip magnitudes that vary from nearly horizontal to vertical, but are mainly >45°.
- The density of discontinuous open fractures varies from 0 to 13 per meter; the density is greatest at 2,406-2,407 m MD. The density of large discontinuous open fractures varies from 0 to 6 per meter, with the highest density occurring at 2,418.5-2,420 m MD and 2,357-2,358 m MD. The density of continuous open fractures varies from 0 to 3 per meter, with the highest densities observed at 1,794.5-1,796.5 m MD, 1,834-1,835 m MD, 1,838-1,839 m MD, and 2,017-2,018 m MD. The density of large continuous open fractures varies from 0 to 8 per meter, and is highest at 2,420-2,421.5 m MD. Litho-

bound open fractures are more localized and are developed mainly in association with intrusion and/or possible intrusive rocks, their density varies from 0 to 6 per meter (with a peak at 2,061-2,062.5 m MD). The fracture density of possible open fracture varies from 0 to 11 per meter, with the highest densities observed at 2,463-2,464.5 m MD.

- A total of 28 possible open faults were identified in the logged interval. They have a dominant strike orientation of NNE-SSW, with ESE and WNW azimuths. Possible-open-fault dip magnitudes are highly variable (from 38° to vertical), but mainly >70°.
- A total of 2 drilling-induced fractures were identified, with a dominant strike orientation of N-S. A total of 13 borehole breakouts were identified, with a dominant strike of E-W/ENE-WSW (perpendicular to the strike orientation of the drilling-induced fractures). Well PG-18 has a deviation of approximately 33° to 40.6° from vertical, so the strikes of drilling induced fractures and borehole breakouts may not align with the trends of maximum and minimum horizontal stress (respectively).
- Four fracture zones were identified, based mainly on fracture strike orientation. They are:
  - Fracture Zone 1 (2,494-2,357 m MD): Comprised mainly of intensely-altered fine-medium-grained and medium-coarse-grained basalt lavas, intermediate fine-medium-grained rock, and basaltic breccia. Open fractures are well developed and are mainly discontinuous, but continuous open fractures, large continuous open fractures, large discontinuous open fractures, litho-bound open fractures and possible open fractures are also observed. Open fractures demonstrate a dominant NNE-SSW strike with WNW and ESE azimuths, and dip magnitudes from nearly horizontal to vertical, but are mainly >70°.

Circulation losses were reported at 6 depths in this interval, with loss rates between 4 L/s and 8 L/s. They may be associated with possible open faults and zones of large continuous and discontinuous open fractures.

One feed zone was identified from temperature logs and the circulation losses. The “size 2” feed zone at 2,420-2,485 m MD may be associated with a high angle (68°) NNE-SSW possible open fault at 2,420.4 m MD, a high angle (86°) NNE-SSW possible open fault at 2,428 m MD, a high angle (70°) NNW-SSE possible open fault at 2,436.1 m MD, a high angle (87°) N-S possible open fault at 2,436.4 m MD, a high angle (79°) NNE-SSW possible open fault at 2,443.4 m MD, a lower angle (47°) NW-SE possible open fault at 2,444.8 m MD, a lower angle (37°) NNE-SSW possible open fault at 2,453.2 m MD, a high angle (83°) NNE-SSW possible open fault at 2,458 m MD, a high angle (89°) NNE-SSW possible open fault at 2,485.6 m MD, a high angle (71°) possible open fault at 2,485.8 m MD, and some large continuous and discontinuous open fractures at 2,417-2,491 m MD which demonstrate a dominant strike orientation of NNE-SSW, with WNW azimuth, and dip magnitudes that vary from 20° to vertical but are mainly >70°. ÍSOR (2017) considers this feed zone to be one of the most permeable the entire logged interval.

- Fracture Zone 2 (2,357-2,252 m MD): Comprised mainly of intensely-altered fine-medium-grained and medium-coarse-grained basalt lavas, and glassy basalt. Open fractures are well developed and are mainly discontinuous, though continuous open fractures, large continuous open fractures, large discontinuous open fractures, litho-bound open fractures and possible open fractures are also observed. The dip statistics of the open fractures demonstrate dominant high degree of scatter (NE-SW, NNE-SSW, N-S, and ENE-WSW strikes with WNW, NW, E, ESE, ENE, and SSE and NNW azimuths), and dip magnitudes from nearly horizontal to vertical, but are mainly >65°.

No losses of circulation occurred within this fracture zone, and no feed zones were recognized in this fracture zone.

- Fracture Zone 3 (2,252-1,956 m MD): Comprised mainly intensely-altered of fine-medium-grained, medium-coarse-grained, to coarse-grained basalt lavas, glassy basalt, and basaltic breccia. Open fractures are well developed and are mainly discontinuous, but continuous open fractures, large continuous open fractures, large discontinuous open fractures, litho-bound open fractures and possible open fractures are also observed. These fractures have a dominant strike orientation of NNE-SSW, with WNW and ESE azimuths, and dip magnitudes vary from nearly horizontal to vertical but are mainly  $>70^\circ$ .

No losses of circulation occurred within this fracture zone, and no feed zones were recognized in this fracture zone.

- Fracture Zone 4 (1,956-1,748 m MD): Comprised mainly of intensely-altered fine-medium-grained, medium-coarse-grained, to coarse-grained basalt lavas, glassy basalt, intermediate coarse-grained rock, and basaltic breccia. Open fractures are well developed, and are mainly discontinuous, but continuous open fractures, large continuous open fractures, large discontinuous open fractures, and possible open fractures are also observed. These open fractures demonstrate dominant strike orientations of NNE-SSW, N-S, and ENE-WSW with WNW, ESE, W, E, and NW azimuths, and dip magnitudes vary from nearly horizontal to vertical but are mainly  $>55^\circ$ .

No losses of circulation occurred within this fracture zone, and no feed zones were recognized in this fracture zone.

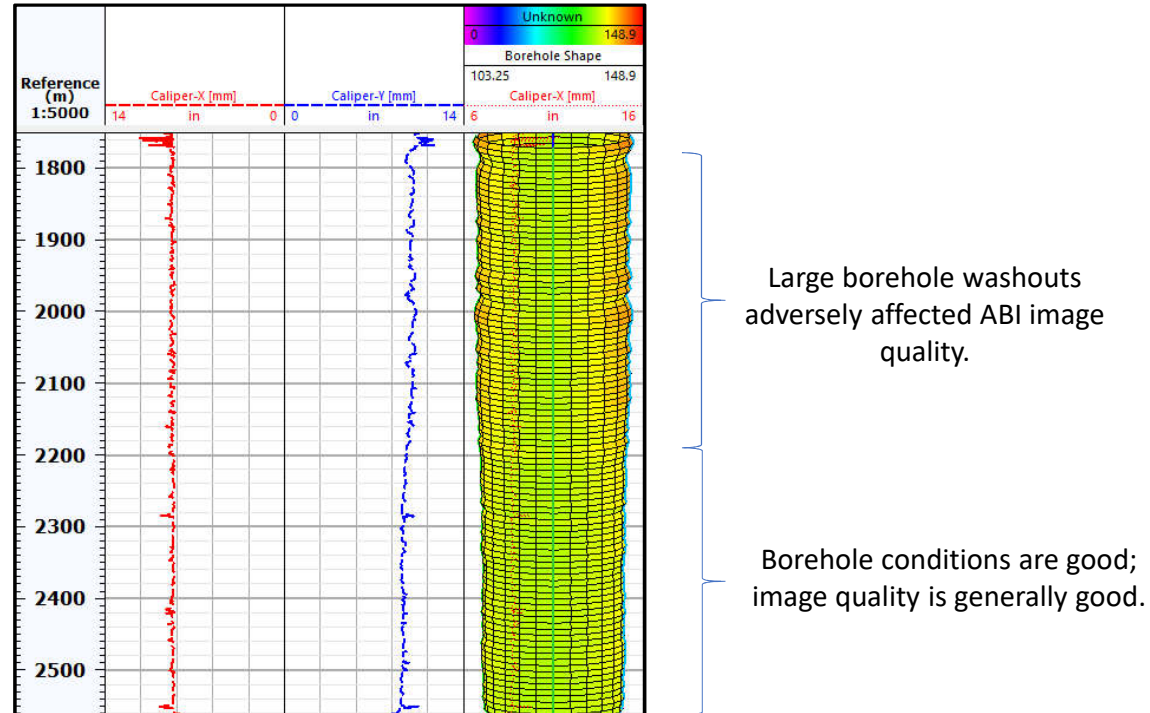
## 5. REFERENCES

- ÍSOR, 2017. Þeistareykir - Well ÞG-18 Phase 3: Drilling for a 7" Perforated Liner down to 2644 m  
Landsvirkjun Report Number: LV-2017-105.
- Massiot, C., Mc. Namara, D., Nicol, A., Townend, J., 2015. Fracture Width and Spacing  
Distribution from Borehole Televiwer Logs and Cores in the Rotokawa Geothermal  
Field, New Zealand.
- Sæmundsson, K., 2007. Jarðfræðin á Þeistareykjum. ÍSOR Report Number: ÍSOR-07270.
- Sæmundsson, K., Sigurgeirsson, M., Grönvold, K., 2011. Þeistareykir Jarðfræðirannsóknir 2011.  
ÍSOR Report Number: ÍSOR-2012/024.

**Figures**

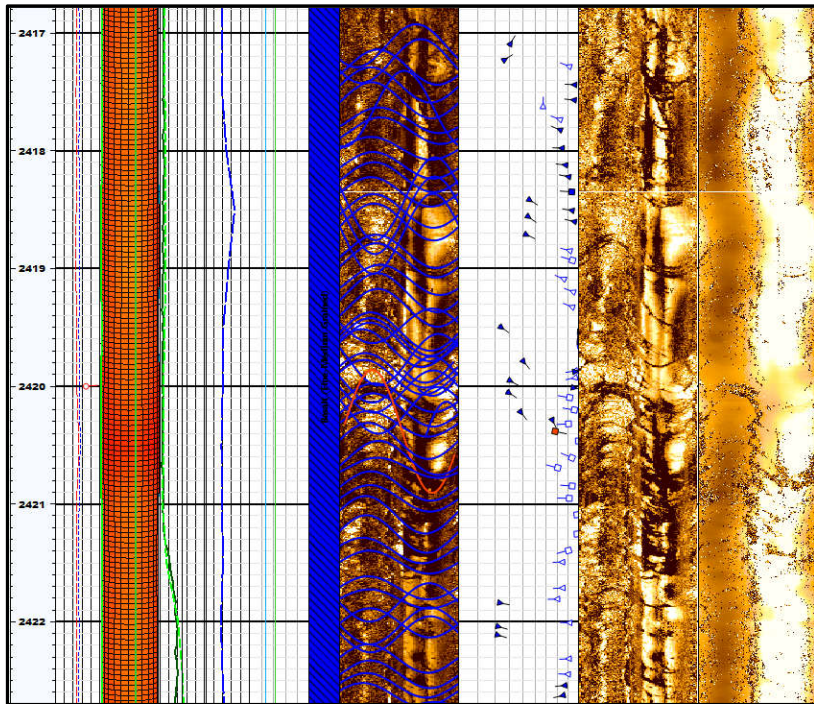
LV-2019-004, 31 January 2019

Figure 2.1.1: ABI Borehole Shape Analysis and Calipers (X and Y) Depth Plot Interval 1,748-2,494 m MD, Well PG-18

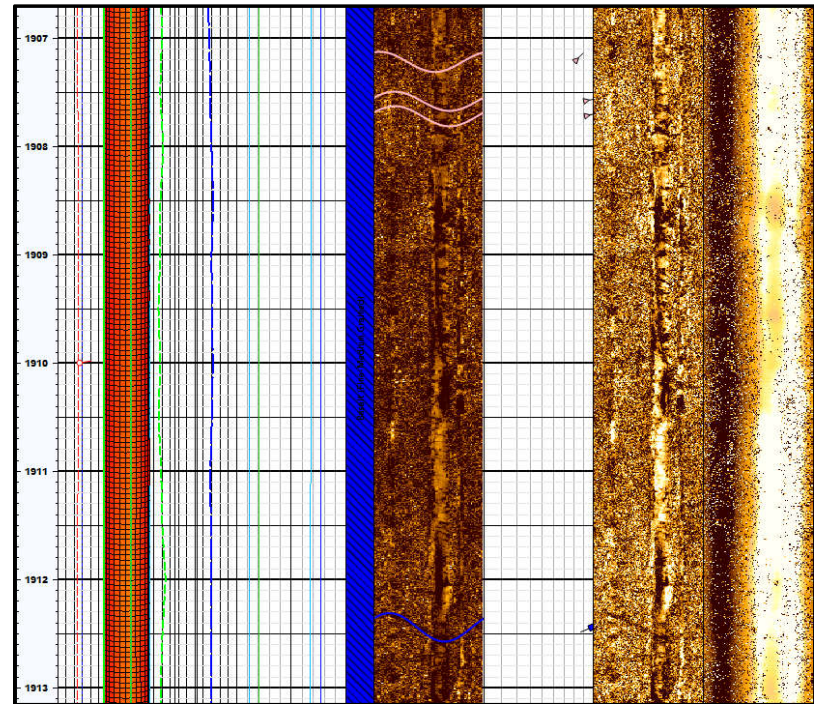


The borehole conditions from 2,494-2,200 m MD are good, with only few large and minor washouts, and the image quality in this interval is generally good. Evident borehole washouts in the interval of 2,200-1,748 m MD adversely affected ABI Image quality, but fractures and faults could still be identified and analyzed.

Figure 2.1.2: Examples of “Good” and “Poor” ABI Image Quality, Well PG-18

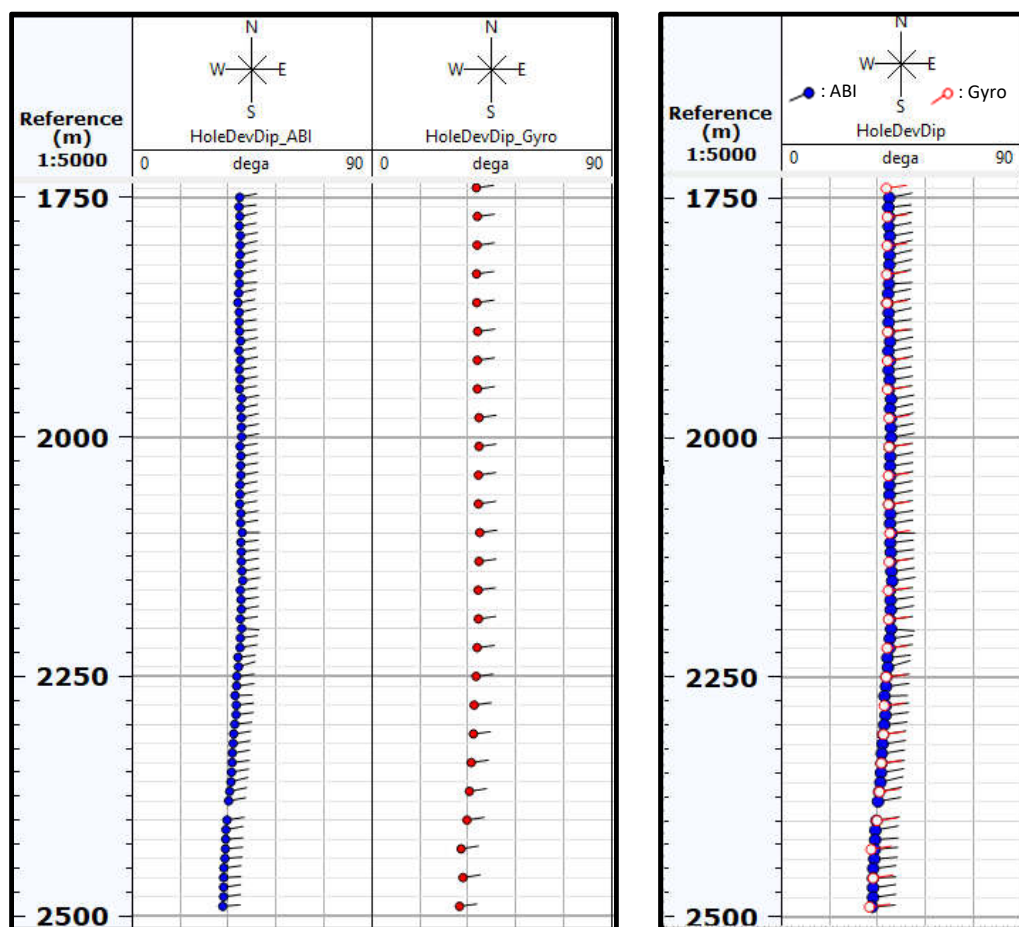


An example of “good” ABI image quality. The image log quality and borehole conditions are generally good in the interval of 2,494-2,200 m MD.



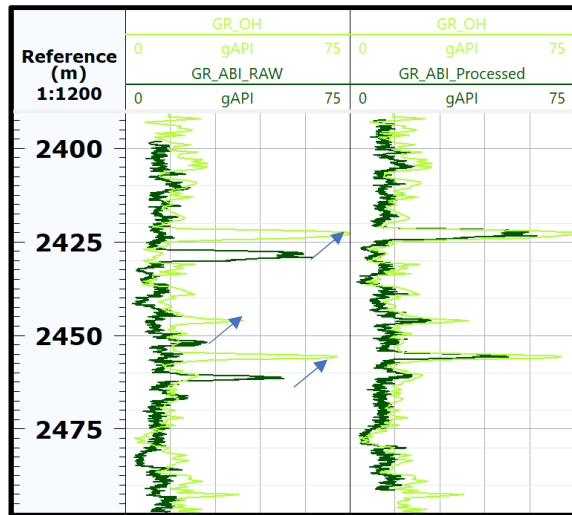
An example of “poor” ABI image quality. Borehole washouts are evident over the interval of 2,200-1,748 m MD and adversely affected ABI image quality.

Figure 2.1.3: Well Deviation and Well Azimuth Data from ABI and Gyro Surveys, Well PG-12

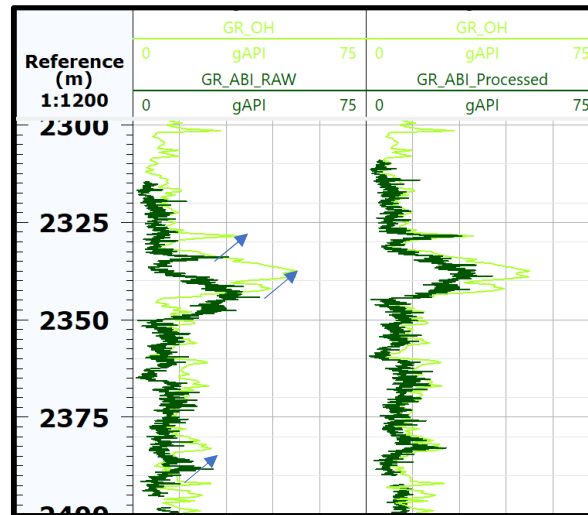


In general, the inclinometry data from the ABI tool agreed with the well deviation and well azimuth data from gyro surveys, indicating that the tool was correctly oriented in the borehole and that the calculated dips are correct.

Figure 2.1.4: Simple (Bulk / Block) Depth Shifts of the ABI Images

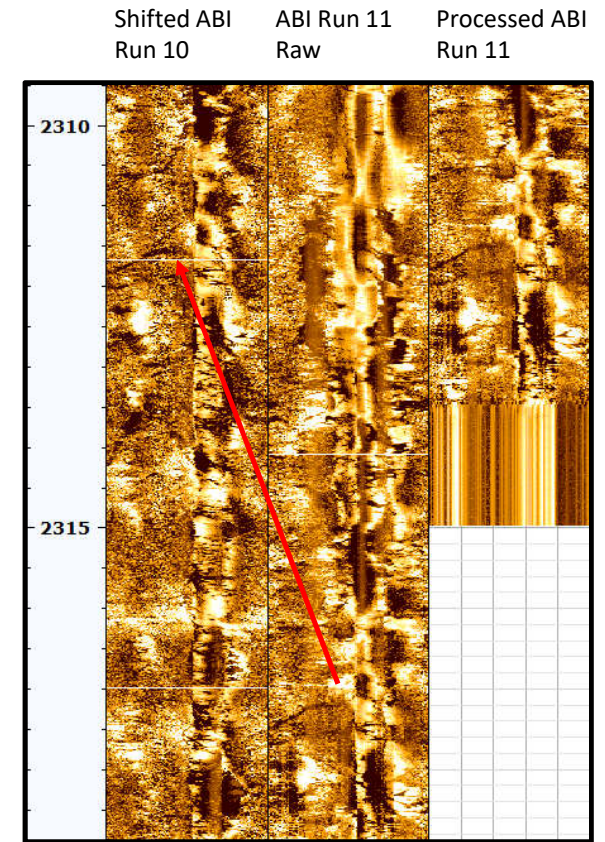


GR-OH vs. GR-ABI Logging run 9; depth shift: 5.8 m



GR-OH vs. GR-ABI Logging run 10; depth shift: 5.4 m

Simple (bulk / block) depth shifts were performed during the ABI processing, in which the ABI logs were shifted/moved up by 5.8 m (for run number 9), 5.4 m (for run number 10), and 5.7 m (for run number 11).



Shifted ABI run 10 vs. shifted ABI run 11; depth shift: 5.7 m

Figure 2.3.1: ABI Image Examples of Discontinuous, Large Discontinuous, Continuous, and Large Continuous Open Fractures

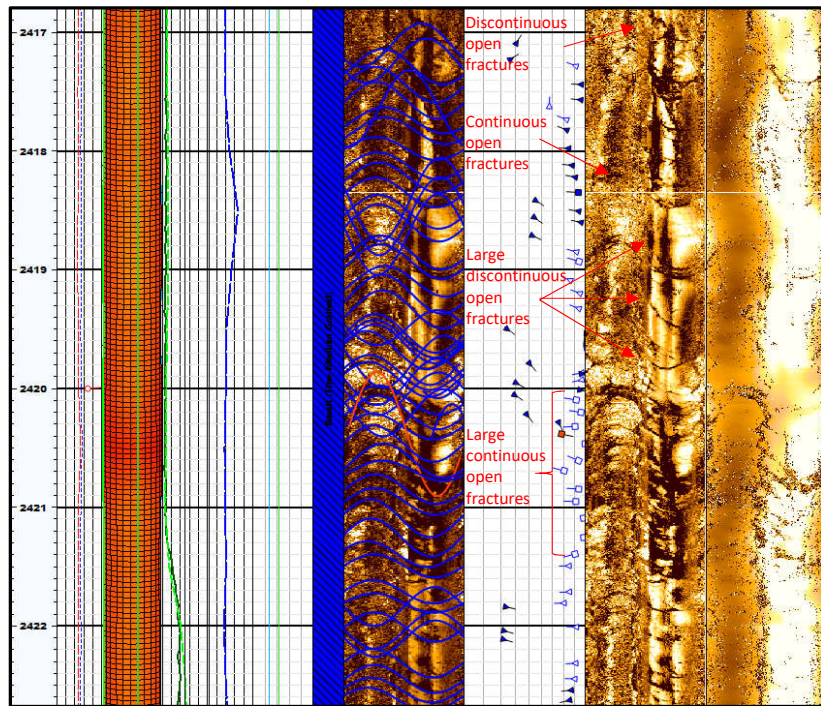


Image example of discontinuous, large discontinuous, continuous, and large continuous open fractures. Discontinuous open fracture is the dominant fracture type in the well PG-18.

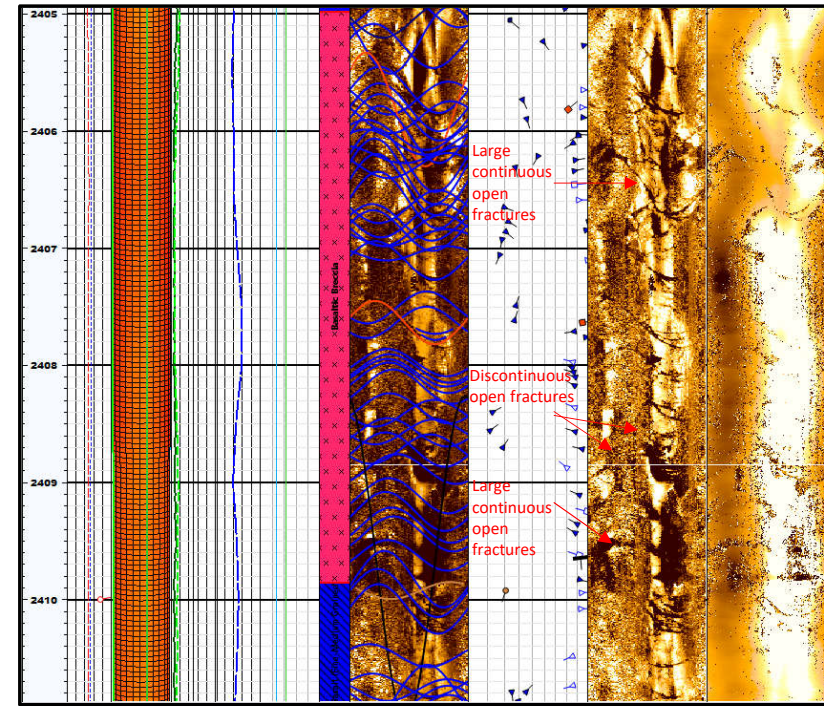


Image example of discontinuous, large discontinuous, and large continuous open fractures.

Figure 2.3.2: ABI Image Examples of Discontinuous, Large Discontinuous, Continuous, and Large Continuous Open Fractures

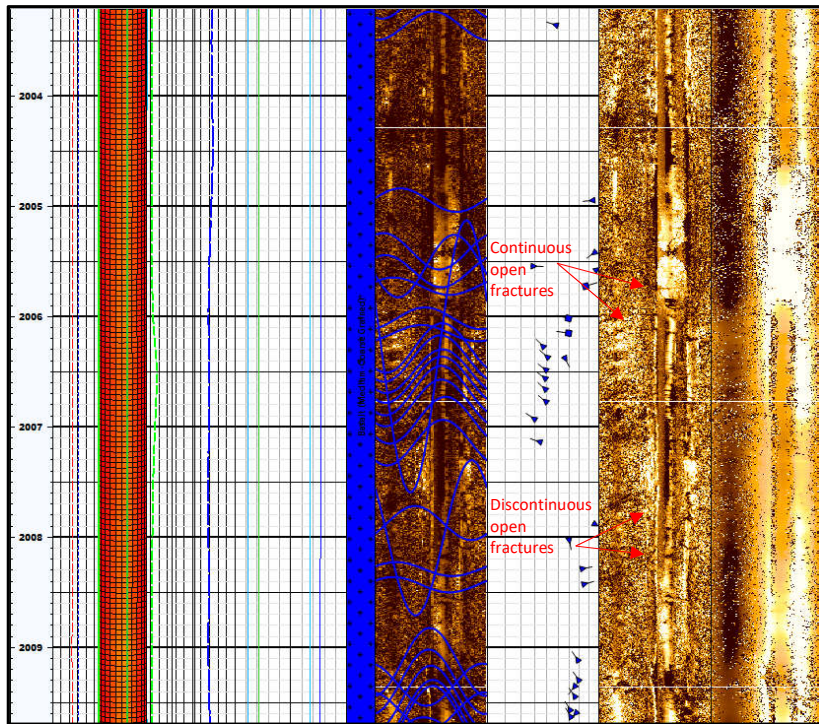


Image example of continuous and discontinuous open fractures.

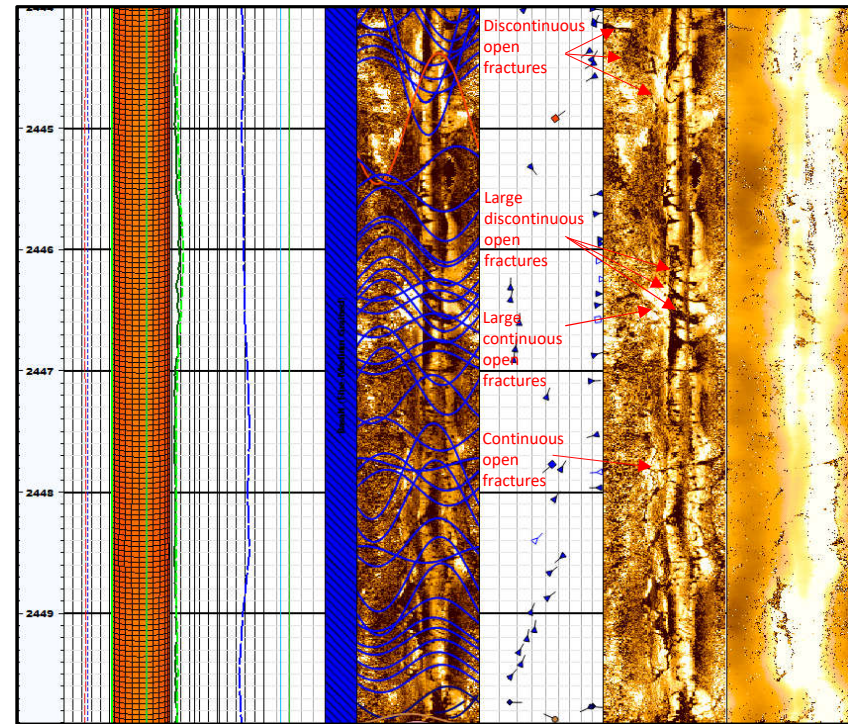
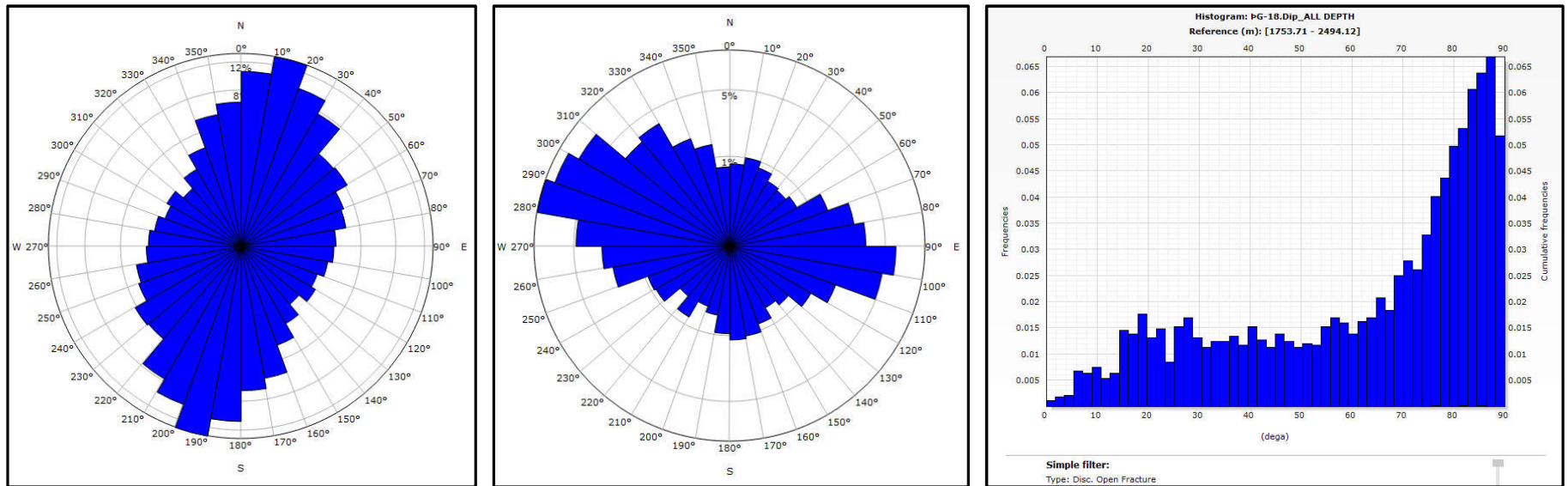


Image example of discontinuous, large discontinuous, continuous, and large continuous open fractures.

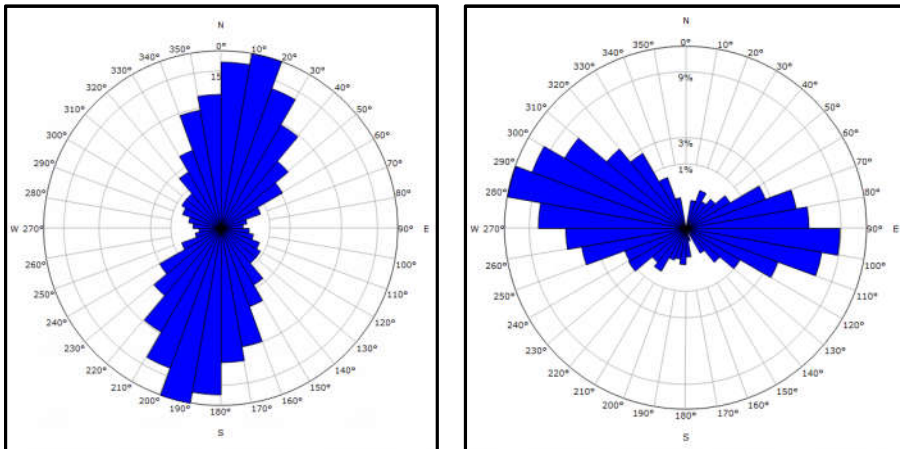
Figure 2.3.3: Dip Statistics of Discontinuous Open Fractures, Interval 2,494-1,748 m MD



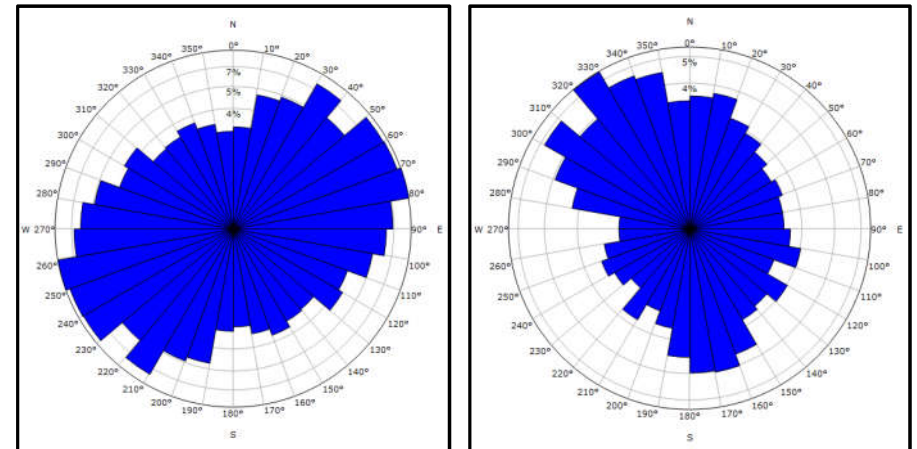
A total of 2,840 discontinuous open fractures were identified over the entire logged interval (2,494-1,748 m MD). Discontinuous-open-fracture dip statistics over the interval demonstrate a dominant strike orientation of NNE-SSW, with WNW and ESE azimuths. Dip magnitudes for this fracture type are highly variable, from horizontal to vertical, but mainly steeper than 70°.

Figure 2.3.4: Dip Statistics of Discontinuous Open Fractures ( $\geq 70^\circ$  Dip Magnitudes and  $< 70^\circ$  Dip Magnitudes), Interval 2,494-1,748 m MD

$\geq 70^\circ$  dip magnitudes

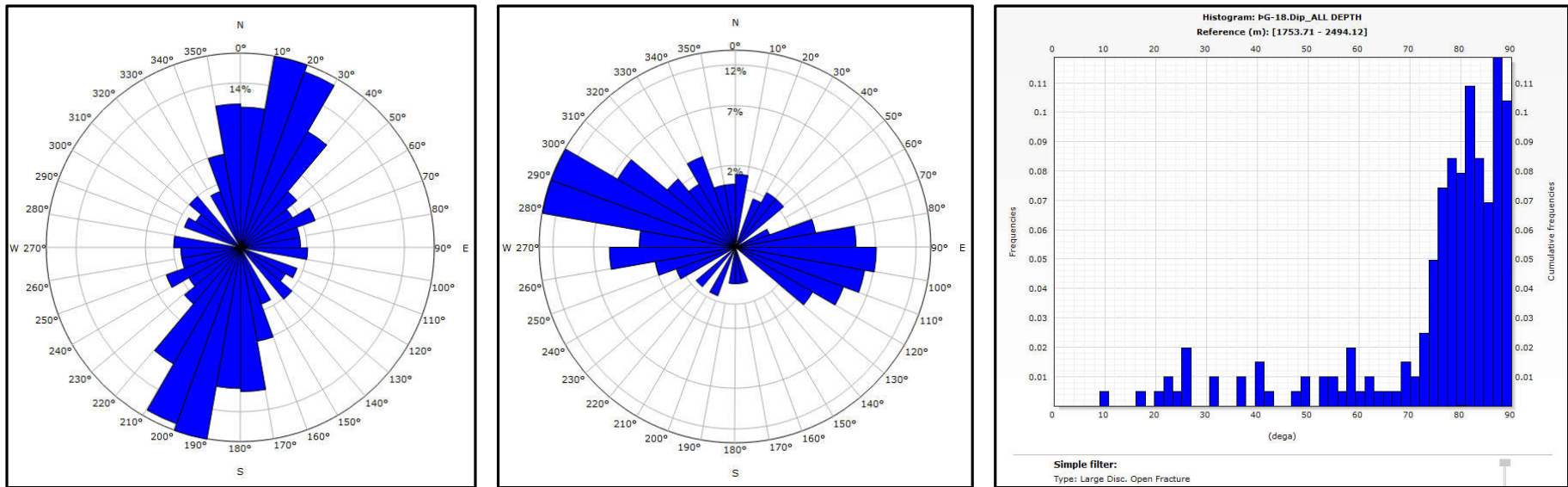


$< 70^\circ$  dip magnitudes



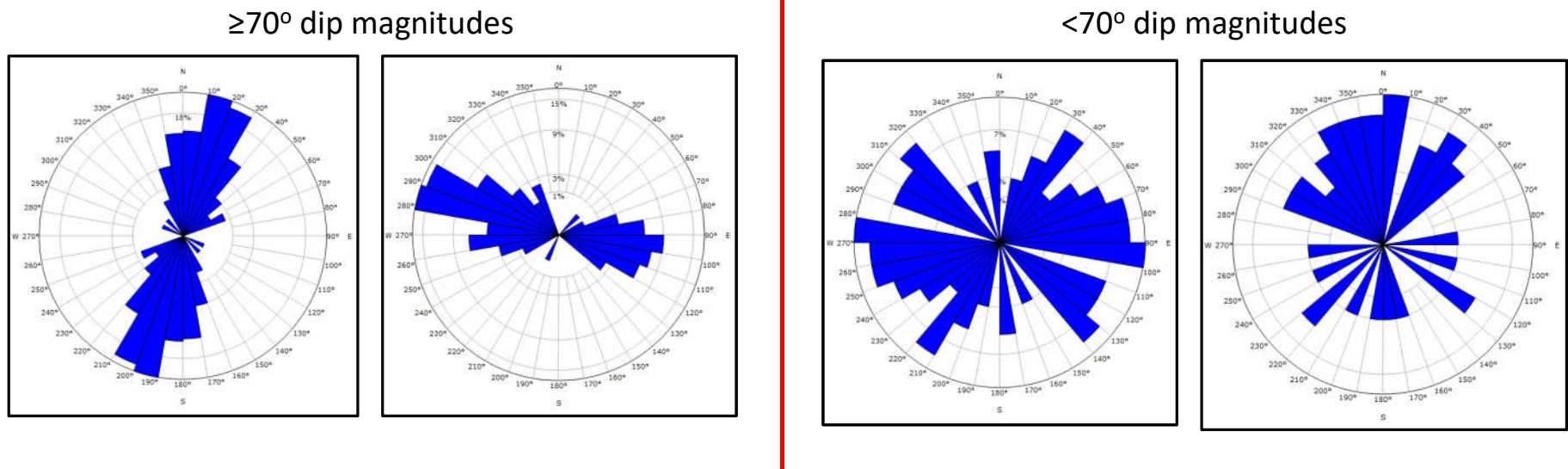
Discontinuous open fractures with dip magnitudes  $\geq 70^\circ$  show a dominant strike orientation of NNE-SSW, with WNW and ESE azimuths. Discontinuous open fractures with dip magnitudes  $< 70^\circ$  show a dominant strike orientation of ENE-WSW, with NNW and SSE azimuths.

Figure 2.3.5: Dip Statistics of Large Discontinuous Open Fractures, Interval 2,494-1,748 m MD



A total of 202 large discontinuous open fractures were identified over the entire logged interval (2,494-1,748 m MD). Large-discontinuous-open-fracture dip statistics over the interval demonstrate a dominant strike orientation of NNE-SSW, with WNW and ESE azimuths. Dip magnitudes for this fracture type are highly variable, from 10° to vertical, but mainly steeper than 70°.

Figure 2.3.6: Dip Statistics of Large Discontinuous Open Fractures ( $\geq 70^\circ$  Dip Magnitudes and  $< 70^\circ$  Dip Magnitudes), Interval 2,494-1,748 m MD

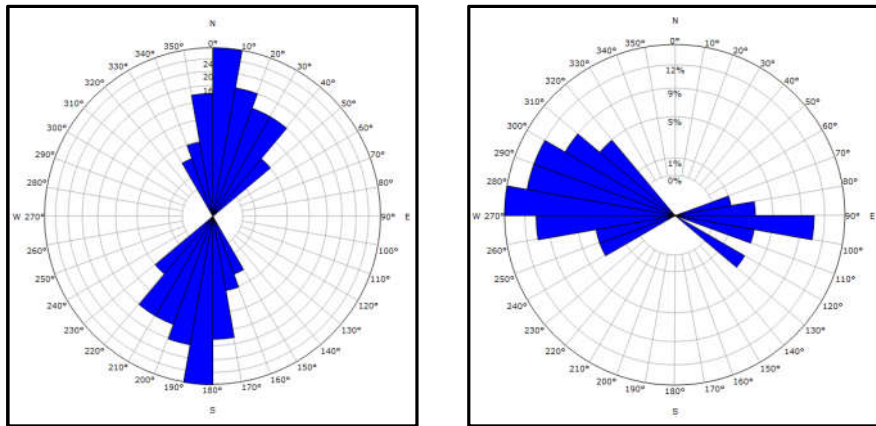


Large discontinuous open fractures with dip magnitudes  $\geq 70^\circ$  show a dominant strike orientation of NNE-SSW, with WNW, ESE azimuths. Large discontinuous open fractures with dip magnitudes  $< 70^\circ$  show a high degree of scatter but E-W strike with Northerly azimuth predominate.

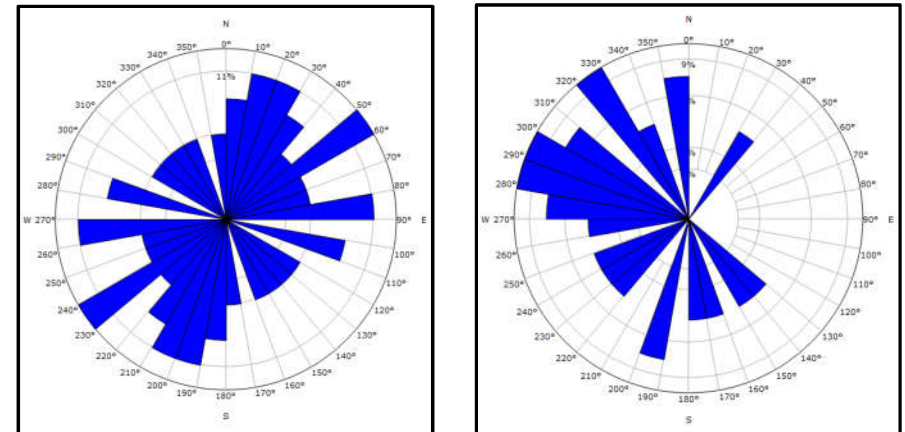


Figure 2.3.8: Dip Statistics of Continuous Open Fractures ( $\geq 65^\circ$  Dip Magnitudes and  $< 65^\circ$  Dip Magnitudes), Interval 2,494-1,748 m MD

$\geq 65^\circ$  dip magnitudes

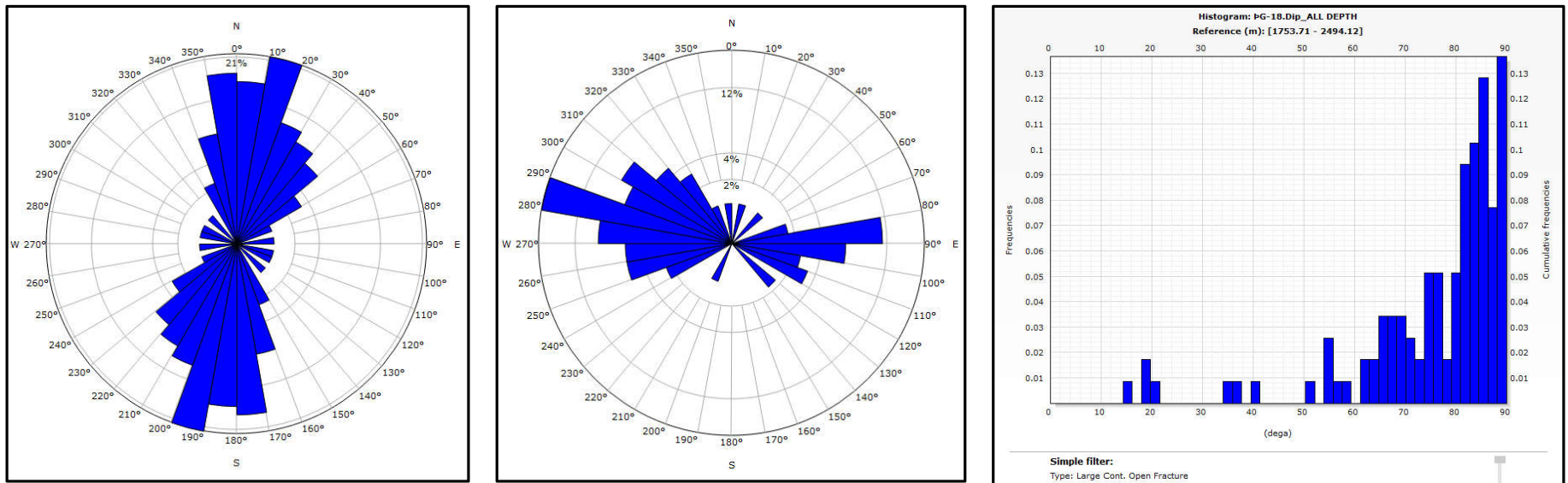


$< 65^\circ$  dip magnitudes



Continuous open fractures with dip magnitudes  $\geq 65^\circ$  show dominant strike orientation of NNE-SSW with WNW and ESE dips. Continuous open fractures with dip magnitudes of  $< 65^\circ$  indicate dominant strike orientations of NNE-SSW, NE-SW, and E-W with WNW, NW, SW, SSW, SSE, and SW azimuths.

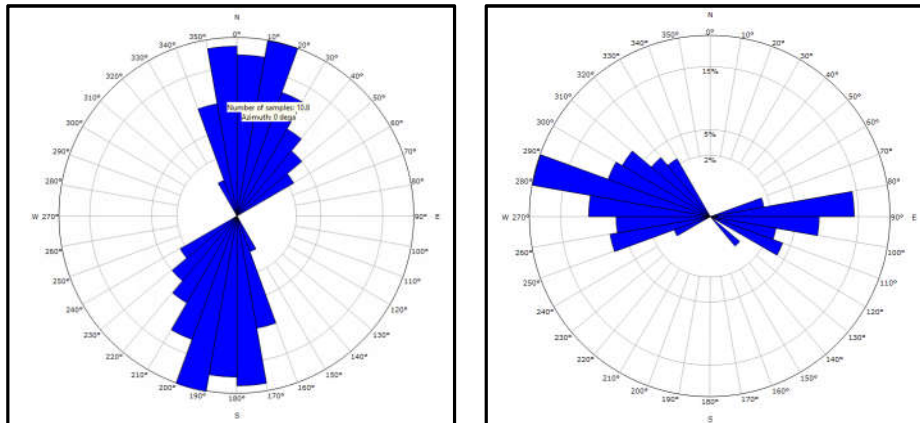
Figure 2.3.9: Dip Statistics of Large Continuous Open Fractures, Interval 2,494-1,748 m MD



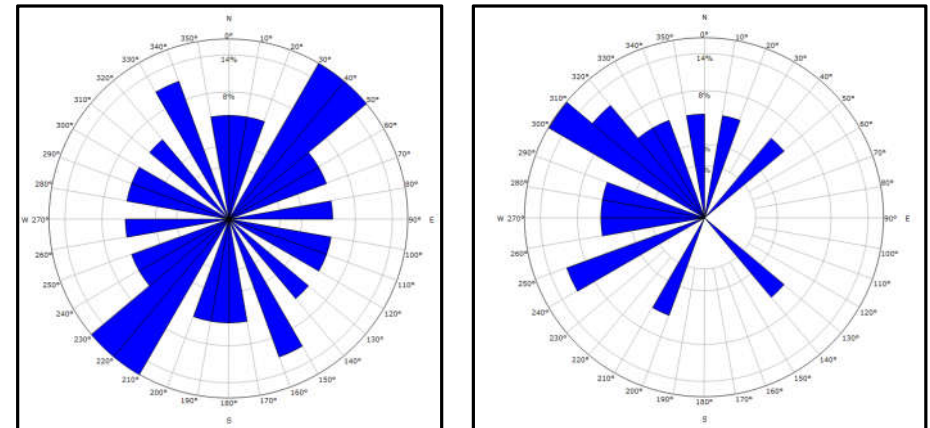
A total of 117 large continuous open fractures were identified over the entire logged interval (2,494-1,748 m MD). Large-continuous-open-fracture dip statistics over the interval demonstrate a dominant strike orientation of NNE-SSW, with WNW, E, and ESE azimuths. Dip magnitudes for this fracture type are highly variable, from 15° to vertical, but mainly steeper than 65°

Figure 2.3.10: Dip Statistics of Large Continuous Open Fractures ( $\geq 65^\circ$  Dip Magnitudes and  $< 65^\circ$  Dip Magnitudes), Interval 2,494-1,748 m MD

$\geq 65^\circ$  dip magnitudes



$< 65^\circ$  dip magnitudes



Large continuous open fractures with dip magnitudes  $\geq 65^\circ$  show a dominant strike orientation of NNE-SSW, with WNW, E, and ESE azimuths (Figure 2.3.10). Discontinuous open fractures with dip magnitudes  $< 65^\circ$  show a high degree of scatter but a NE-SW strike with NW azimuth predominates.

Figure 2.3.11: ABI Image Examples of Litho-bound Open Fractures

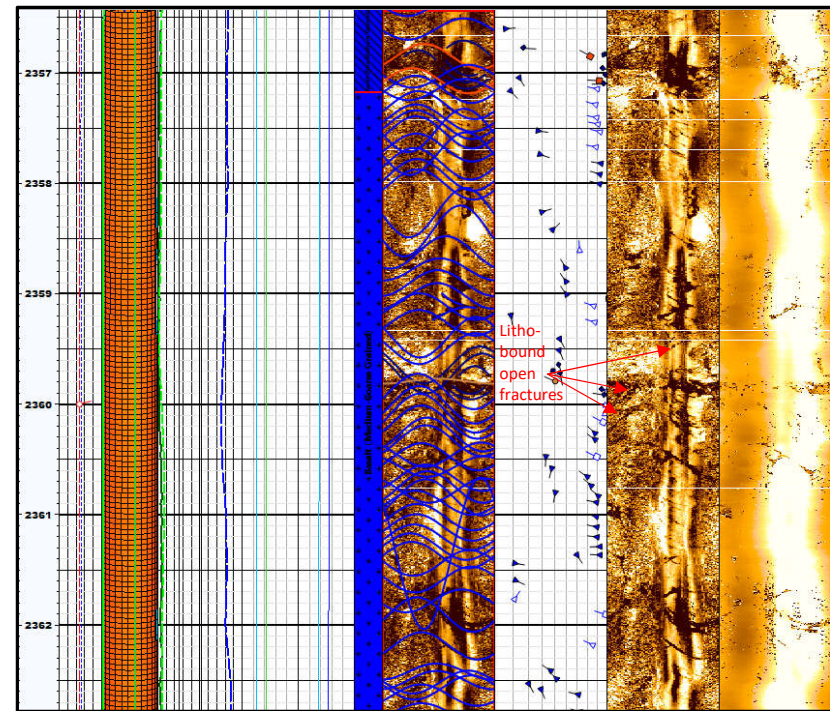
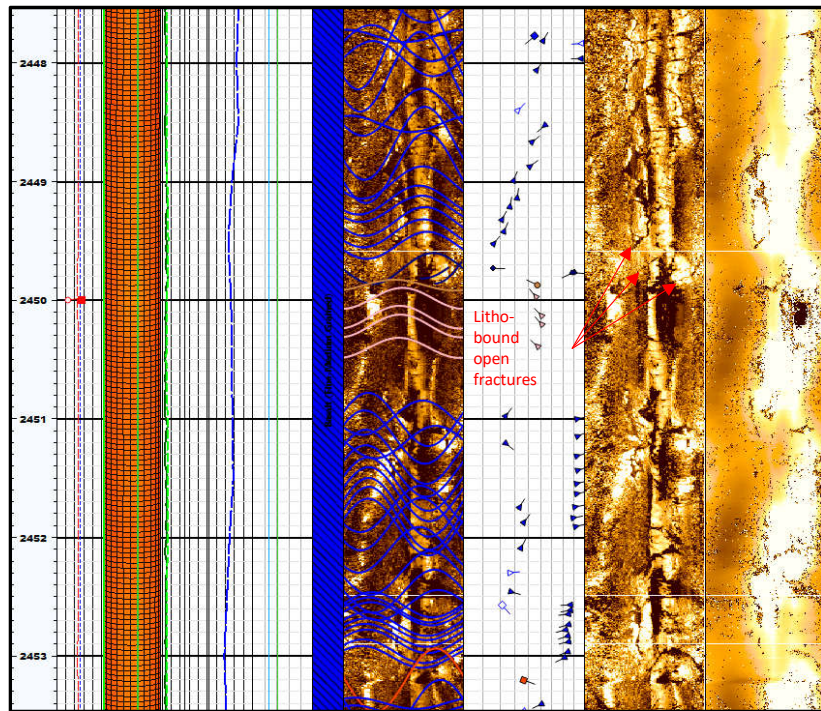
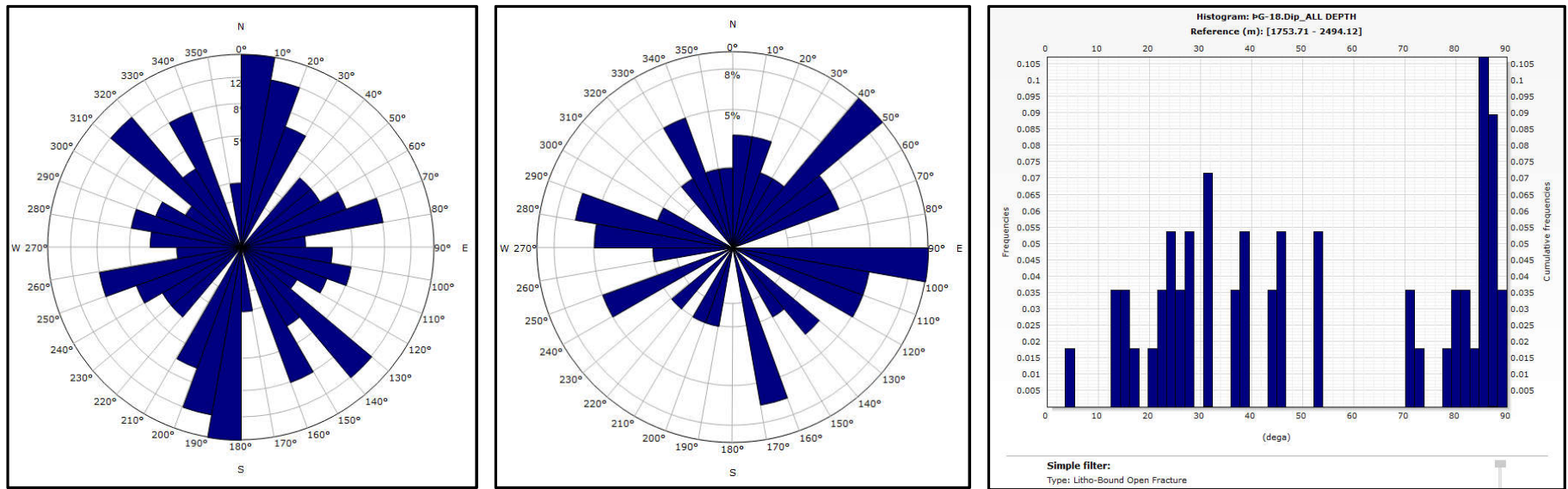


Image example of litho-bound open fractures. This fracture type has a low amplitude and is compartmentalized within individual lithologic units bounded and/or terminated by lithologic boundaries. The development of this fracture type is mainly associated with intrusion and/or possible intrusive rocks.

Image example of litho-bound open fractures.

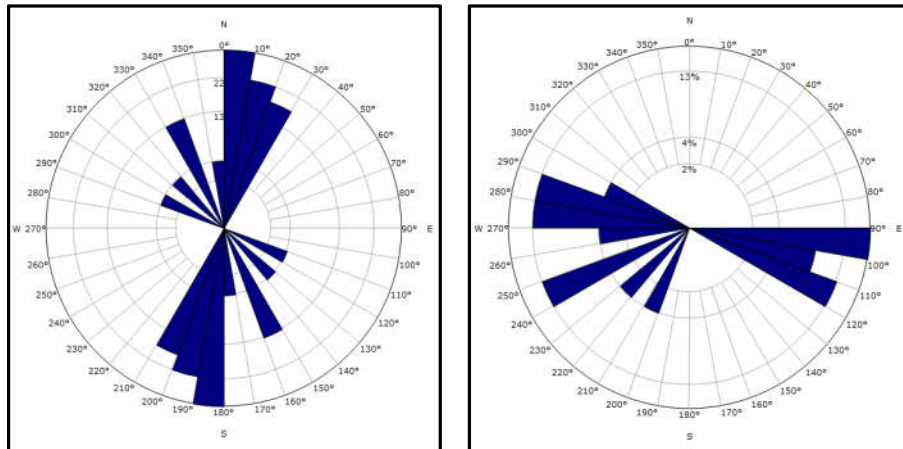
Figure 2.3.12: Dip Statistics of Litho-bound Open Fractures, Interval 2,494-1,748 m MD



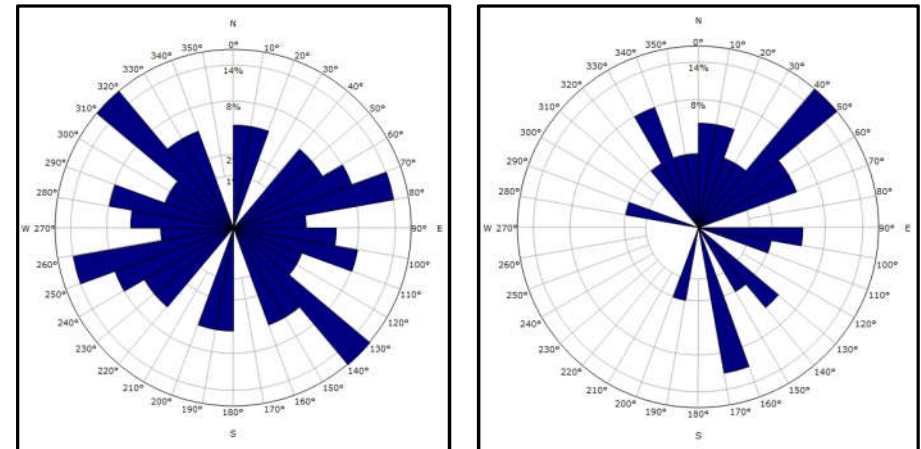
Only 56 litho-bound open fractures were recognized in the entire logged interval (2,494-1,748 m MD). Litho-bound-open-fracture dip statistics over the interval demonstrate dominant strike orientations of NNE-SSW, NW-SE, and ENE-WSW, with ESE, WNW, NE, and SSE azimuths. Dip magnitudes for this fracture type are highly variable, from nearly horizontal to vertical.

Figure 2.3.13: Dip Statistics of Litho-bound Open Fractures ( $\geq 70^\circ$  Dip Magnitudes and  $< 70^\circ$  Dip Magnitudes), Interval 2,494-1,748 m MD

$\geq 70^\circ$  dip magnitudes



$< 70^\circ$  dip magnitudes



Litho-bound open fractures with dip magnitudes  $\geq 70^\circ$  show a dominant strike orientation of NNE-SSW, with ESE and WNW azimuths. Discontinuous open fractures with dip magnitudes  $< 70^\circ$  show a high degree of scatter but NW-SE and ENE-WSW strikes with NE and SSE azimuths predominate.

Figure 2.3.14: ABI Image Examples of Possible Open Fractures

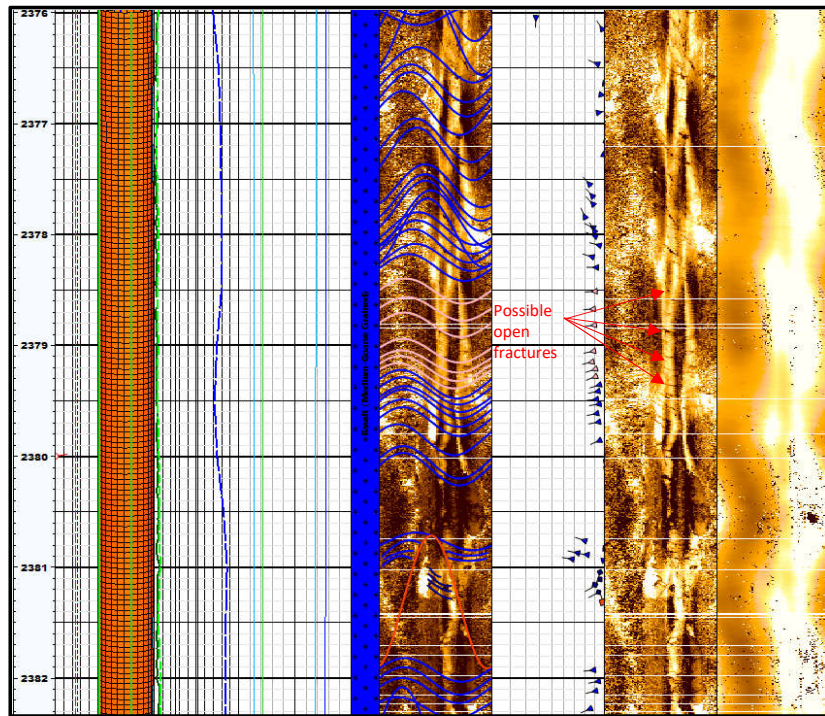


Image example of possible open fractures. This fracture type has a low amplitude and is discontinuous across the borehole diameter, due to poor image quality caused by bad hole condition or logging artifacts

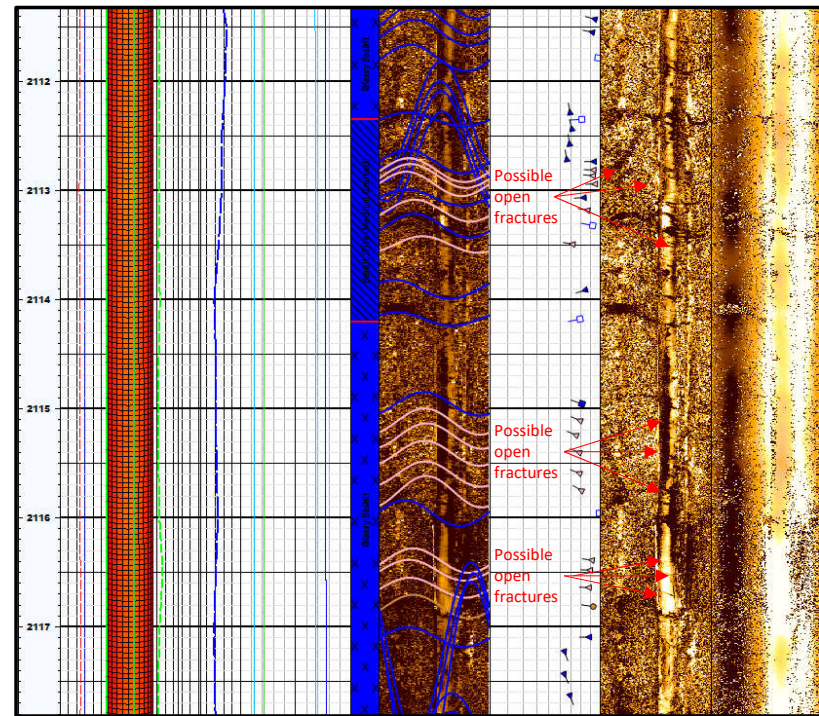
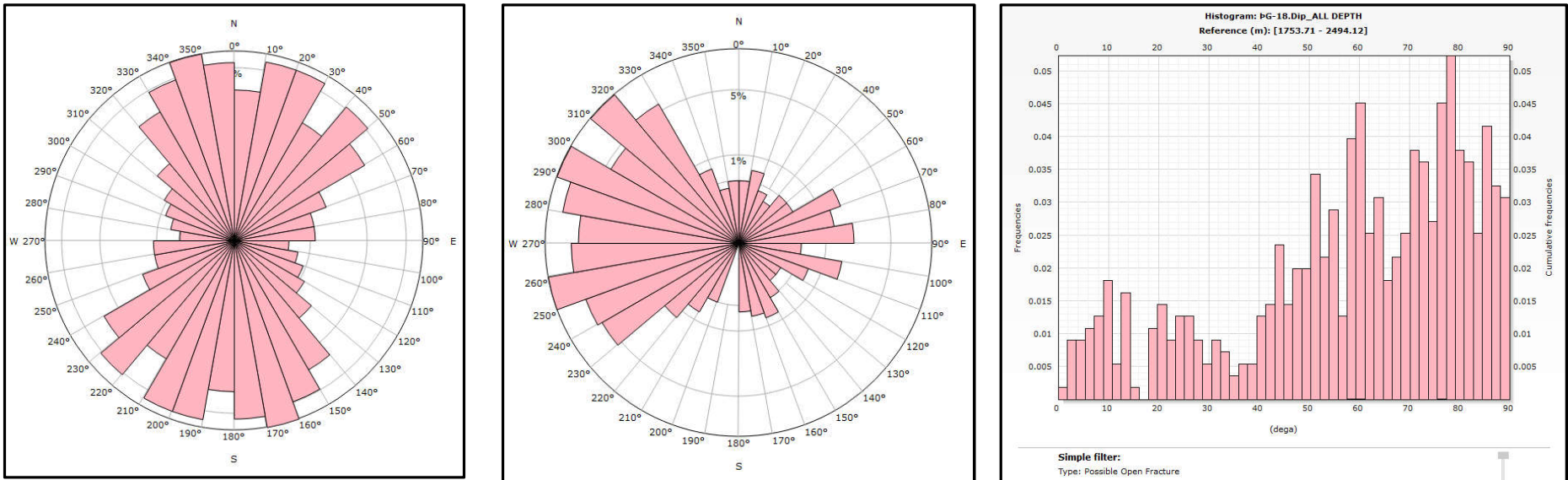


Image example of possible open fractures.

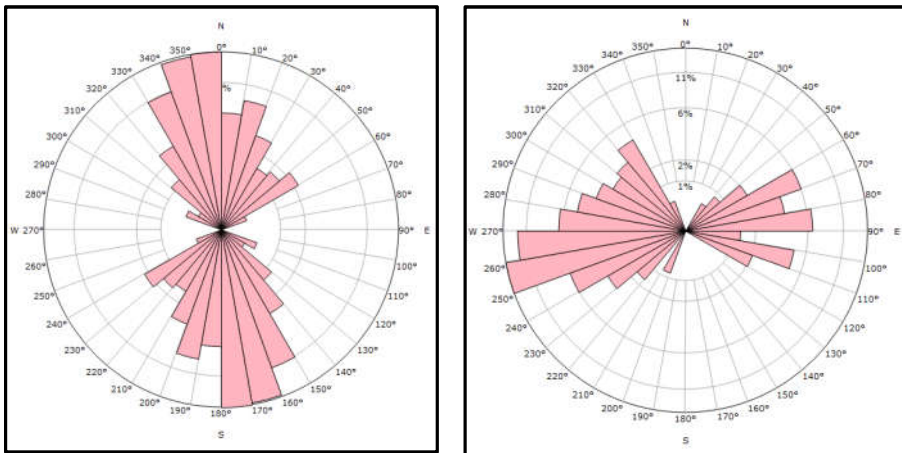
Figure 2.3.15: Dip Statistics of Possible Open Fractures, Interval 2,494-1,748 m MD



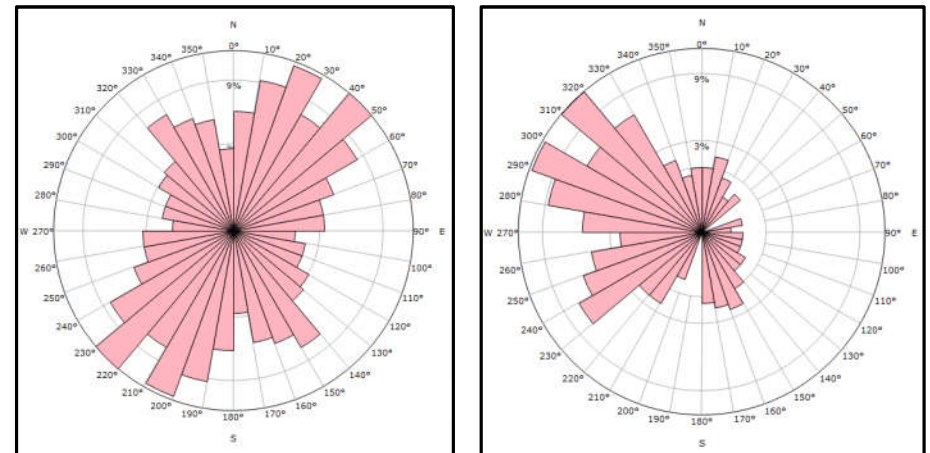
A total of 554 possible open fractures were recognized over the entire logged interval (2,494-1,748 m MD). Possible-open-fracture dip statistics in the interval demonstrate dominant strike orientations of NNW-SSE, NNE-SSW, and NE-SW, with westward (WNW, W, WSW) azimuth, and dip magnitudes that vary from nearly horizontal to vertical, but mainly  $>45^\circ$ .

Figure 2.3.16: Dip Statistics of Possible Open Fractures ( $\geq 70^\circ$  Dip Magnitudes and  $< 70^\circ$  Dip Magnitudes), Interval 2,494-1,748 m MD

$\geq 70^\circ$  dip magnitudes



$< 70^\circ$  dip magnitudes



Possible open fractures with dip magnitudes of  $\geq 70^\circ$  show dominant strike orientations of NNW-SSE, with WSW and ENE azimuths. Possible open fractures with dip magnitudes of  $< 70^\circ$  demonstrate dominant strike orientations of NNE-SSW and NE-SW, with WNW and NW azimuths.

Figure 2.3.17: ABI Image Examples of Possible Open Fault

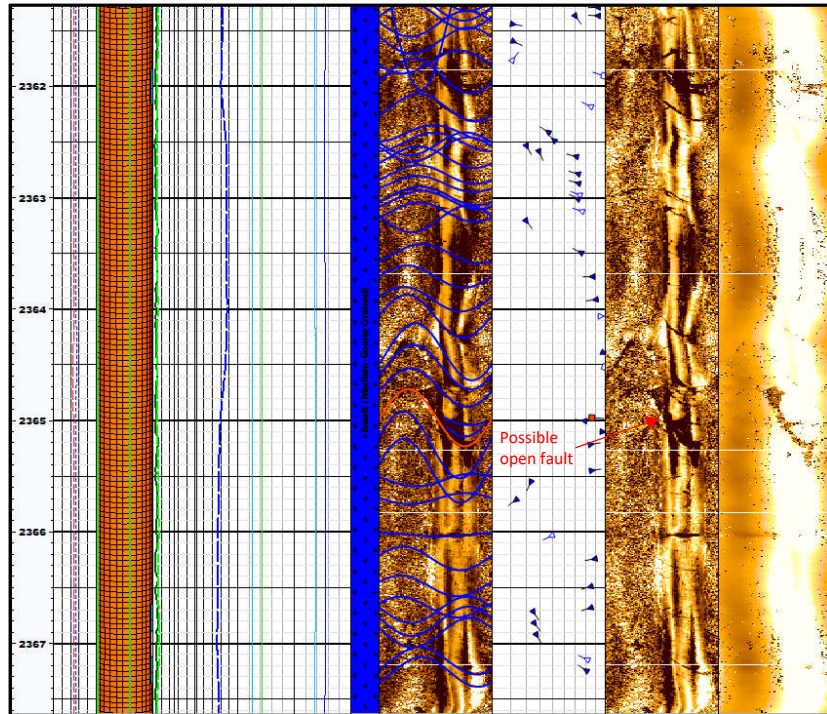


Image example of possible open fault at 2,365 m MD. Continuous, discontinuous, large discontinuous, and large continuous open fractures are well developed near the fault plane. Abrupt terminations of fractures are also observed on the fault's plane.

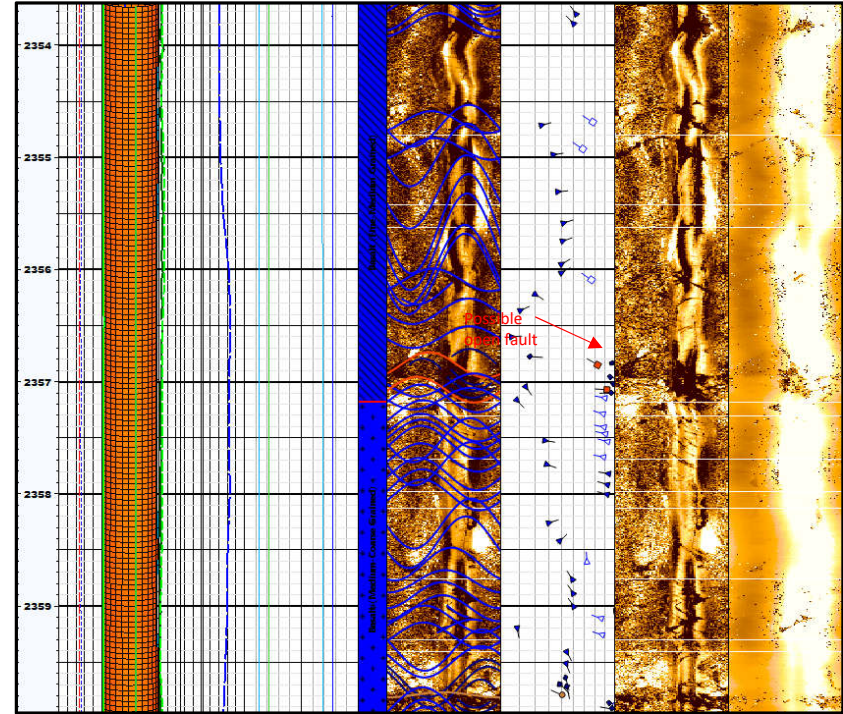


Image example of possible open faults at 2,356.9 m MD and 2,357.1 m MD. Continuous, discontinuous, large discontinuous, and large continuous open fractures are well developed near the fault plane. Large low-amplitude events and abrupt terminations of fractures are also observed on the fault's plane.

Figure 2.3.18: ABI Image Examples of Possible Open Fault

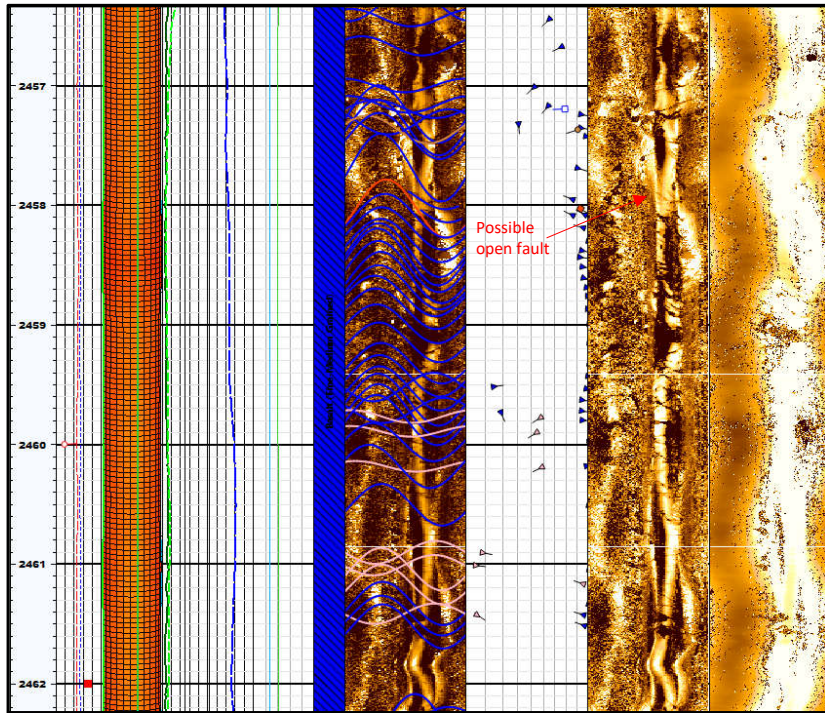


Image example of possible open fault at 2,458 m MD. Continuous, discontinuous, and large continuous open fractures are well developed near the fault plane. Sharp facies change and abrupt terminations of fractures are also observed on the fault's plane.

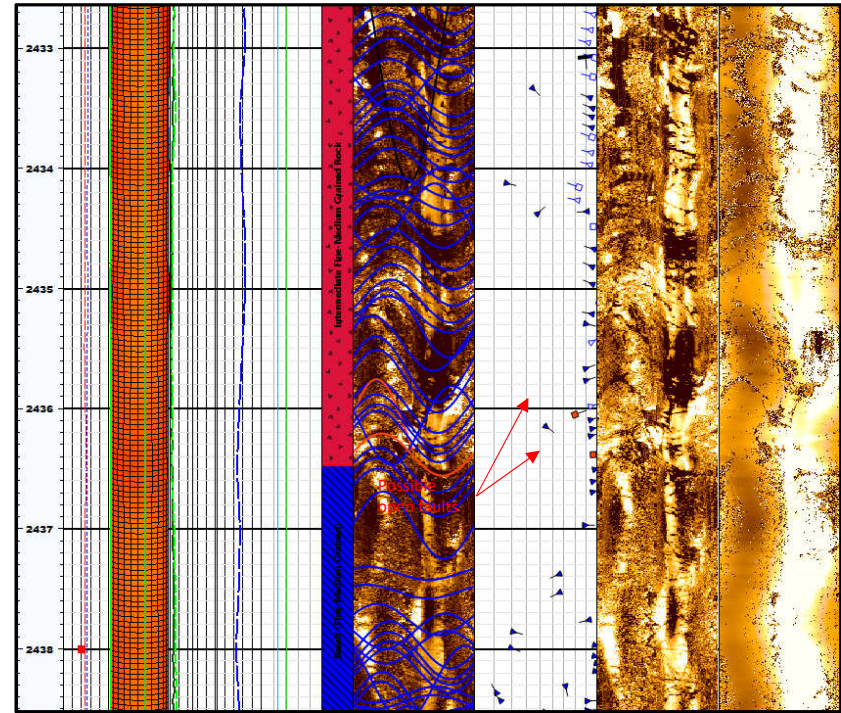
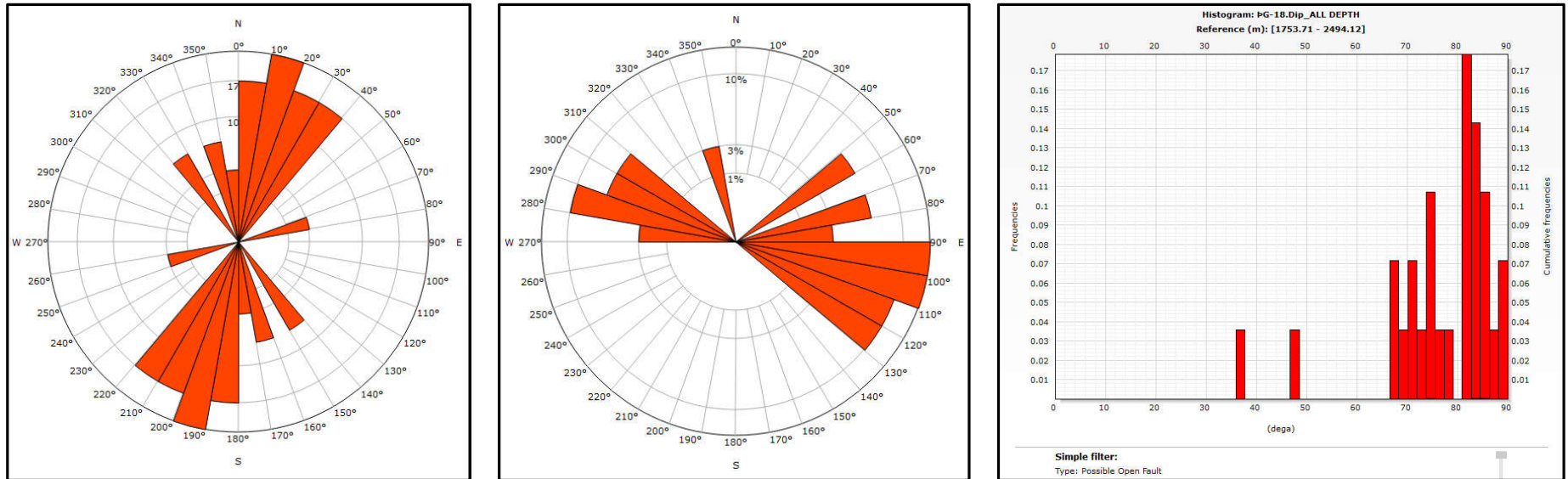


Image example of possible open faults at 2,436 m MD and 2,436.4 m MD. Continuous, discontinuous, large discontinuous, and large continuous open fractures are well developed near the fault plane. Abrupt terminations of fractures and sharp facies change are also observed on the fault's plane.

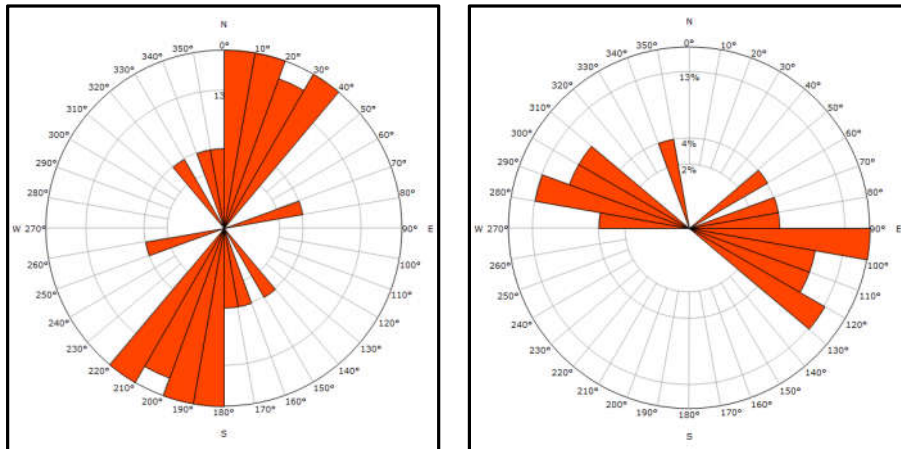
Figure 2.3.19: Dip Statistics of Possible Open Faults, Interval 2,494-1,748 m MD



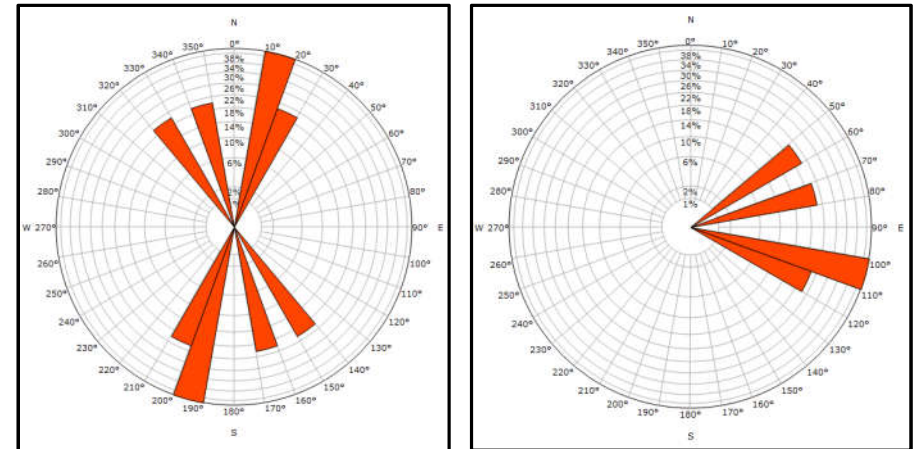
A total of 28 possible open faults were identified in the logged interval. Possible-open-fault dip statistics demonstrate a dominant strike orientation of NNE-SSW, with ESE and WNW azimuths. Dip magnitudes vary from 38° to vertical, but are mainly >70°.

Figure 2.3.20: Dip Statistics of Possible Open Faults ( $\geq 70^\circ$  Dip Magnitudes and  $< 70^\circ$  Dip Magnitudes), Interval 2,494-1,748 m MD

$\geq 70^\circ$  dip magnitudes



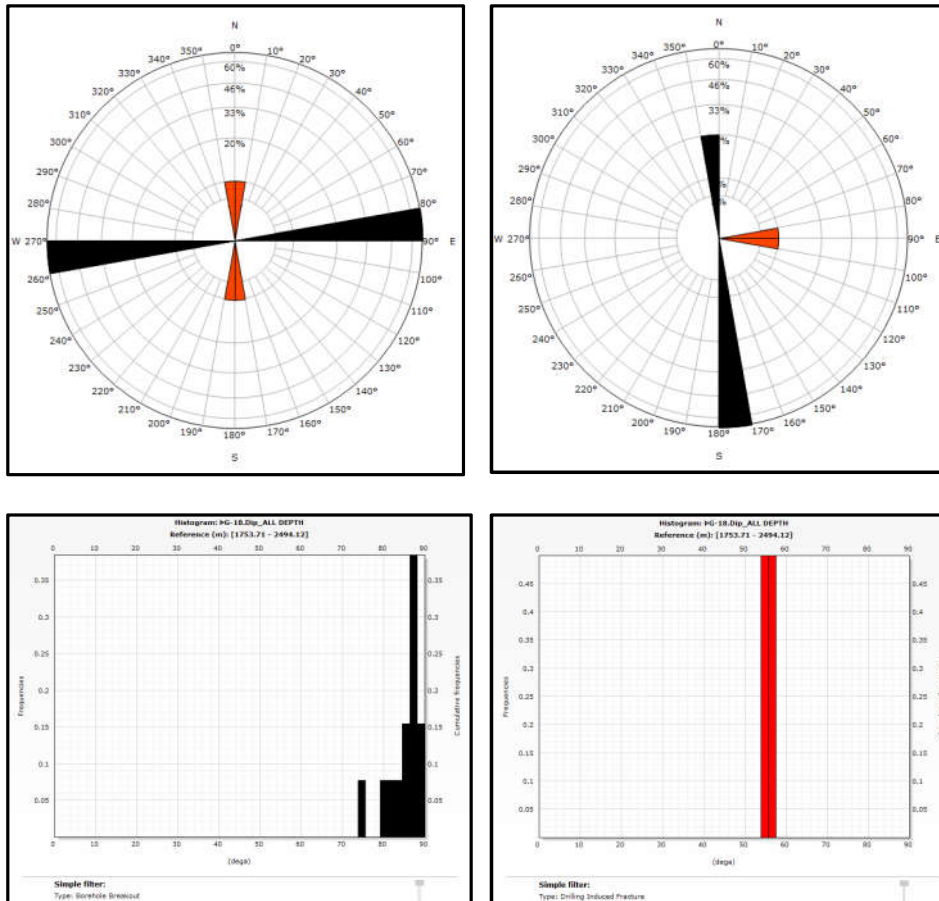
$< 70^\circ$  dip magnitudes



Possible open faults with dip magnitudes  $\geq 70^\circ$  show dominant strike orientations of NNE-SSW with ESE and WNW azimuth; those with dip magnitudes  $< 70^\circ$  have dominant strike orientations of NNE-SSW and NNW-SSE with ESE and ENE azimuths.



Figure 2.3.22: Dip Statistics of Borehole Breakouts and Drilling Induced Fractures, Interval 2,494-1,748 m MD



A total of 2 drilling-induced fractures were identified, both of the two drilling induced fractures have a strike orientation of N-S. A total of 13 borehole breakouts were identified, with dip statistics showing a dominant strike of E-W/ENE-WSW (perpendicular to the strike orientation of the drilling-induced fractures)

Figure 2.3.23: ABI Image Examples of Lithologic Boundary

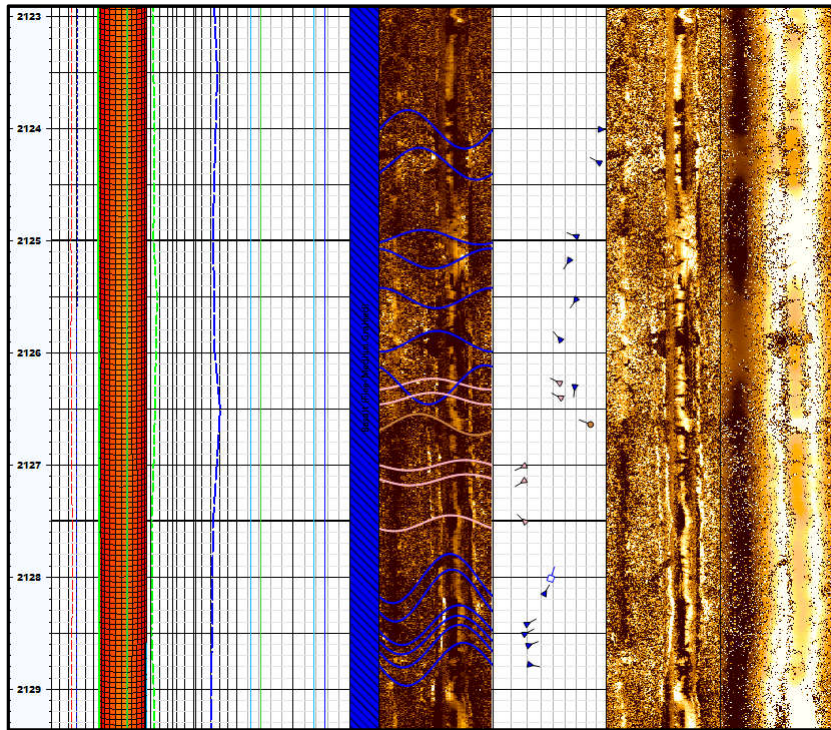


Image example of lithologic boundary.

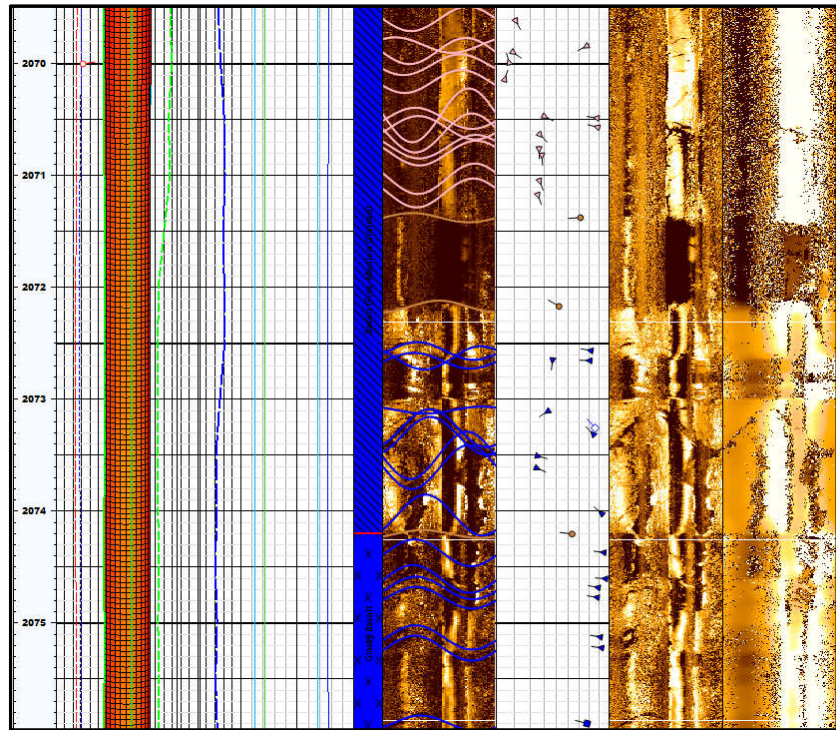
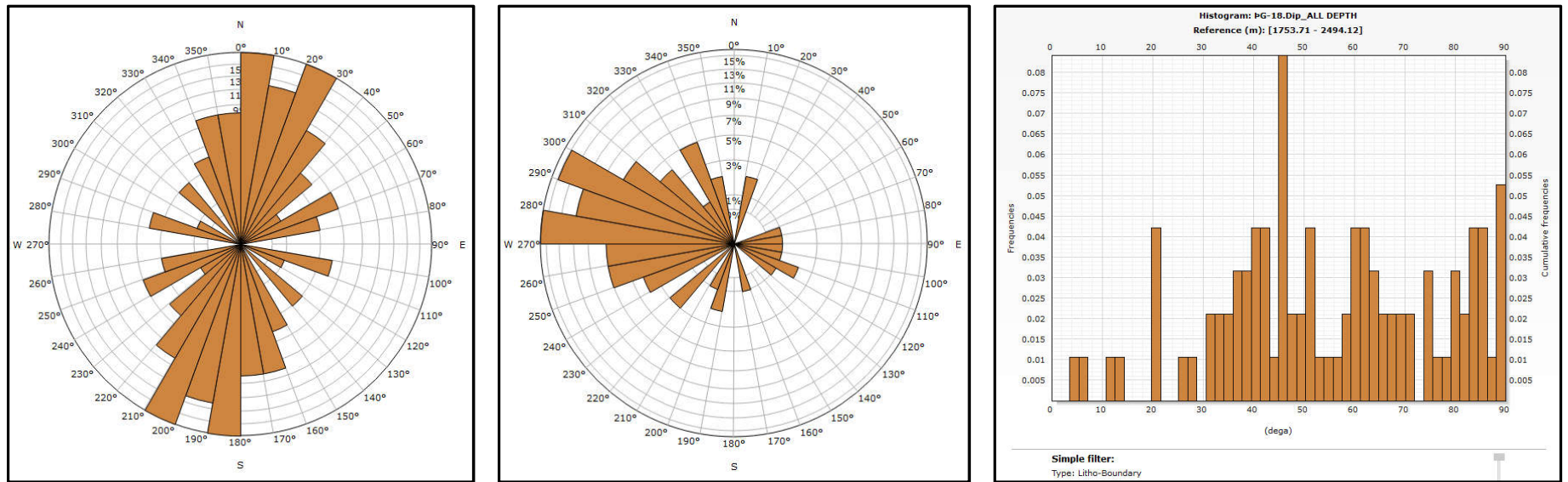


Image example of lithologic boundary.

Figure 2.3.24: Dip Statistics of Lithologic Boundary, Interval 2,494-1,748 m MD



Lithologic boundary dip statistics over the interval of 2,494-1,748 m MD. Dip statistics of lithologic boundaries show a dominant azimuth orientation of westerly (WSW, W, WNW). Dip magnitudes are also highly variable, from nearly horizontal to vertical.

Figure 3.1: Fracture Zonation, Interval 2,494-1,753 m MD, Well PG-18

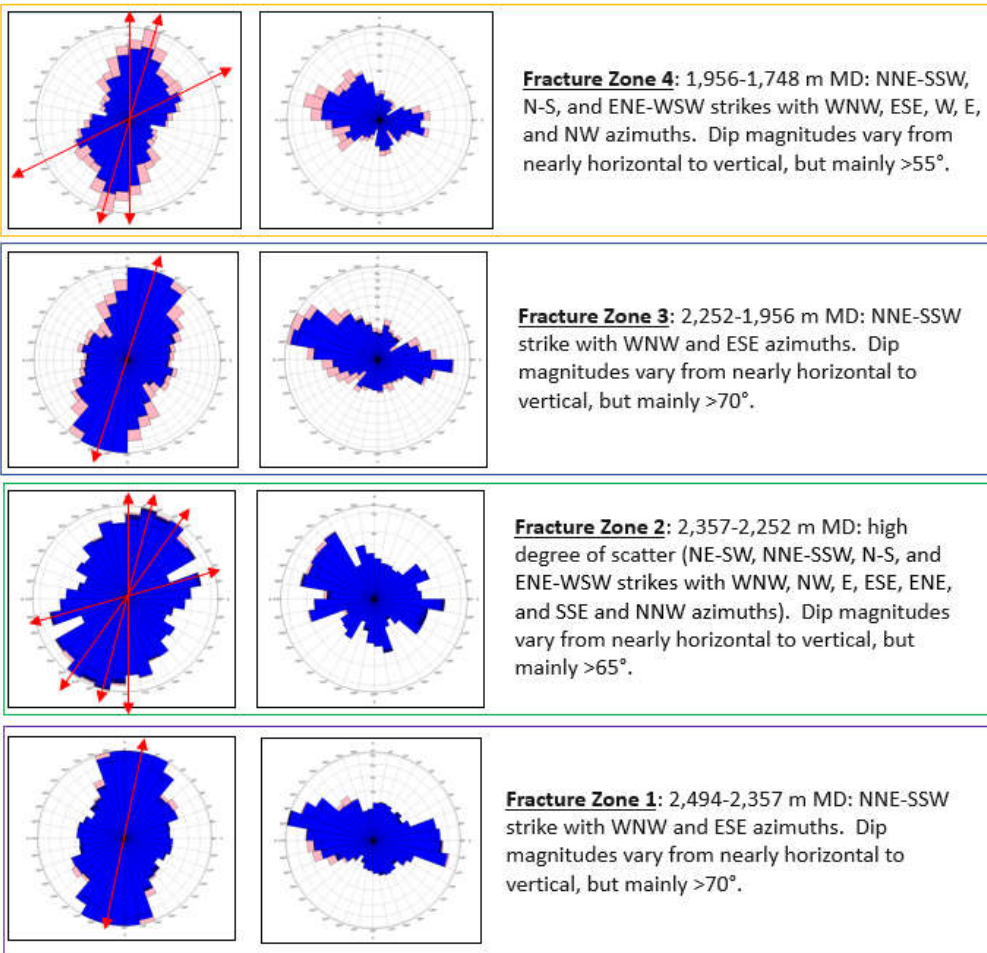
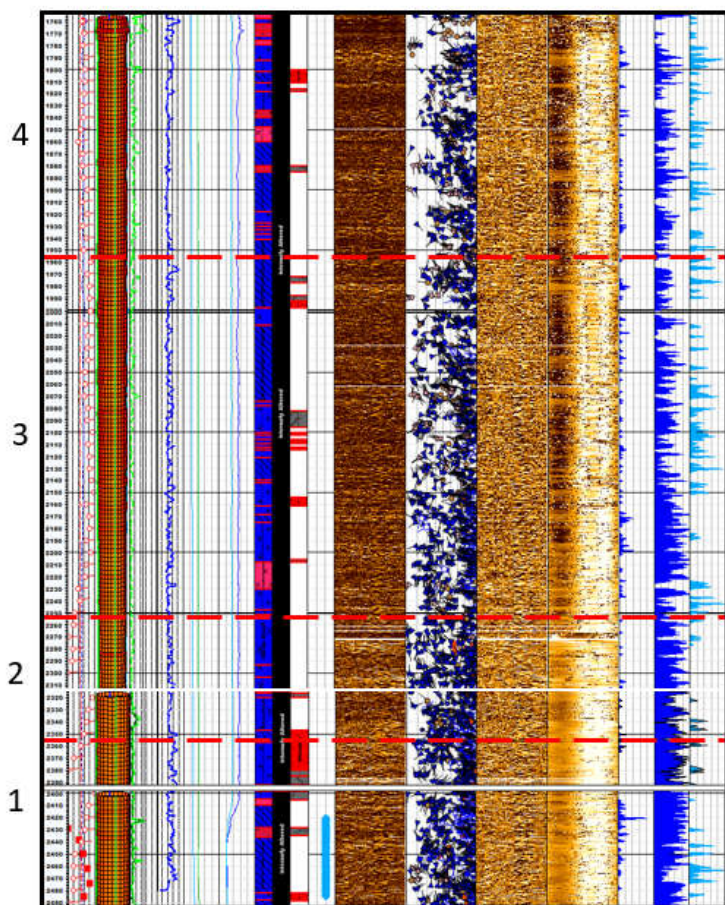
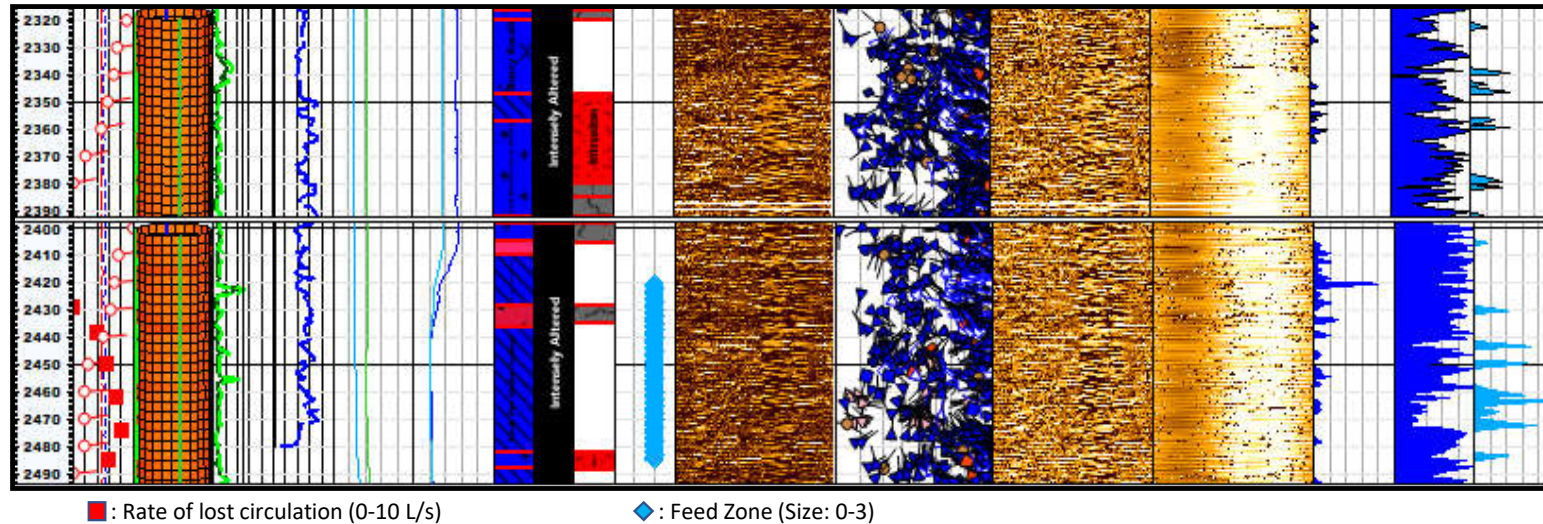
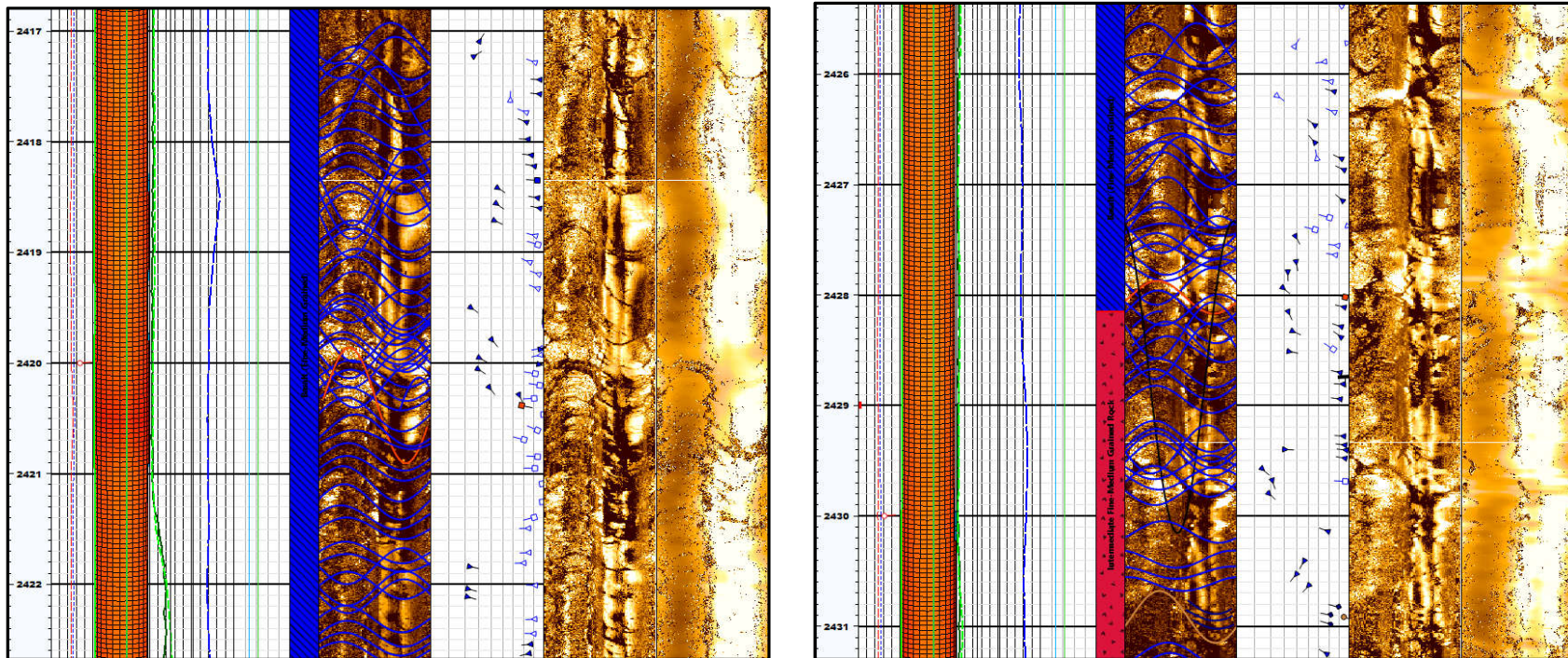


Figure 3.2: Zones of Lost Circulation and Feed Zone, Fracture Zone 1 (2,494-2,357 m MD)



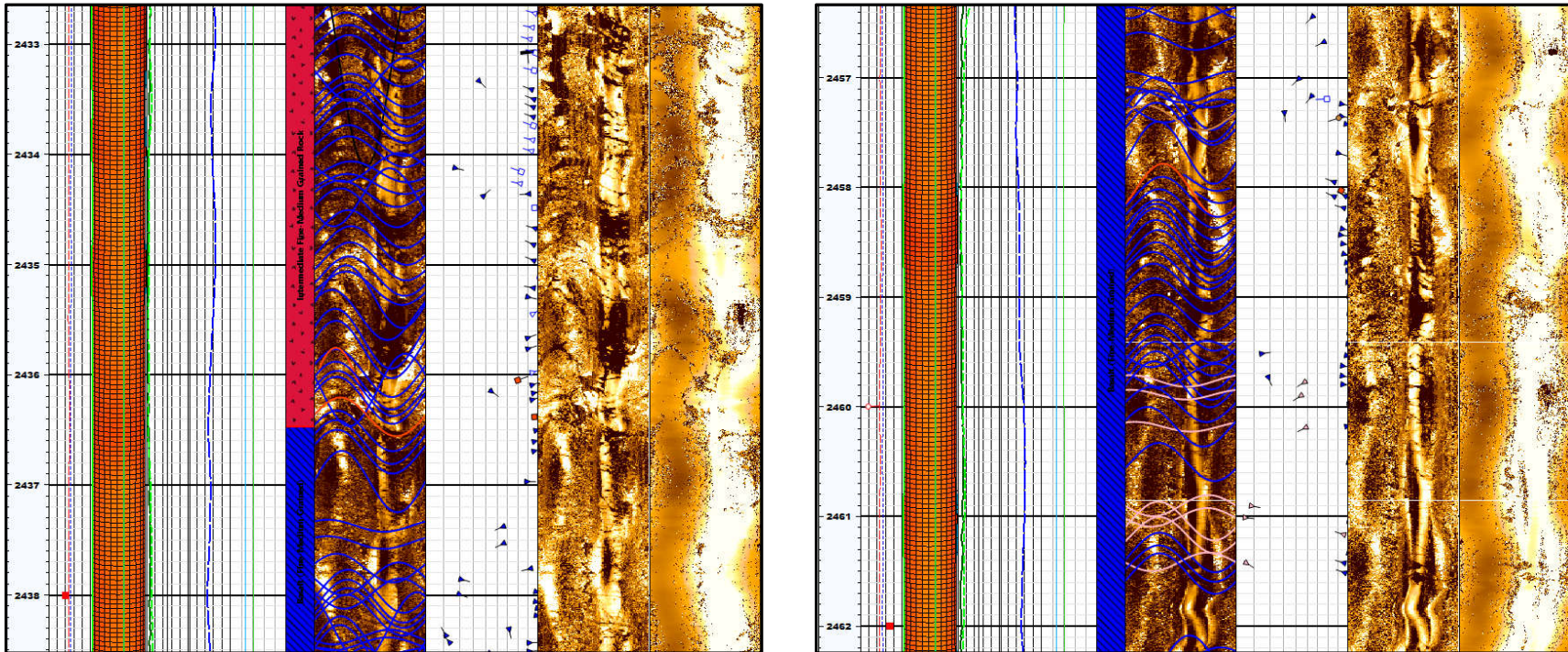
Circulation losses occurred within Fracture Zone 1 at 2,438 m MD (4 L/s), 2,450 m MD (5.5 L/s), 2,462 m MD (7 L/s), 2,474 m MD (8 L/s), and 2,485 m MD (6 L/s). The rate of circulation loss increased from 4 L/s to 8 L/s between 2,438 m MD to 2,474 m MD. This could be associated with a high angle (79°) NNE-SSW possible open fault at 2,443.4 m MD, a lower angle (47°) NW-SE possible open fault at 2,444.8 m MD, a lower angle (37°) NNE-SSW possible open fault at 2,453.2 m MD, a high angle (83°) NNE-SSW possible open fault at 2,458 m MD, and zone of large continuous and discontinuous open fractures at 2,439-2,478 m MD, which demonstrate dominant strike orientations of N-S, NNE-SSE, and NE-SW with NNW, ESE, E, W, and NW azimuths, and dip magnitudes that vary from approximately 20° to vertical, but are mainly >70°.

Figure 3.3: Examples of Feed Zone, Fracture Zone 1 (2,494-2,357 m MD)



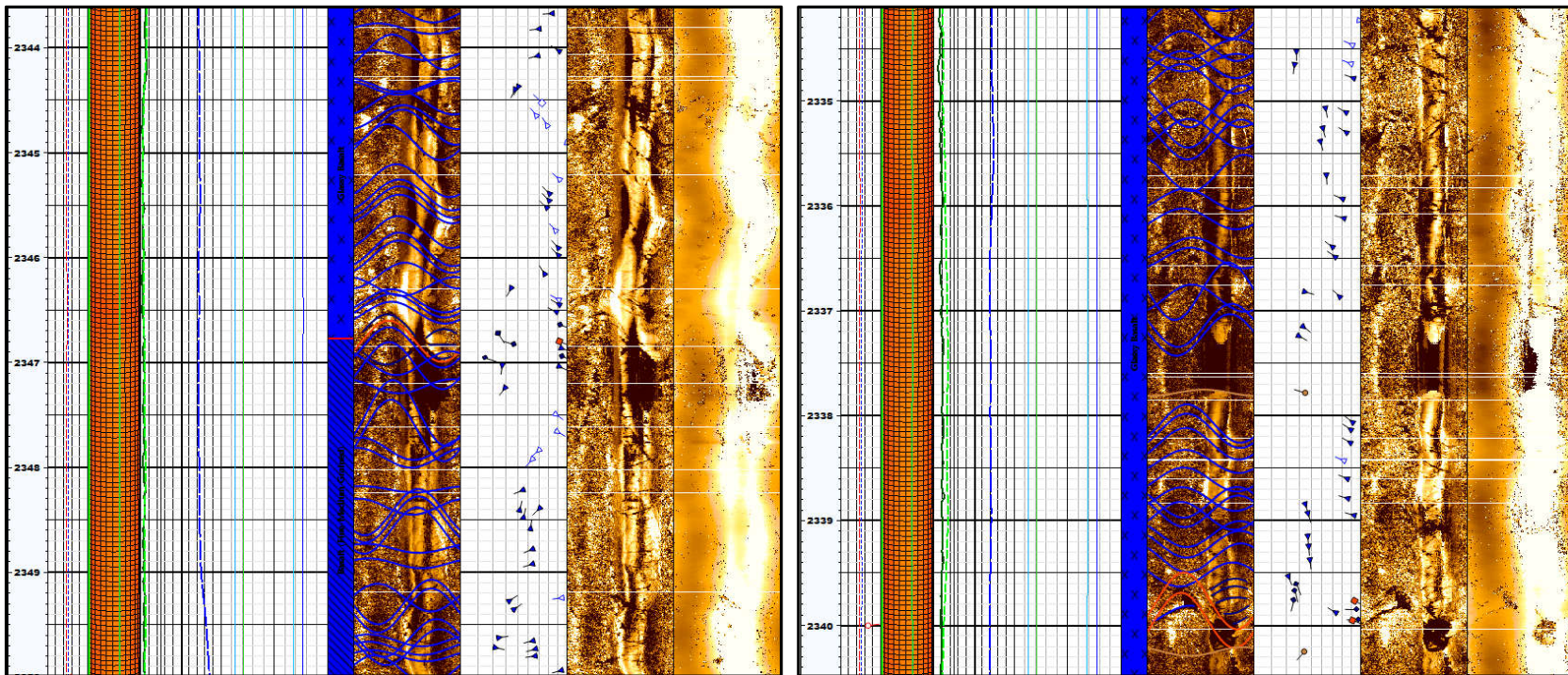
The “size 2” feed zone at 2,420-2,485 m MD is possibly associated with a high angle (68°) NNE-SSW possible open fault at 2,420.4 m MD, a high angle (86°) NNE-SSW possible open fault at 2,428 m MD, a high angle (70°) NNW-SSE possible open fault at 2,436.1 m MD, a high angle (87°) N-S possible open fault at 2,436.4 m MD, a high angle (79°) NNE-SSW possible open fault at 2,443.4 m MD, a lower angle (47°) NW-SE possible open fault at 2,444.8 m MD, a lower angle (37°) NNE-SSW possible open fault at 2,453.2 m MD, a high angle (83°) NNE-SSW possible open fault at 2,458 m MD, a high angle (89°) NNE-SSW possible open fault at 2,485.6 m MD, a high angle (71°) possible open fault at 2,485.8 m MD, and some large continuous and discontinuous open fractures at 2,417-2,491 m MD which demonstrate a dominant strike orientation of NNE-SSW, with WNW azimuth, and dip magnitudes that vary from 20° to vertical but are mainly >70°.

Figure 3.4: Examples of Feed Zone, Fracture Zone 1 (2,494-2,357 m MD)



The “size 2” feed zone at 2,420-2,485 m MD is possibly associated with a high angle (68°) NNE-SSW possible open fault at 2,420.4 m MD, a high angle (86°) NNE-SSW possible open fault at 2,428 m MD, a high angle (70°) NNW-SSE possible open fault at 2,436.1 m MD, a high angle (87°) N-S possible open fault at 2,436.4 m MD, a high angle (79°) NNE-SSW possible open fault at 2,443.4 m MD, a lower angle (47°) NW-SE possible open fault at 2,444.8 m MD, a lower angle (37°) NNE-SSW possible open fault at 2,453.2 m MD, a high angle (83°) NNE-SSW possible open fault at 2,458 m MD, a high angle (89°) NNE-SSW possible open fault at 2,485.6 m MD, a high angle (71°) possible open fault at 2,485.8 m MD, and some large continuous and discontinuous open fractures at 2,417-2,491 m MD which demonstrate a dominant strike orientation of NNE-SSW, with WNW azimuth, and dip magnitudes that vary from 20° to vertical but are mainly >70°.

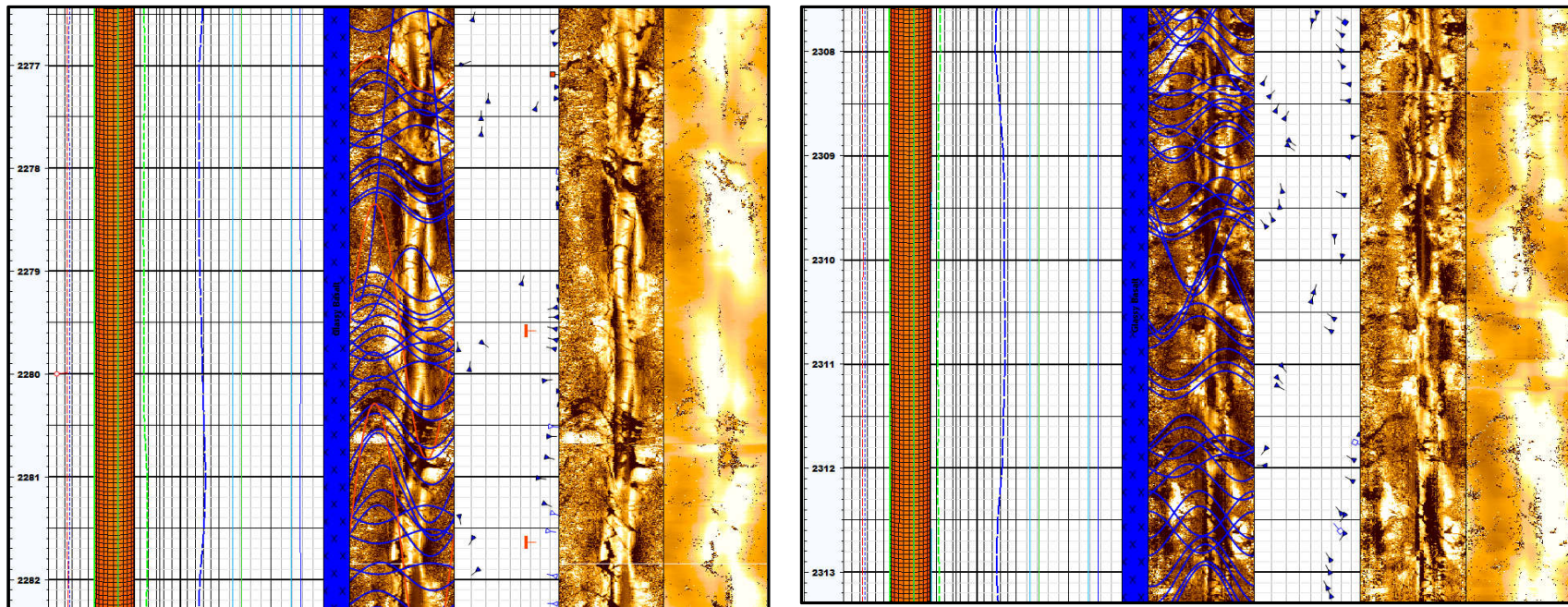
Figure 3.5: Examples of Large Continuous Open Fractures, Large Discontinuous Open Fractures, and Possible Open Faults in Fracture Zone 2 (2,357-2,252 m MD)



Large continuous and discontinuous open fractures in Fracture Zone 2 (2,357-2,252 m MD) are observed at 2,344-2,357 m MD, 2,338-2,340 m MD, 2,311.5-2,313 m MD, 2,277-2,285 m MD, 2,263-2,267 m MD, 2,253-2,255 m MD, 2,333-2,335 m MD, and 2,326-2,330 m MD, which demonstrate a dominant strike orientation of NNE-SSW with WNW and ESE azimuths, and dip magnitudes that vary from approximately  $20^\circ$  to vertical, but are mainly  $>75^\circ$ .

Possible open faults were recognized at 2,357 m MD, 2,356.8 m MD, 2,346.8 m MD, 2,340 m MD, 2,339.7 m MD, 2,319.5 m MD, 2,303.4 m MD, and 2,277.1 m MD, which demonstrate a dominant strike orientation of NNE-SSW with ESE and WNW azimuths, and dip magnitudes range from  $70^\circ$  to nearly vertical ( $85^\circ$ ).

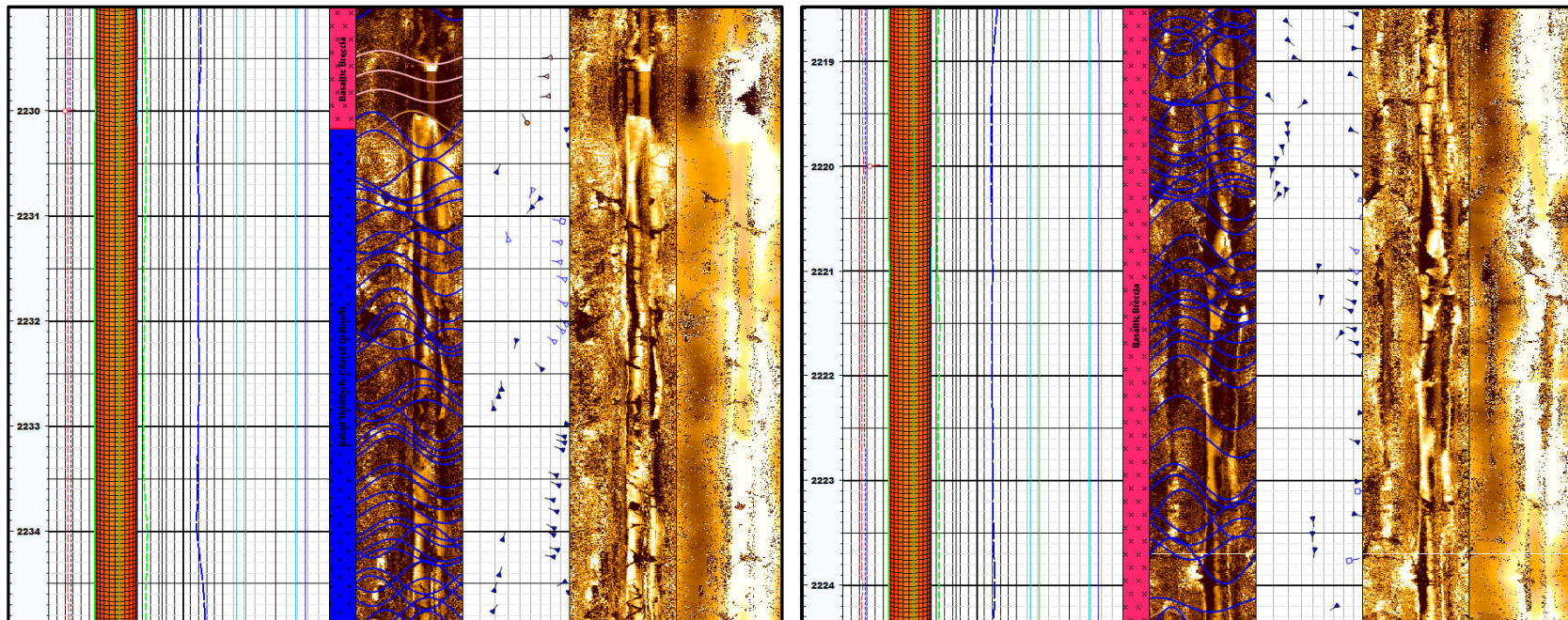
Figure 3.6: Examples of Large Continuous Open Fractures, Large Discontinuous Open Fractures, and Possible Open Faults in Fracture Zone 2 (2,357-2,252 m MD)



Large continuous and discontinuous open fractures in Fracture Zone 2 (2,357-2,252 m MD) are observed at 2,344-2,357 m MD, 2,338-2,340 m MD, 2,311.5-2,313 m MD, 2,277-2,285 m MD, 2,263-2,267 m MD, 2,253-2,255 m MD, 2,333-2,335 m MD, and 2,326-2,330 m MD, which demonstrate a dominant strike orientation of NNE-SSW with WNW and ESE azimuths, and dip magnitudes that vary from approximately  $20^\circ$  to vertical, but are mainly  $>75^\circ$ .

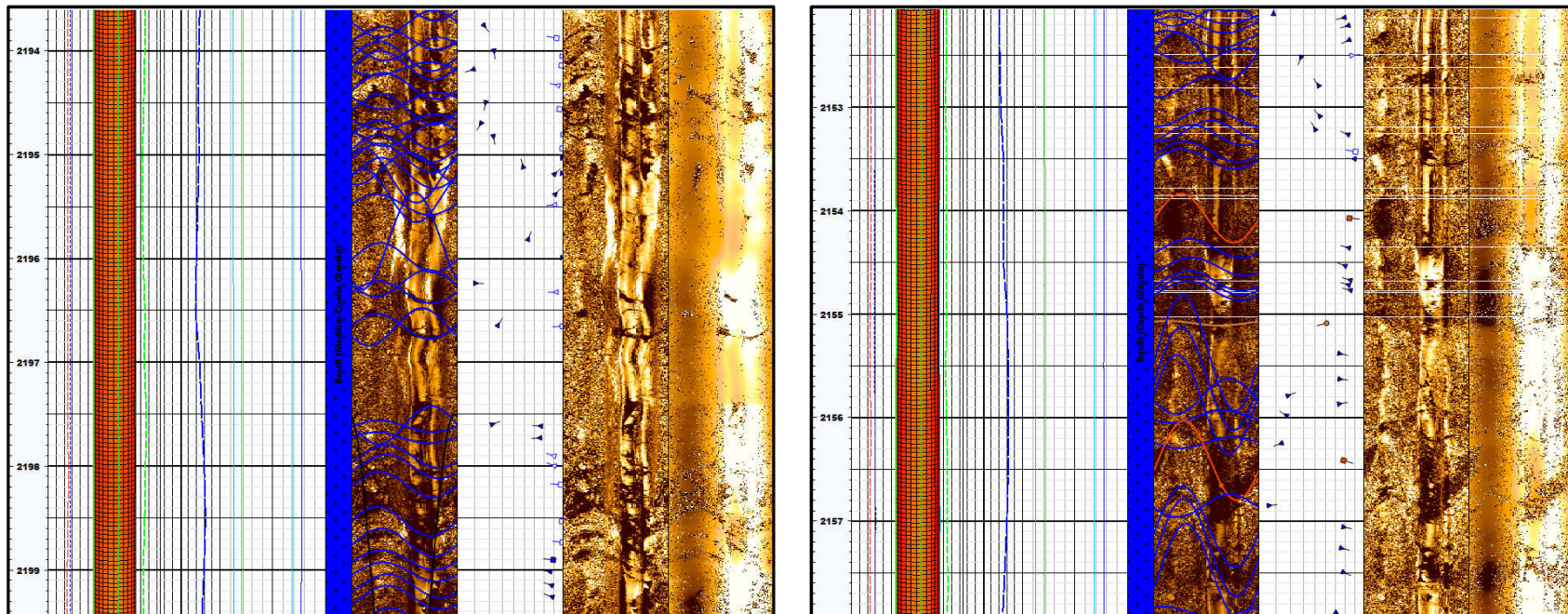
Possible open faults were recognized at 2,357 m MD, 2,356.8 m MD, 2,346.8 m MD, 2,340 m MD, 2,339.7 m MD, 2,319.5 m MD, 2,303.4 m MD, and 2,277.1 m MD, which demonstrate a dominant strike orientation of NNE-SSW with ESE and WNW azimuths, and dip magnitudes range from  $70^\circ$  to nearly vertical ( $85^\circ$ ).

Figure 3.7: Examples of Large Continuous and Discontinuous Open Fractures in Fracture Zone 3 (2,252-1,956 m MD)



Large continuous and discontinuous open fractures in Fracture Zone 3 (2,252-1,956 m MD) are observed at 2,230-2,233 m MD, 2,223-2,224 m MD, 2,220-2,221 m MD, 2,215 m MD, 2,213.7 m MD, 2,205-2,206 m MD, 2,201.8 m MD, 2,197.5-2,199 m MD, 2,193-2,197 m MD, 2,185-2,190 m MD, 2,177-2,179 m MD, 2,170-2,174 m MD, 2,167-2,168 m MD, 2,156.5-2,161 m MD, 2,152-2,154 m MD, 2,139-2,141 m MD, 2,132.5 m MD, 2,128 m MD, 2,116-2,122 m MD, 2,111-2,115 m MD, 2,103 m MD, 2,100 m MD, 2,094-2,096 m MD, 2,087-2,089 m MD, 2,072-2,074 m MD, 2,036-2,043 m MD, 2,033-2,034 m MD, 1,990.5 m MD, and 1,978-1,983 m MD, which demonstrate a dominant strike orientation of NNE-SSW with WNW and ESE azimuths, and dip magnitudes that vary from approximately 15° to vertical, but are mainly >80°.

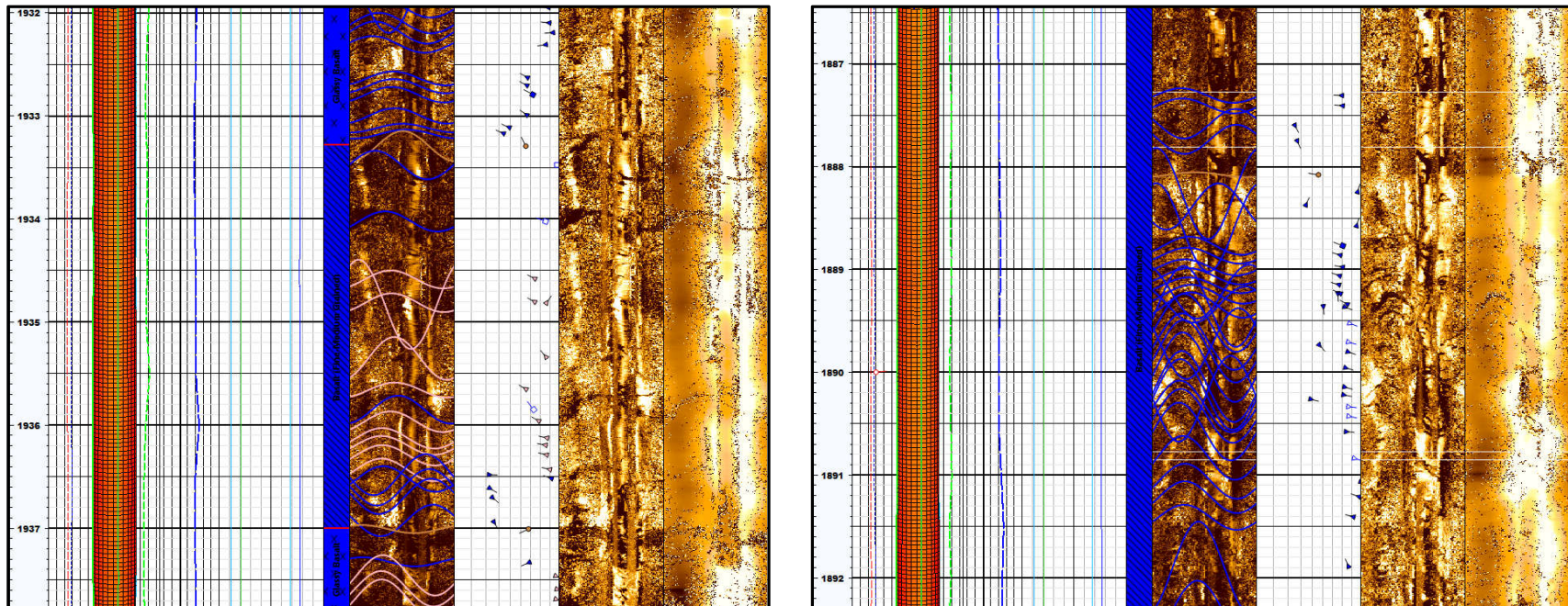
Figure 3.8: Examples of Large Continuous and Discontinuous Open Fractures, and Possible Open Faults in Fracture Zone 3 (2,252-1,956 m MD)



Large continuous and discontinuous open fractures in Fracture Zone 3 (2,252-1,956 m MD) are observed at 2,230-2,233 m MD, 2,223-2,224 m MD, 2,220-2,221 m MD, 2,215 m MD, 2,213.7 m MD, 2,205-2,206 m MD, 2,201.8 m MD, 2,197.5-2,199 m MD, 2,193-2,197 m MD, 2,185-2,190 m MD, 2,177-2,179 m MD, 2,170-2,174 m MD, 2,167-2,168 m MD, 2,156.5-2,161 m MD, 2,152-2,154 m MD, 2,139-2,141 m MD, 2,132.5 m MD, 2,128 m MD, 2,116-2,122 m MD, 2,111-2,115 m MD, 2,103 m MD, 2,100 m MD, 2,094-2,096 m MD, 2,087-2,089 m MD, 2,072-2,074 m MD, 2,036-2,043 m MD, 2,033-2,034 m MD, 1,990.5 m MD, and 1,978-1,983 m MD, which demonstrate a dominant strike orientation of NNE-SSW with WNW and ESE azimuths, and dip magnitudes that vary from approximately 15° to vertical, but are mainly >80°.

Possible open faults were recognized at 2,156.5 m MD and 2,154 m MD, which demonstrate a dominant strike orientation of NNE-SSW with ESE azimuth, and dip magnitudes range from 67° to 75°.

Figure 3.9: Examples of Large Continuous and Discontinuous Open Fractures in Fracture Zone 4 (1,956-1,748 m MD)



Large continuous and discontinuous open fractures in Fracture Zone 4 (1,956-1,748 m MD) are observed at 1,928-1,937 m MD, 1,898-1,902 m MD, 1,887-1,891.5 m MD, 1,851-1,855 m MD, 1,819.8 m MD, 1,788-1,797.5 m MD, and 1,784-1,787 m MD, which demonstrate dominant strike orientations of N-S, NNE-SSW, and NNW-SSE with ESE, W, WNW, ENE, and WSW azimuths, and dip magnitudes that vary from approximately 20° to vertical, but are mainly >75°.

**Appendix A**

LV-2019-004, 31 January 2019

# ABI Image Processing and Interpretation of Well ÞG-18, Þeistareykir Field, Þingeyjarsveit, Iceland

Tito Satria Putra Perdana, Senior Geologist  
GeothermEx – A Schlumberger Company, San Francisco Bay Area, California, USA  
09 January 2019

## Disclaimer

*Any interpretation, research, analysis, data, results, estimates, or recommendation furnished with the services or otherwise communicated by GeothermEx to its customers at any time in connection with the services are opinions based on inferences from measurements, empirical relationships and/or assumptions. These inferences, empirical relationships and/or assumptions are not infallible, and professionals in the industry may differ with respect to such inferences, empirical relationships and/or assumptions. Accordingly, GeothermEx cannot and does not warrant the accuracy, correctness or completeness of any such interpretation, research, analysis, data, results, estimates or recommendation.*

*Customer acknowledges that it is accepting the services "as is," that GeothermEx makes no representation or warranty, express or implied, of any kind or description in respect thereto. Specifically, Customer acknowledges that GeothermEx does not warrant that any interpretation, research, analysis, data, results, estimates, or recommendation is fit for a particular purpose, including but not limited to compliance with any government request or regulatory requirement. Customer further acknowledges that such services are delivered with the explicit understanding and agreement that any action taken based on the services received shall be at its own risk and responsibility, and no claim shall be made against GeothermEx as a consequence thereof.*

# Agenda

Objective and Data Used

ABI Log Data Acquisition

ABI Log Data Quality and Borehole Conditions

ABI Manual Dip Classification

ABI Plot Formats (Deliverables)

ABI Dip Statistics and Image Examples

ABI Open Fracture Zonations

Comparison of Fractures, Faults, Drilling Induced Fractures, Breakouts, and Lithological Boundaries in PG-15, PG-17, PG-12, and PG-18

## Objectives and Data Used

### Objective:

The main objective of this study was to provide detailed fracture analysis of well PG-18 including fracture classification and orientation.

### Data Used:

- Image log (ABI)
- Caliper logs
- Open-Hole Logs: gamma Ray (GR), neutron porosity (NN) log
- Temperature logs
- Spinner logs
- Lost circulation intervals
- Lithological log plot (from cutting analysis)
- Intrusion log plot
- Alteration log plot
- Feed zone interval

# ABI Log Data Acquisitions

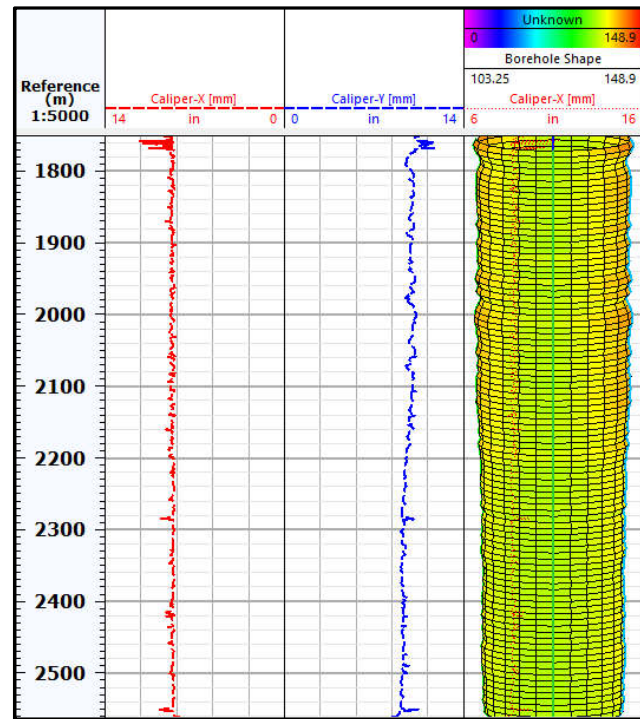
Tool Type	ABI
Intervals (m MD)	8.5 inch: 2,494-1,748 m MD
Dates Logged	26 August 2017
Bit Sizes (inch)	8.5
Borehole Coverage (%)	100
Well deviation (degrees)	~33 to ~40.6
Well azimuth (degrees)	~80.5 to ~83
Drilling fluid Type	Mud / Water

The acoustic borehole scanner tool “ABI” was logged on 26 August 2017, in the well PG-18 located in the Þeistareykir Field, Þingeyjarsveit county, Iceland.

The ABI logging was conducted in 3 runs: 2,494-2,392 m MD, 2,393-2,309 m MD, and 2,313.5-1,748 m MD.

ABI acoustic borehole scanner tool generates an image of the borehole wall by transmitting ultrasound pulses from rotating sensor and recording the amplitude and travel time of the signals reflected at the interface between mud and formation ([www.alt.lu](http://www.alt.lu)).

# ABI Log Data Quality and Borehole Conditions

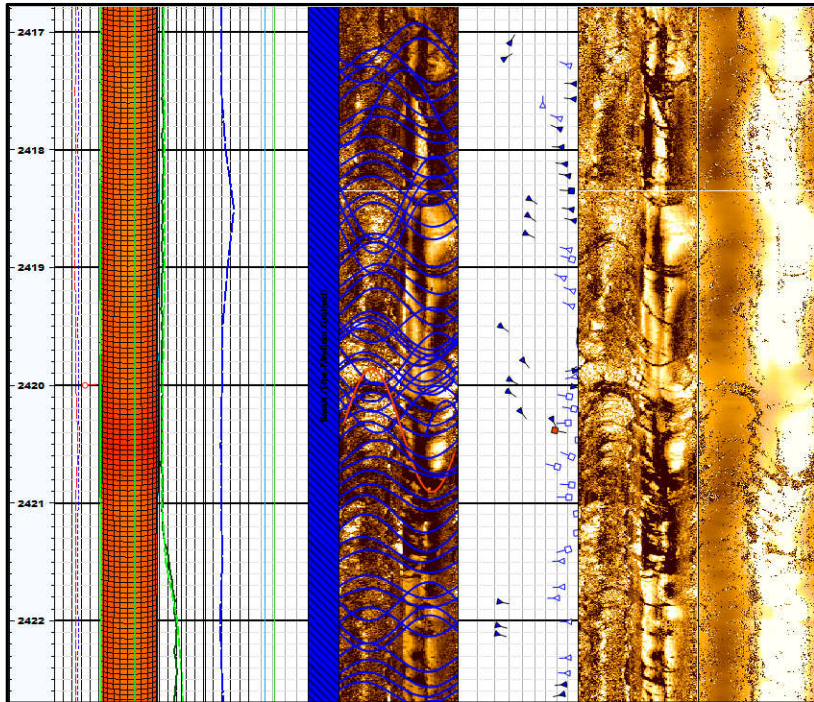


Large borehole washouts adversely affected ABI image quality.

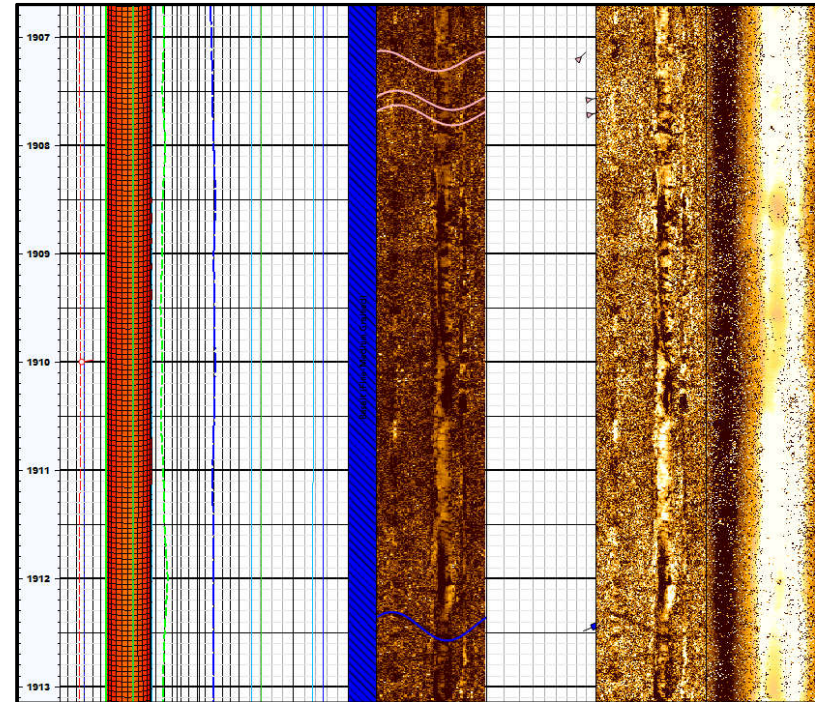
Borehole conditions are good; image quality is generally good.

The borehole conditions from 2,494-2,200 m MD are good, with only few large and minor washouts, and the image quality in this interval is generally good. Evident borehole washouts in the interval of 2,200-1,748 m MD adversely affected ABI Image quality, but fractures and faults could still be identified and analyzed.

# ABI Log Data Quality and Borehole Conditions

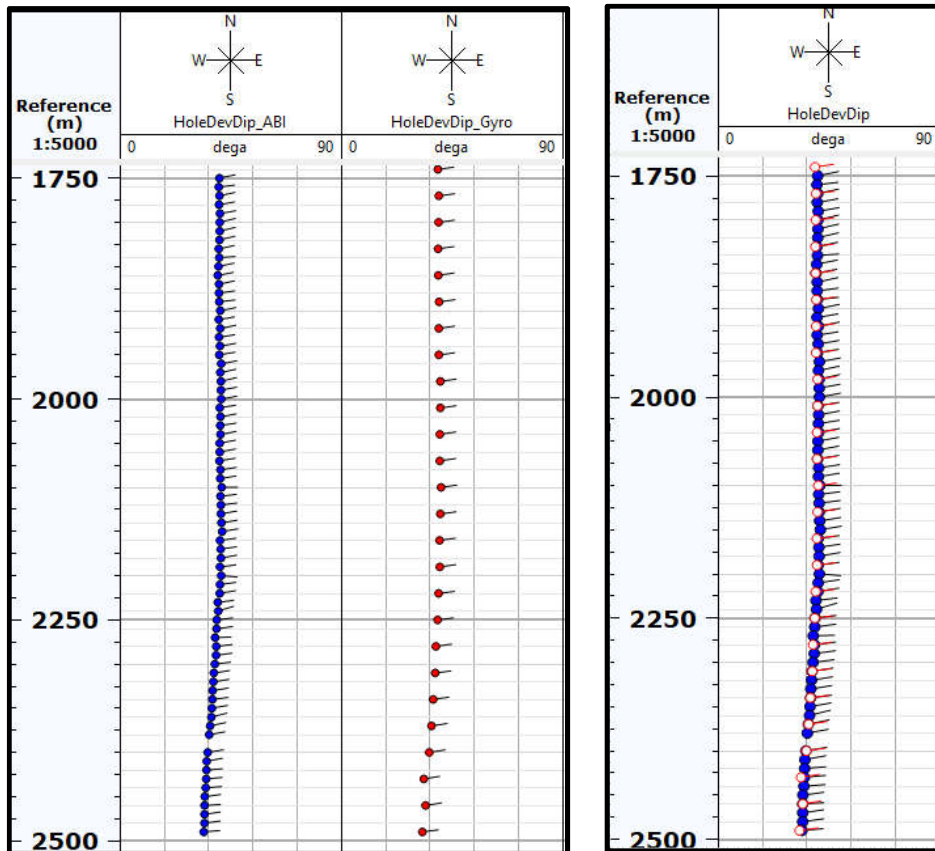


An example of “good” ABI image quality. The image log quality and borehole conditions are generally good in the interval of 2,494-2,200 m MD.



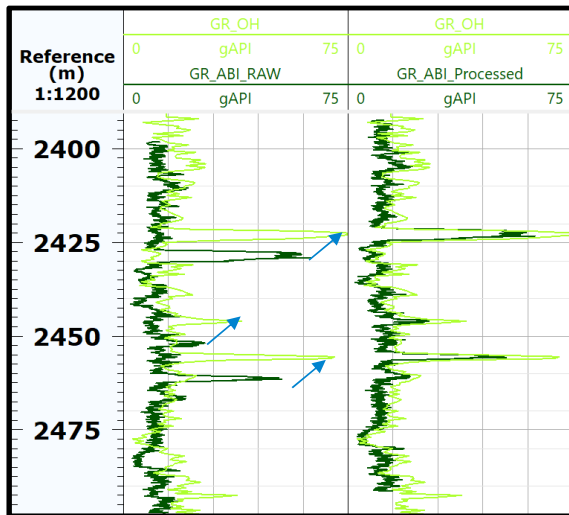
An example of “poor” ABI image quality. Borehole washouts are evident over the interval of 2,200-1,748 m MD and adversely affected ABI image quality.

# ABI Log Data Quality and Borehole Conditions

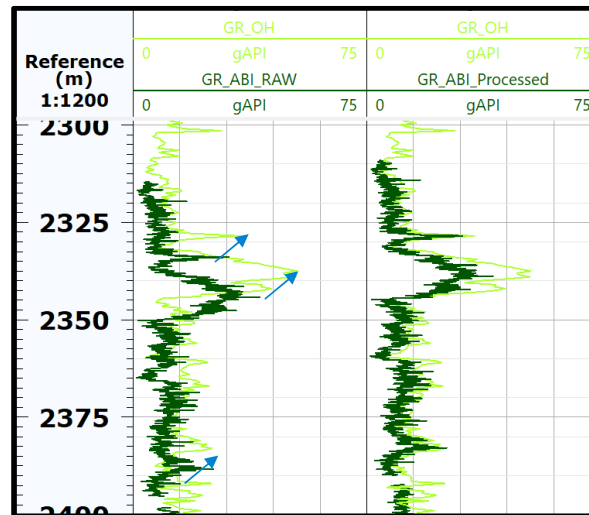


In general, the inclinometry data from the ABI tool agreed with the well deviation and well azimuth data from gyro surveys, indicating that the tool was correctly oriented in the borehole and that the calculated dips are correct.

# ABI Image Log Depth Shift / Depth Matched

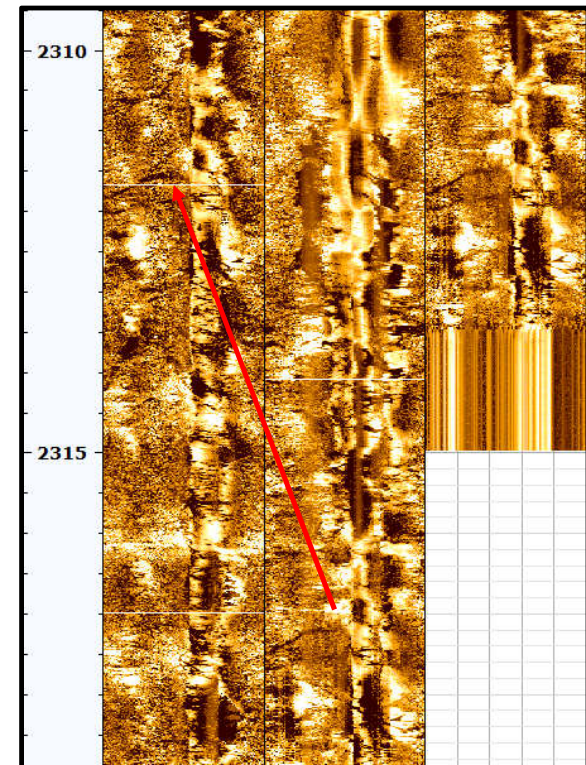


GR-OH vs. GR-ABI Logging run 9; depth shift: -5.8 m



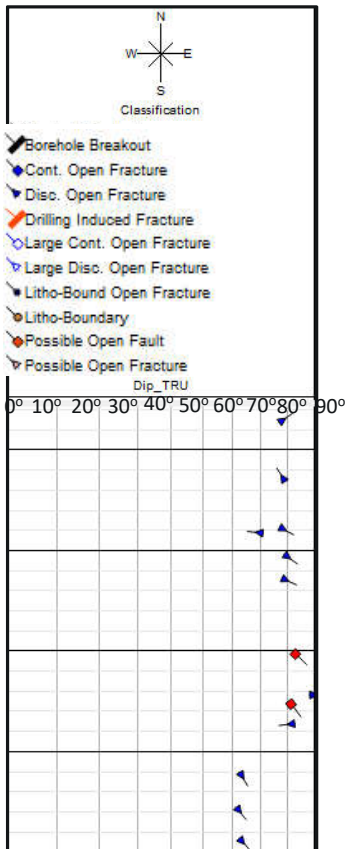
GR-OH vs. GR-ABI Logging run 10; depth shift: -5.4 m

Shifted ABI Run 10    ABI Run 11 Raw    Processed ABI Run 11



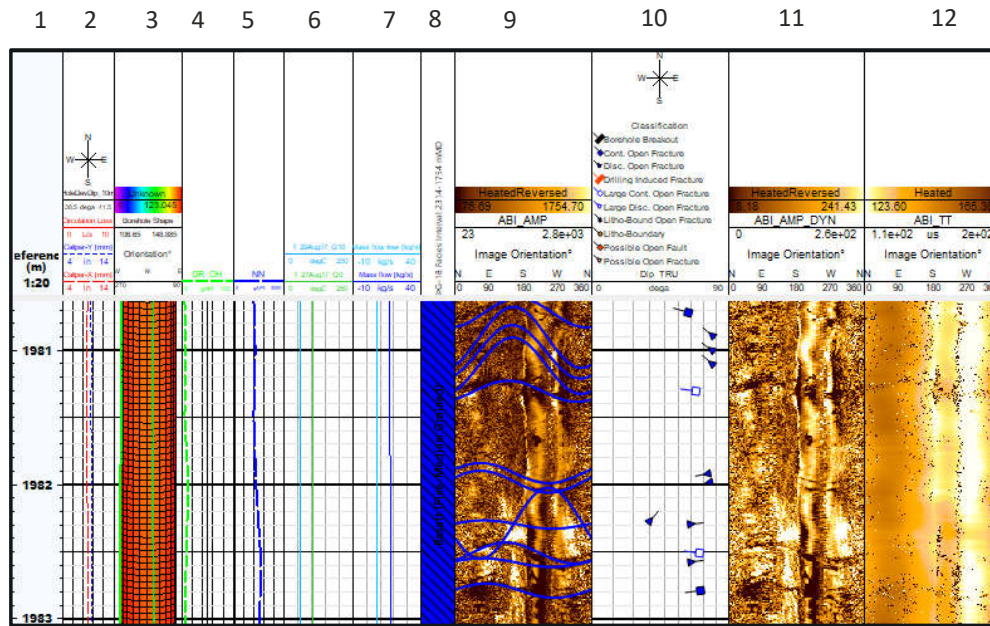
Shifted ABI run 10 vs. shifted ABI run 11; depth shift: -5.7 m

# Manual Dip Classification



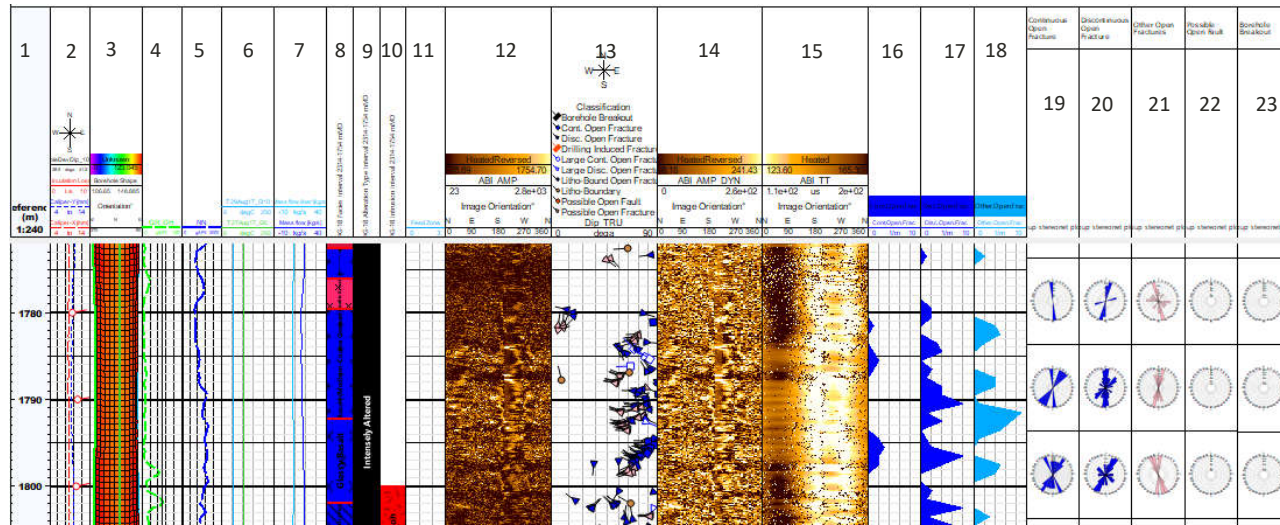
Feature Name	Description
Lithological Boundary	Apparently non-erosional boundary / contact between different lithologies / facies. Solid brown circle.
Continuous Open Fracture	Fracture with low-amplitude image, continuous across borehole diameter. Solid blue square.
Large Continuous Open Fracture	Fracture with large low-amplitude event, continuous across borehole diameter. Blue triangle.
Discontinuous Open Fracture	Fracture with low-amplitude image, discontinuous across borehole diameter. Solid blue square.
Large Discontinuous Open Fracture	Fracture with large low-amplitude event, discontinuous across borehole diameter. Blue square.
Litho-bound Open Fracture	Fracture with low amplitude, compartmentalized within individual lithologic unit bounded and/or terminated by lithologic boundaries. Solid dark blue diamond.
Possible Open Fracture	Fracture with low-amplitude image, discontinuous across borehole diameter (not seen across borehole diameter due to the poor-quality image caused by bad hole or artifact). Solid light pink triangle.
Possible Open Fault	Continuous planar features cutting bedding and/or fracture with a tentative evidence for movement. Solid red square.
Drilling Induced Fracture	Fractures that track vertically down but do not cross the borehole, or appear as discontinuous "gashes" on opposing sides of the borehole. These features appear with high amplitude on images. Red strike.
Borehole Breakout	Vertical irregular low amplitude areas on opposing sides of the borehole wall. Black strike.

# Plot Format: ABI Interpretation (Scale 1:20)



- Track 1 : Measured depth
- Track 2 : Caliper data, borehole inclinometry, and lost circulation
- Track 3 : Borehole shape
- Track 4 : Gamma ray logs (standard open-hole log and ABI)
- Track 5 : Neutron-porosity log
- Track 6 : Temperature logs
- Track 7 : Spinner logs
- Track 8 : Lithology / facies from cutting analysis
- Track 9 : ABI amplitude static image and sinusoid of dips
- Track 10 : True dip tadpole
- Track 11 : ABI amplitude dynamic image
- Track 12 : ABI travel time static image

# Plot Format: ABI Composite (Scale 1:240)



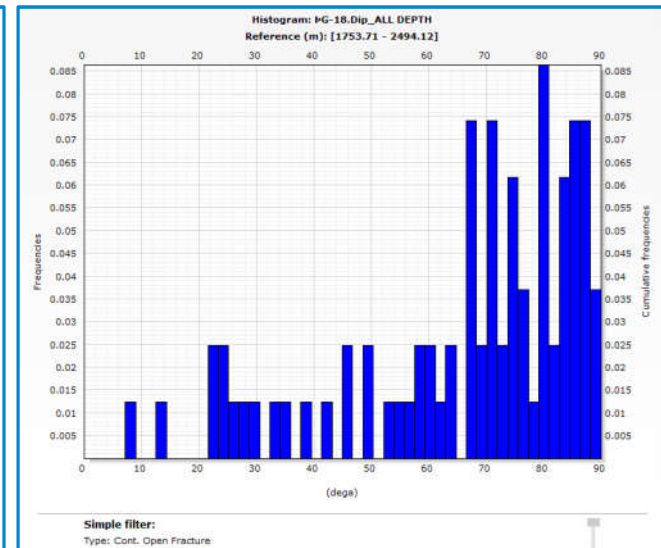
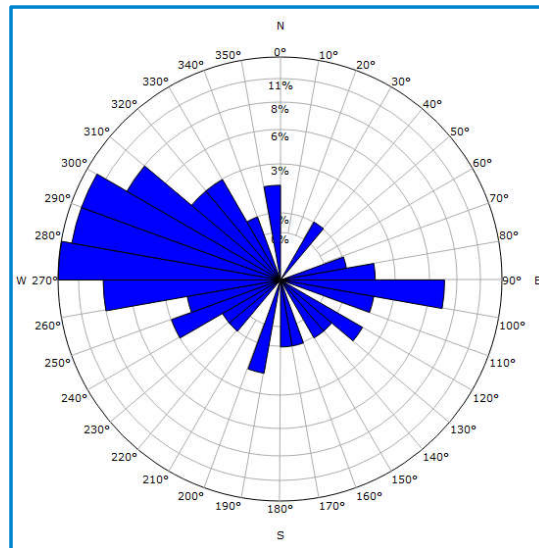
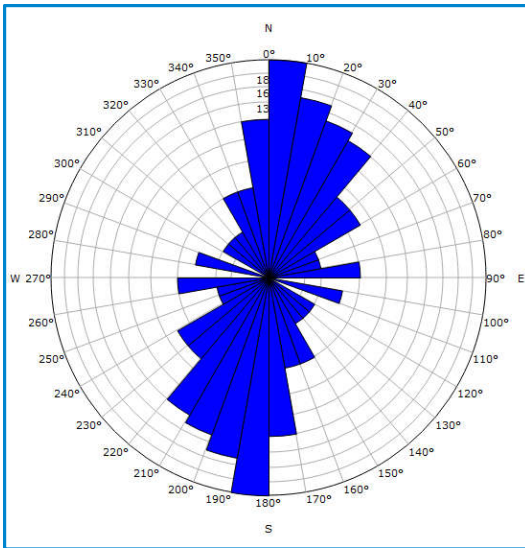
- Track 14 : ABI amplitude dynamic image
- Track 15 : ABI travel time static image
- Track 16 : Fracture density – continuous open frac
- Track 17 : Fracture density – discontinuous open frac
- Track 18 : Fracture density – other open fracs
- Track 19 : Fan plot continuous open frac
- Track 20 : Fan plot discontinuous open frac
- Track 21 : Fan plot other open fracs
- Track 22 : Fan plot possible open fault
- Track 23 : Fan plot borehole breakout and drilling induced frac

- Track 1 : Measured depth
- Track 2 : Caliper data, borehole inclinometry, and lost circulation
- Track 3 : Borehole shape
- Track 4 : Gamma rays
- Track 5 : Neutron-porosity logs
- Track 6 : Temperature Logs
- Track 7 : Spinner logs

- Track 8 : Lithologies / facies from cutting analysis
- Track 9 : Alteration types
- Track 10 : Intrusion intervals
- Track 11 : Feed zones
- Track 12 : ABI amplitude static image
- Track 13 : True dip tadpoles

# ABI Dip Statistics and Image Examples

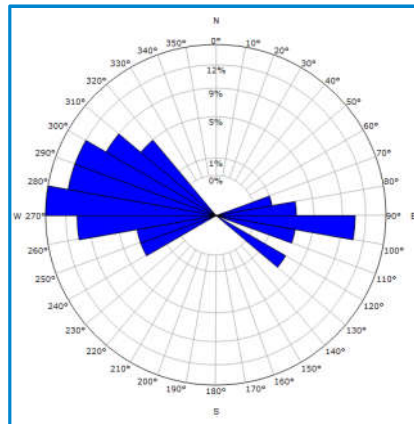
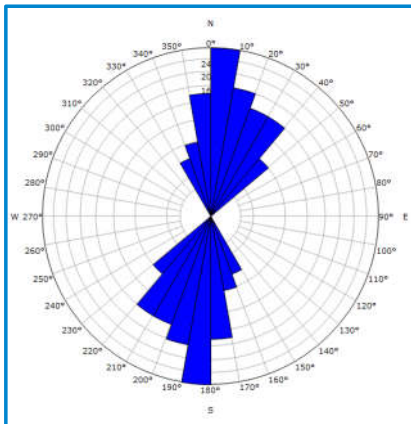
# Dip Statistics: Continuous Open Fracture



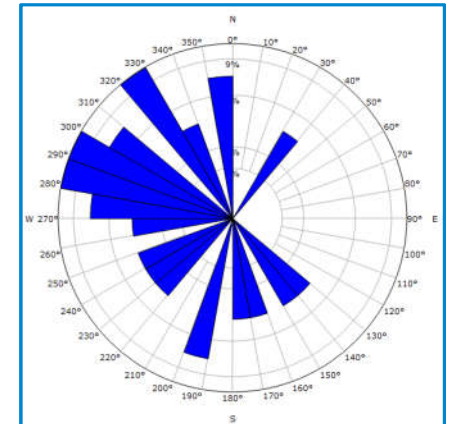
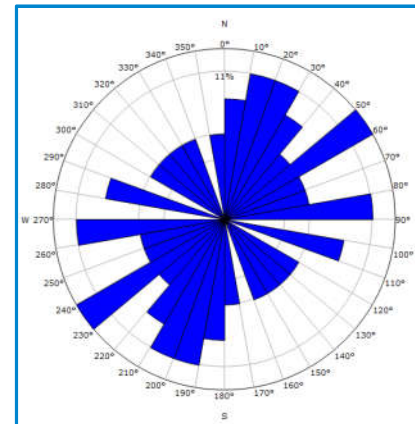
A total of 81 continuous open fractures were identified over the entire logged interval (2,494-1,748 m MD). Continuous-open-fracture dip statistics in the interval indicate a dominant strike orientation of NNE-SSW with WNW and ESE azimuths. The dip magnitudes of the continuous open fractures vary from nearly horizontal (approximately 8°) to vertical, but they are mainly steeper than 65°.

# Dip Statistics: Continuous Open Fracture

≥65° dip magnitudes

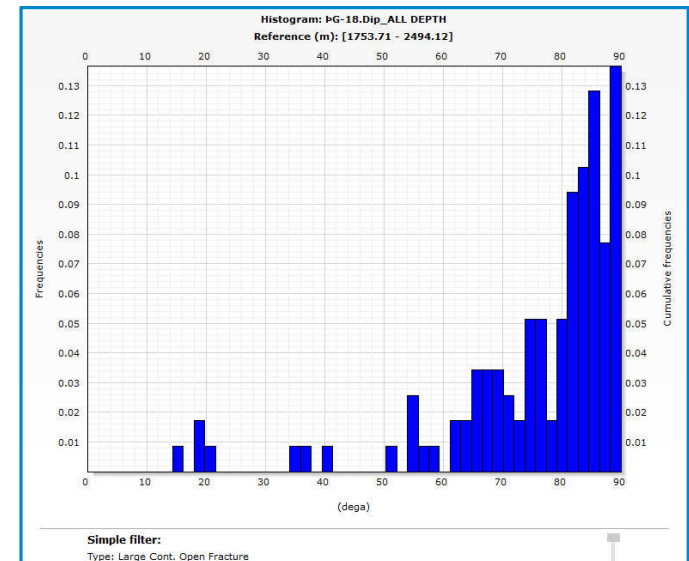
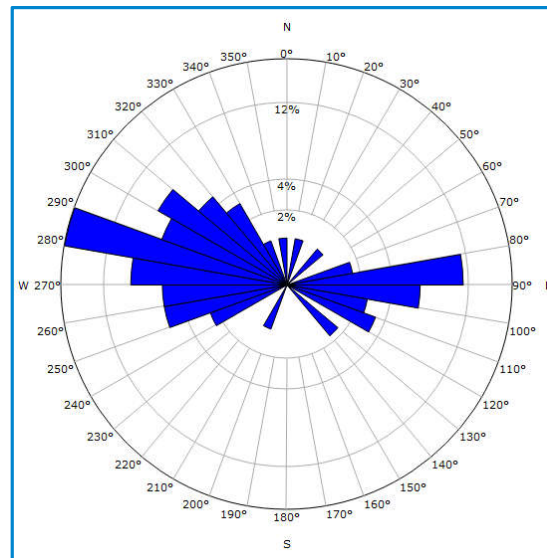
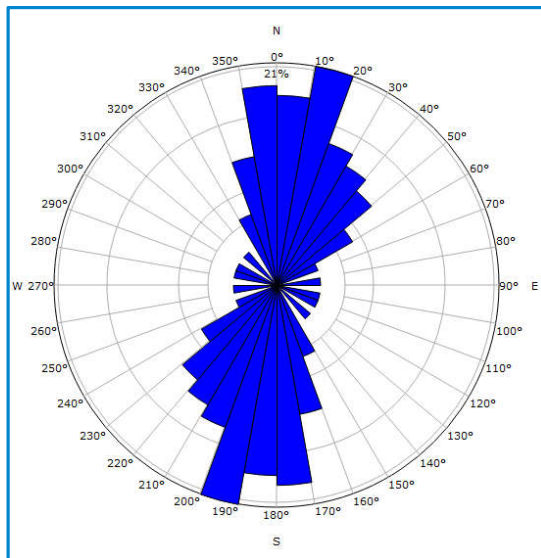


<65° dip magnitudes



Continuous open fractures with dip magnitudes  $\geq 65^\circ$  show dominant strike orientation of NNE-SSW with WNW and ESE dips. Continuous open fractures with dip magnitudes of  $< 65^\circ$  indicate dominant strike orientations of NNE-SSW, NE-SW, and E-W with WNW, NW, SW, SSW, SSE, and SW azimuths.

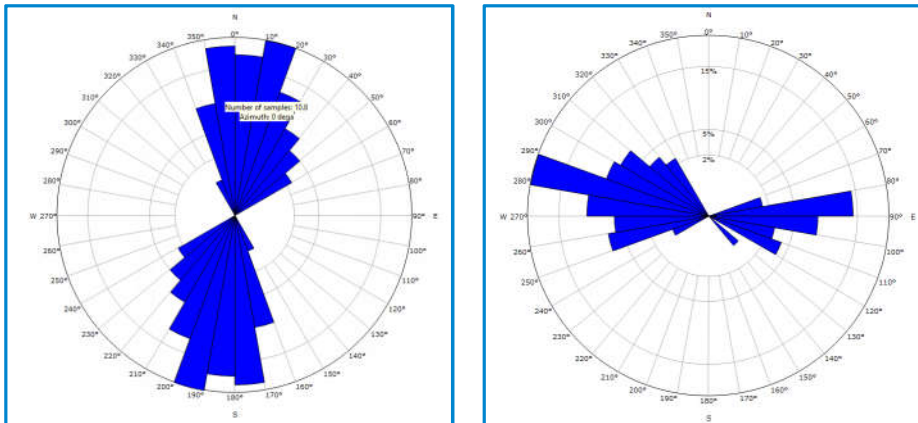
# Dip Statistics: Large Continuous Open Fracture



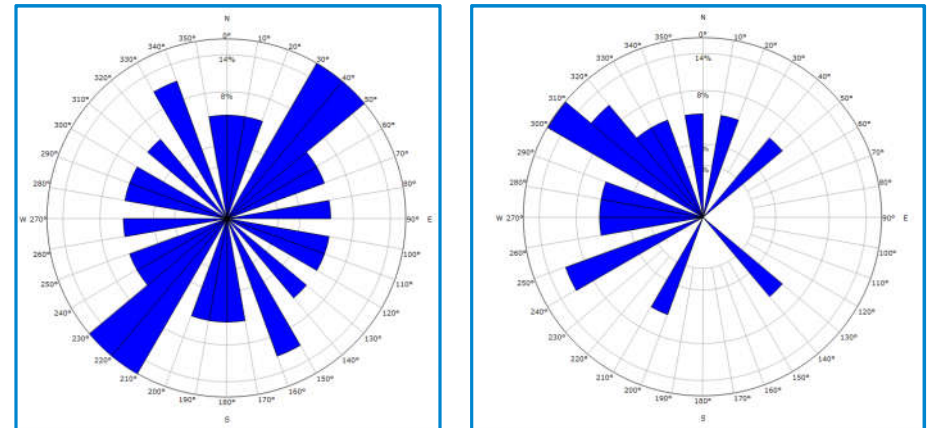
A total of 117 large continuous open fractures were identified over the entire logged interval (2,494-1,748 m MD). Large-continuous-open-fracture dip statistics over the interval demonstrate a dominant strike orientation of NNE-SSW, with WNW, E, and ESE azimuths. Dip magnitudes for this fracture type are highly variable, from 15° to vertical, but mainly steeper than 65°

# Dip Statistics: Large Continuous Open Fracture

≥65° dip magnitudes

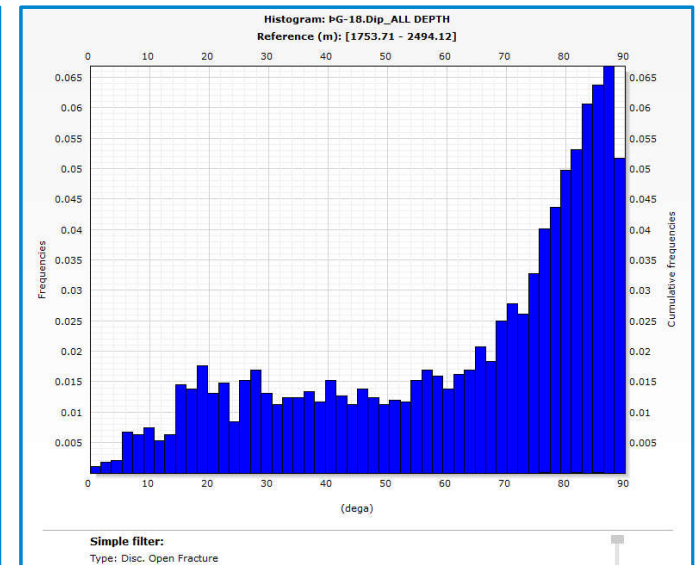
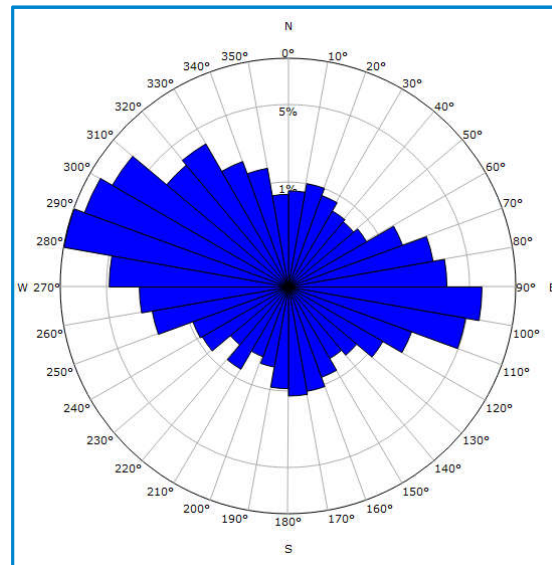
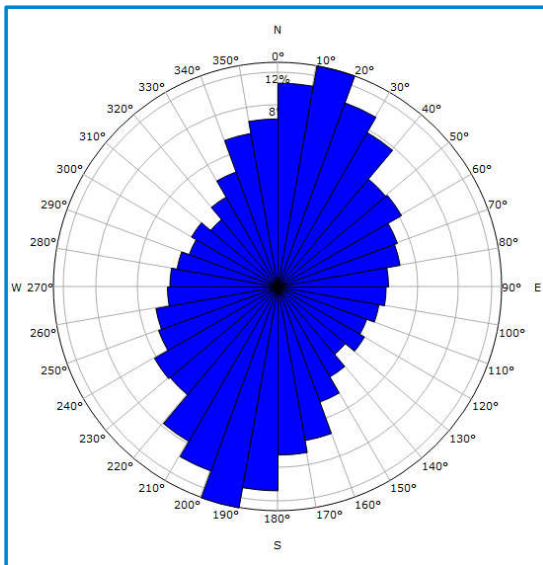


<65° dip magnitudes



Large discontinuous open fractures with dip magnitudes  $\geq 65^\circ$  show a dominant strike orientation of NNE-SSW, with WNW, E, and ESE azimuths (Figure 2.3.10). Discontinuous open fractures with dip magnitudes  $< 65^\circ$  show a high degree of scatter but a NE-SW strike with NW azimuth predominates.

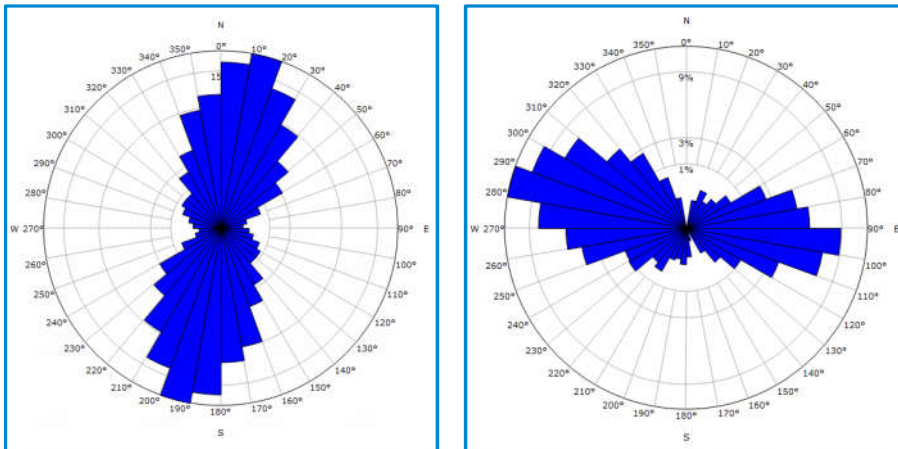
# Dip Statistics: Discontinuous Open Fracture



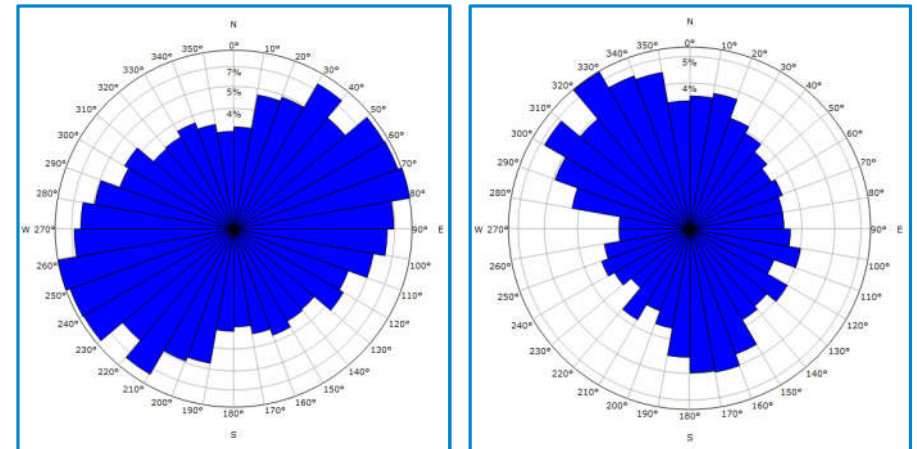
A total of 2,840 discontinuous open fractures were identified over the entire logged interval (2,494-1,748 m MD). Discontinuous-open-fracture dip statistics over the interval demonstrate a dominant strike orientation of NNE-SSW, with WNW and ESE azimuths. Dip magnitudes for this fracture type are highly variable, from horizontal to vertical, but mainly steeper than 70°.

# Dip Statistics: Discontinuous Open Fracture

$\geq 70^\circ$  dip magnitudes

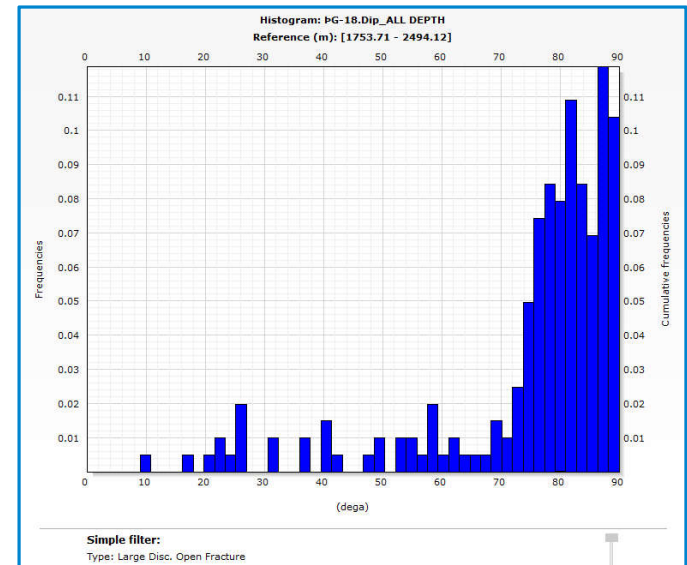
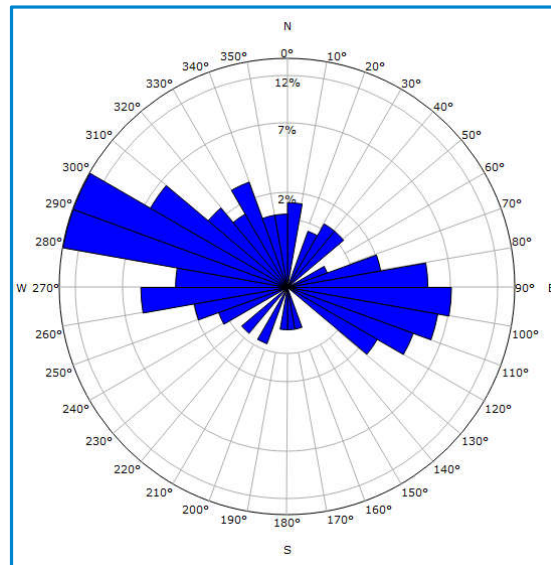
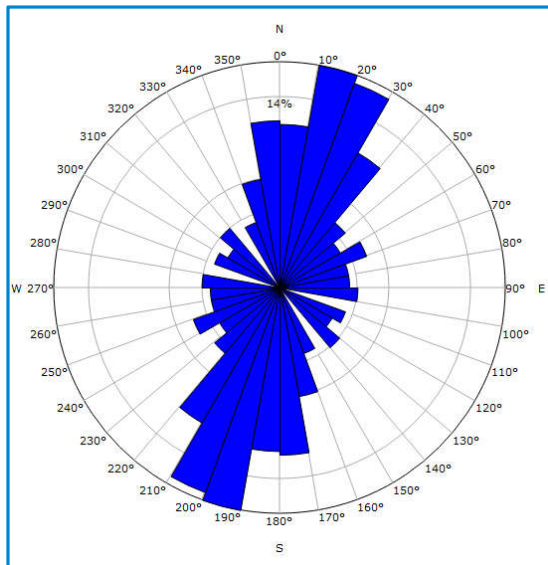


$< 70^\circ$  dip magnitudes



Discontinuous open fractures with dip magnitudes  $\geq 70^\circ$  show a dominant strike orientation of NNE-SSW, with WNW and ESE azimuths. Discontinuous open fractures with dip magnitudes  $< 70^\circ$  show a dominant strike orientation of ENE-WSW, with NNW and SSE azimuths.

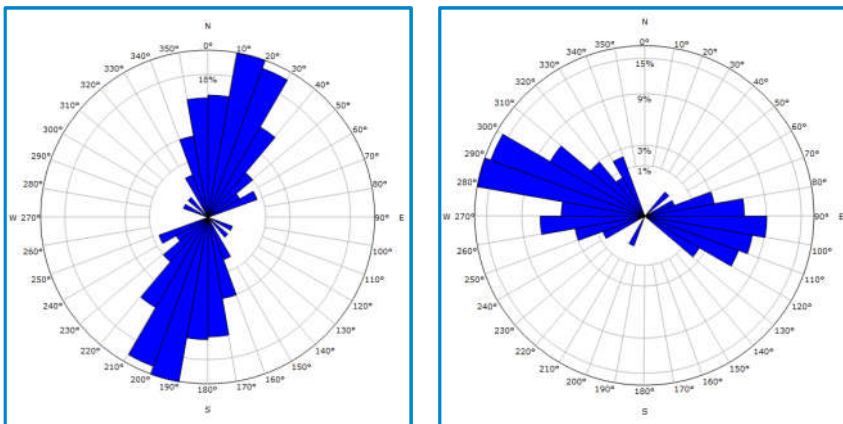
# Dip Statistics: Large Discontinuous Open Fracture



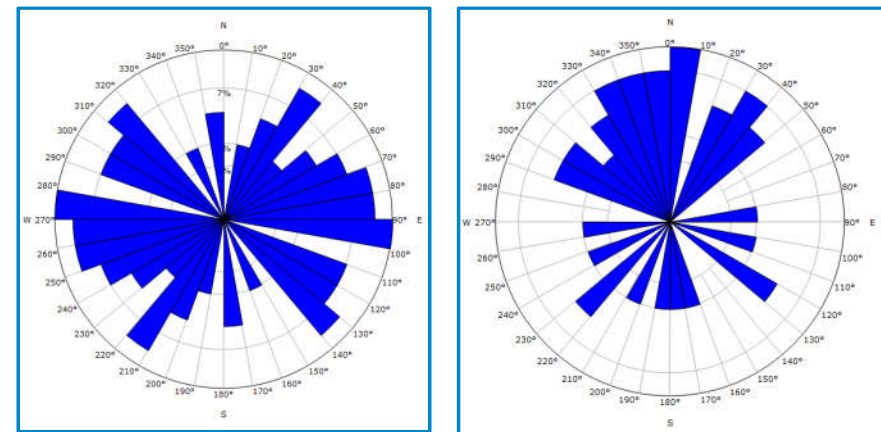
A total of 202 large discontinuous open fractures were identified over the entire logged interval (2,494-1,748 m MD). Large-discontinuous-open-fracture dip statistics over the interval demonstrate a dominant strike orientation of NNE-SSW, with WNW and ESE azimuths. Dip magnitudes for this fracture type are highly variable, from 10° to vertical, but mainly steeper than 70°.

# Dip Statistics: Large Discontinuous Open Fracture

$\geq 70^\circ$  dip magnitudes



$< 70^\circ$  dip magnitudes



Large discontinuous open fractures with dip magnitudes  $\geq 70^\circ$  show a dominant strike orientation of NNE-SSW, with WNW, ESE azimuths. Large discontinuous open fractures with dip magnitudes  $< 70^\circ$  show a high degree of scatter but E-W strike with Northerly azimuth predominate.

# Image Examples: Discontinuous, Large Discontinuous, Continuous and Large Continuous Open Fractures

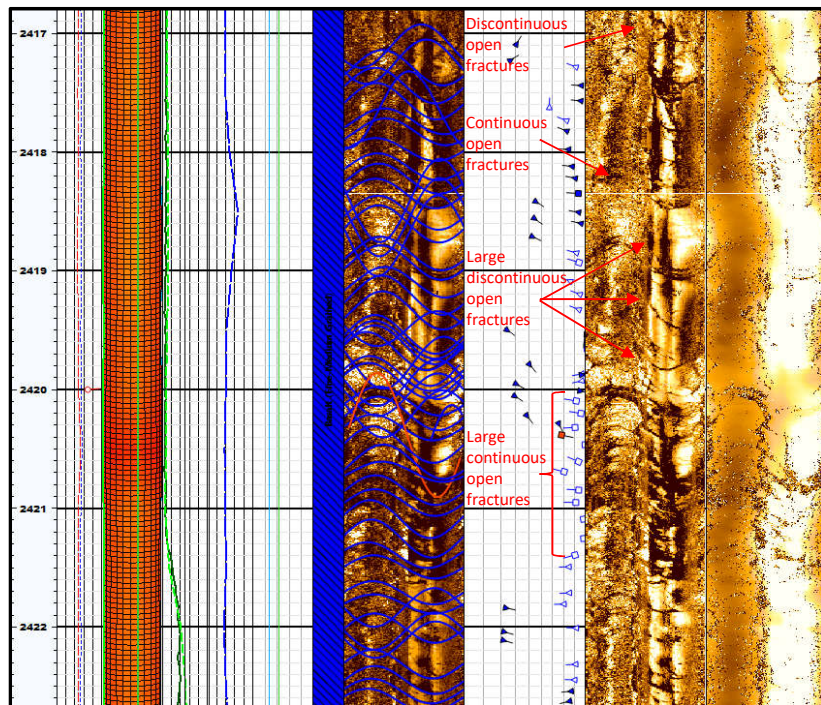


Image example of discontinuous, large discontinuous, continuous, and large continuous open fractures. Discontinuous open fracture is the dominant fracture type in the well PG-18.

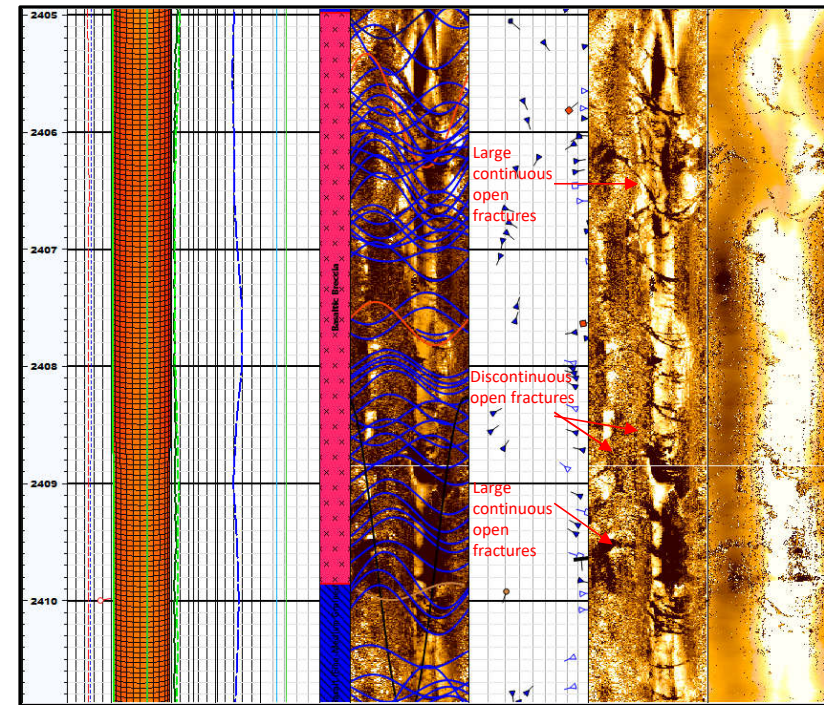


Image example of discontinuous, large discontinuous, and large continuous open fractures.

# Image Examples: Discontinuous, Large Discontinuous, Continuous and Large Continuous Open Fractures

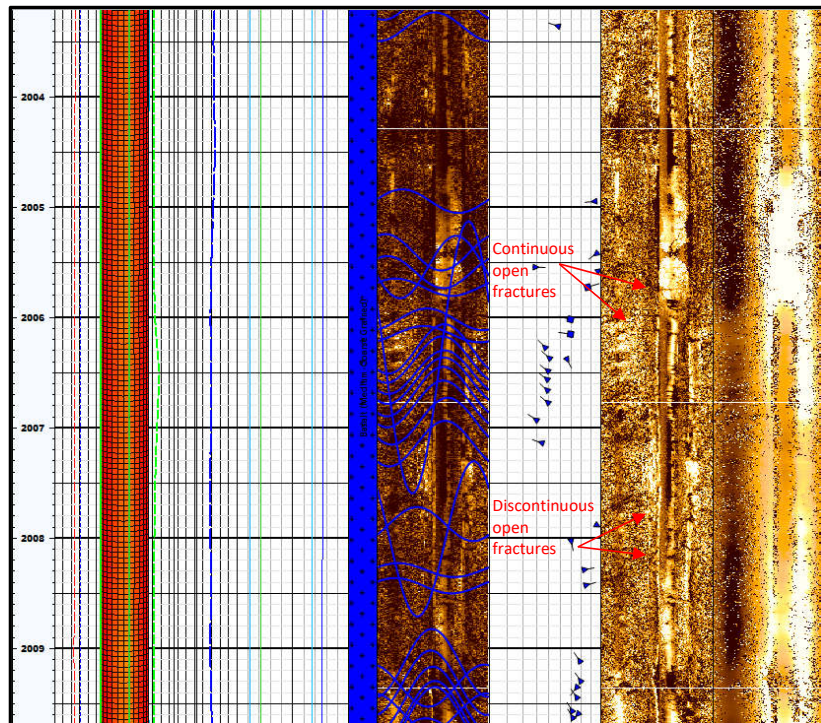


Image example of continuous and discontinuous open fractures.

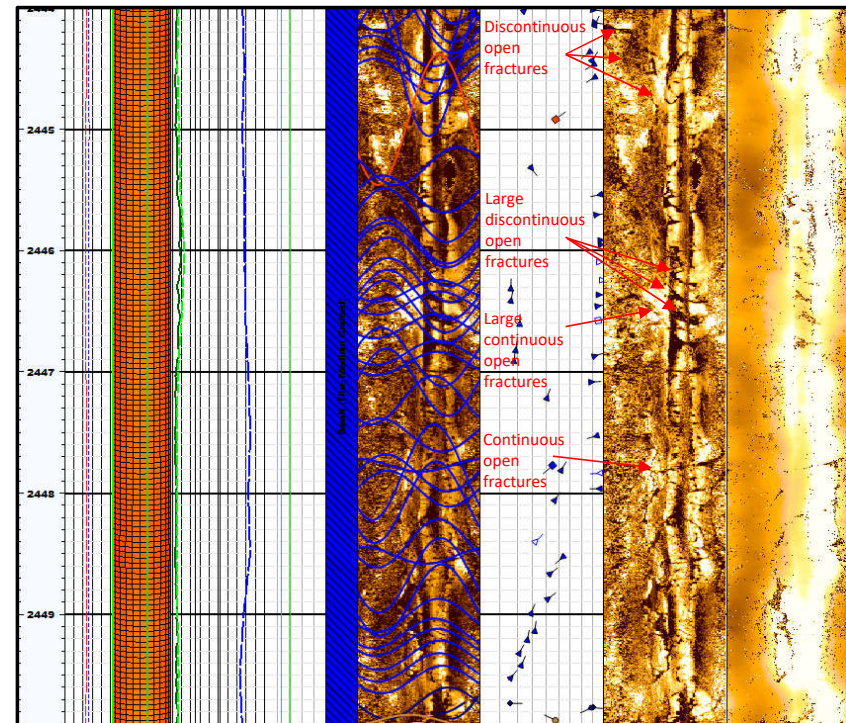
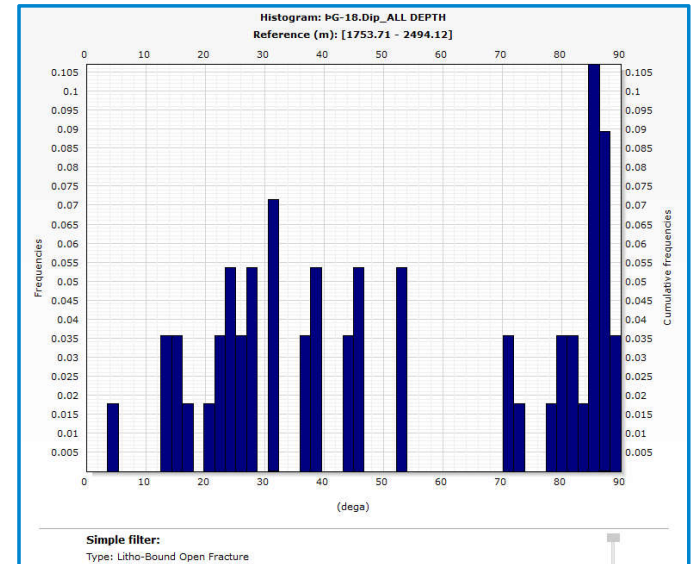
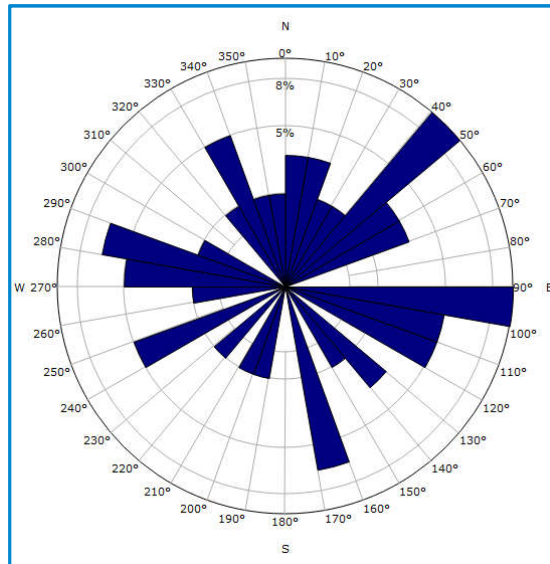
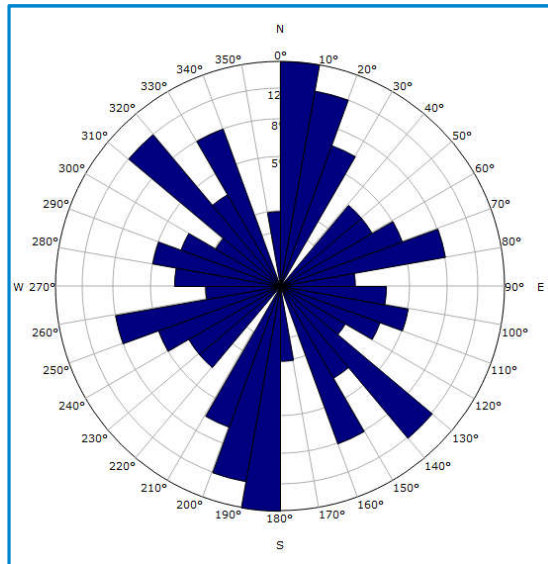


Image example of discontinuous, large discontinuous, continuous, and large continuous open fractures.

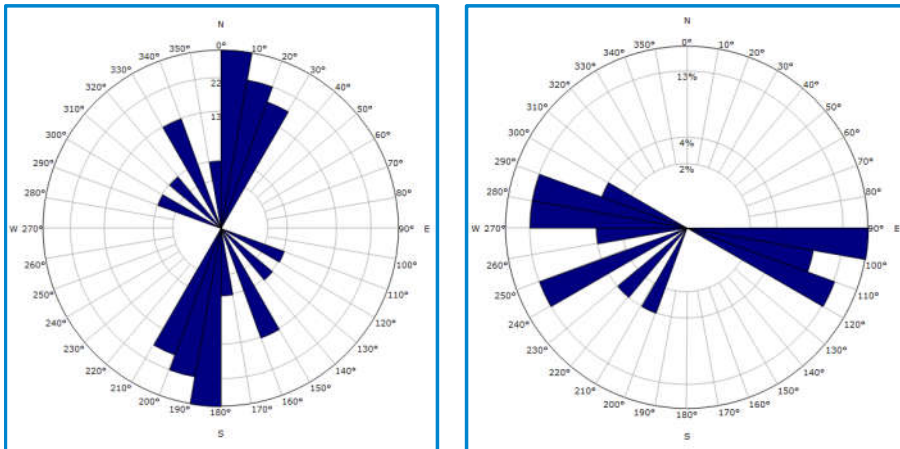
# Dip Statistics: Litho-bound Open Fracture



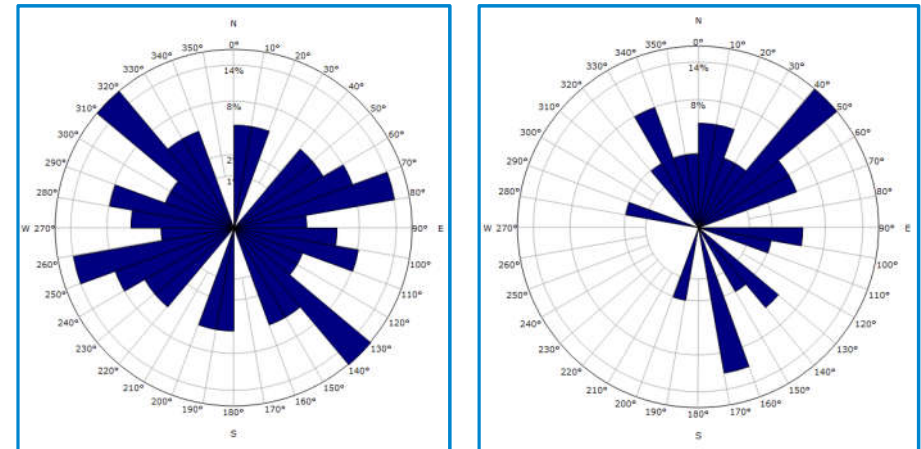
Only 56 litho-bound open fractures were recognized in the entire logged interval (2,494-1,748 m MD). Litho-bound-open-fracture dip statistics over the interval demonstrate dominant strike orientations of NNE-SSW, NW-SE, and ENE-WSW, with ESE, WNW, NE, and SSE azimuths. Dip magnitudes for this fracture type are highly variable, from nearly horizontal to vertical.

# Dip Statistics: Litho-bound Open Fracture

$\geq 70^\circ$  dip magnitudes



$< 70^\circ$  dip magnitudes



Litho-bound open fractures with dip magnitudes  $\geq 70^\circ$  show a dominant strike orientation of NNE-SSW, with ESE and WNW azimuths. Discontinuous open fractures with dip magnitudes  $< 70^\circ$  show a high degree of scatter but NW-SE and ENE-WSW strikes with NE and SSE azimuths predominate.

# Image Examples: Litho-bound Open Fractures

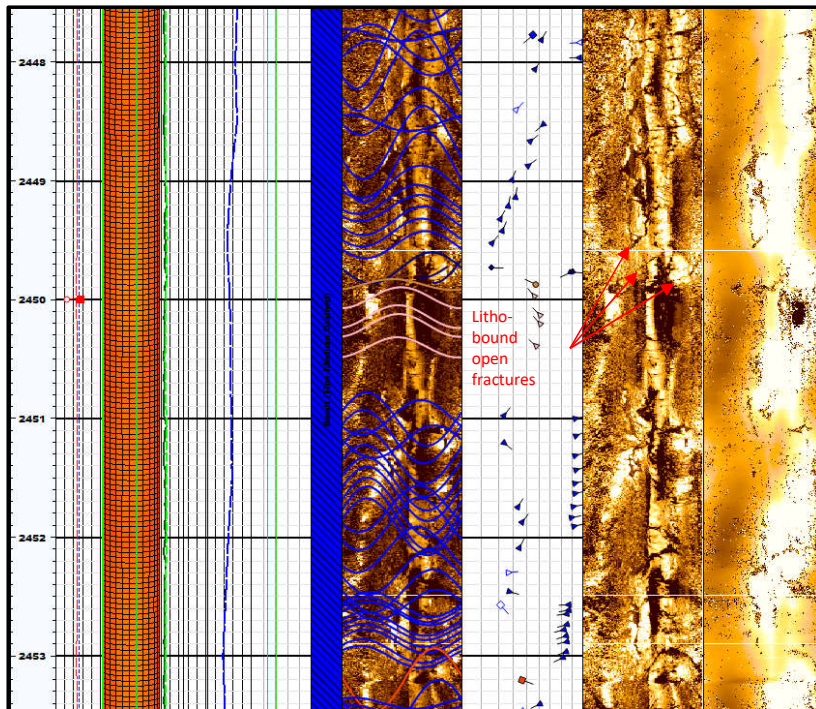


Image example of litho-bound open fractures. This fracture type has a low amplitude and is compartmentalized within individual lithologic units bounded and/or terminated by lithologic boundaries. The development of this fracture type is mainly associated with intrusion and/or possible intrusive rocks.

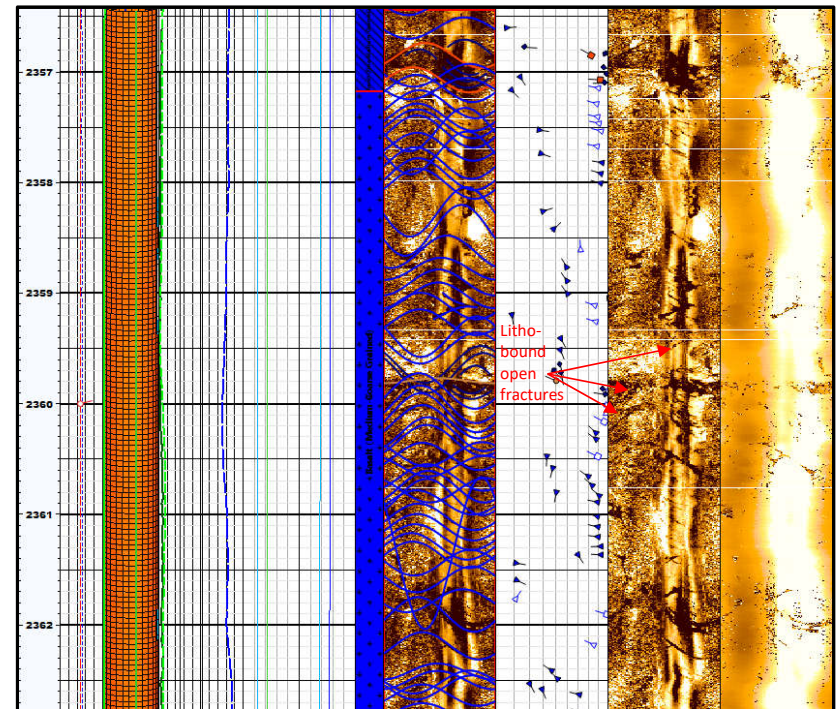
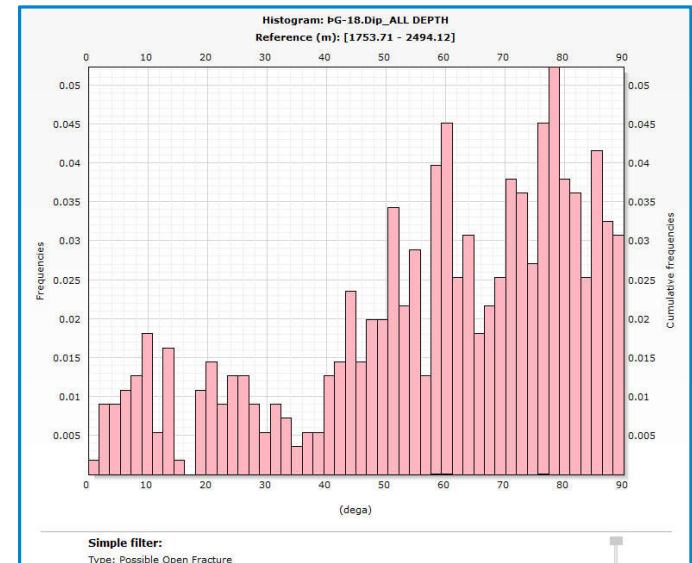
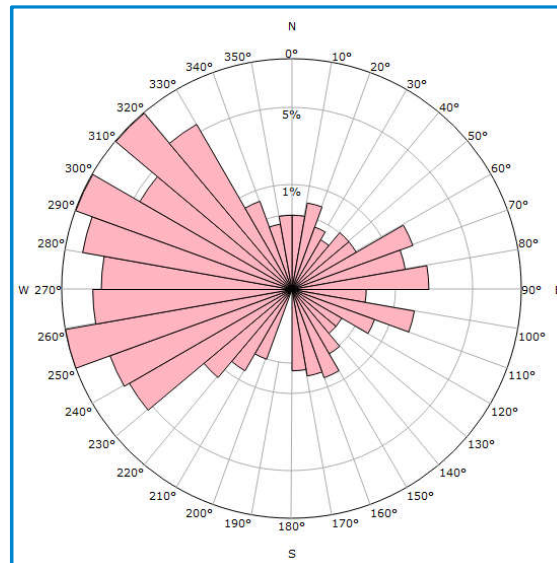
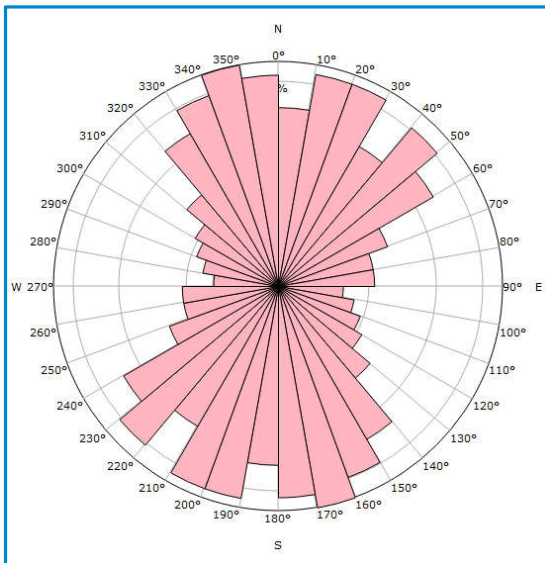


Image example of litho-bound open fractures.

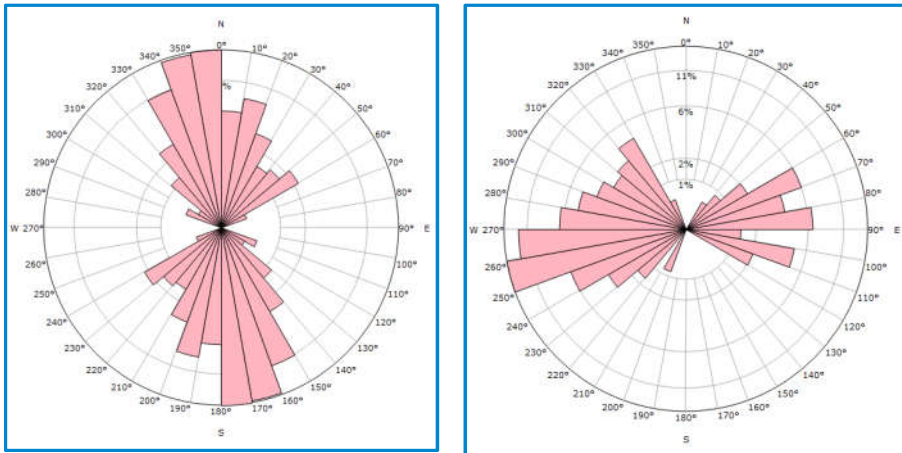
# Dip Statistics: Possible Open Fracture



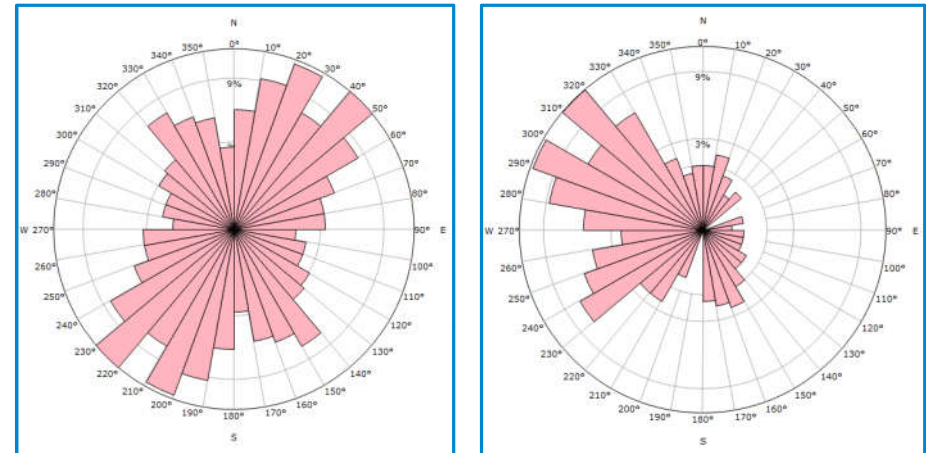
A total of 554 possible open fractures were recognized over the entire logged interval (2,494-1,748 m MD). Possible-open-fracture dip statistics in the interval demonstrate dominant strike orientations of NNW-SSE, NNE-SSW, and NE-SW, with westward (WNW, W, WSW) azimuth, and dip magnitudes that vary from nearly horizontal to vertical, but mainly  $>45^\circ$ .

# Dip Statistics: Possible Open Fracture

$\geq 70^\circ$  dip magnitudes



$< 70^\circ$  dip magnitudes



Possible open fractures with dip magnitudes of  $\geq 70^\circ$  show dominant strike orientations of NNW-SSE, with WSW and ENE azimuths. Possible open fractures with dip magnitudes of  $< 70^\circ$  demonstrate dominant strike orientations of NNE-SSW and NE-SW, with WNW and NW azimuths.

# Image Examples: Possible Open Fracture

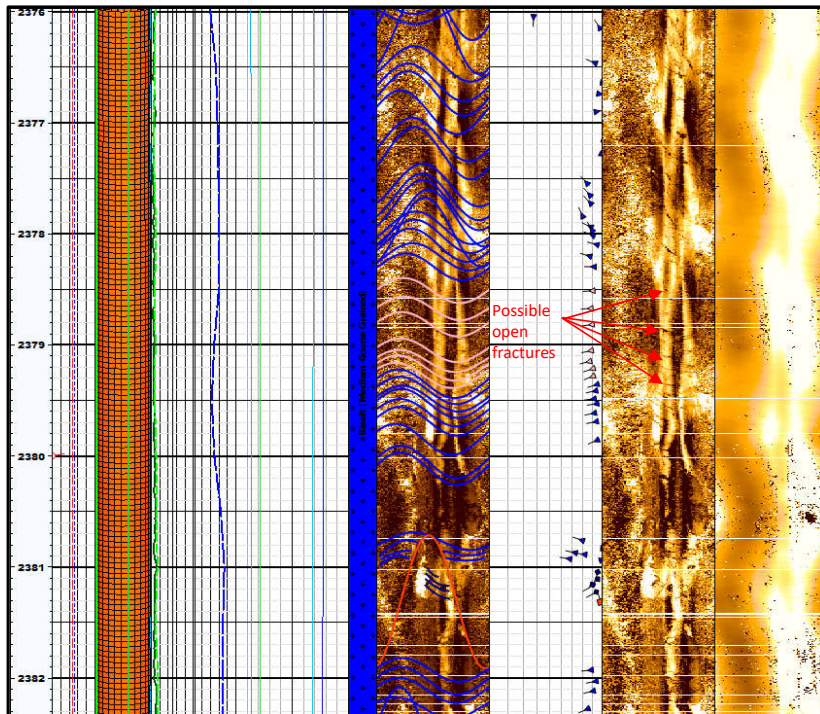


Image example of possible open fractures. This fracture type has a low amplitude and is discontinuous across the borehole diameter, due to poor image quality caused by bad hole condition or logging artifacts

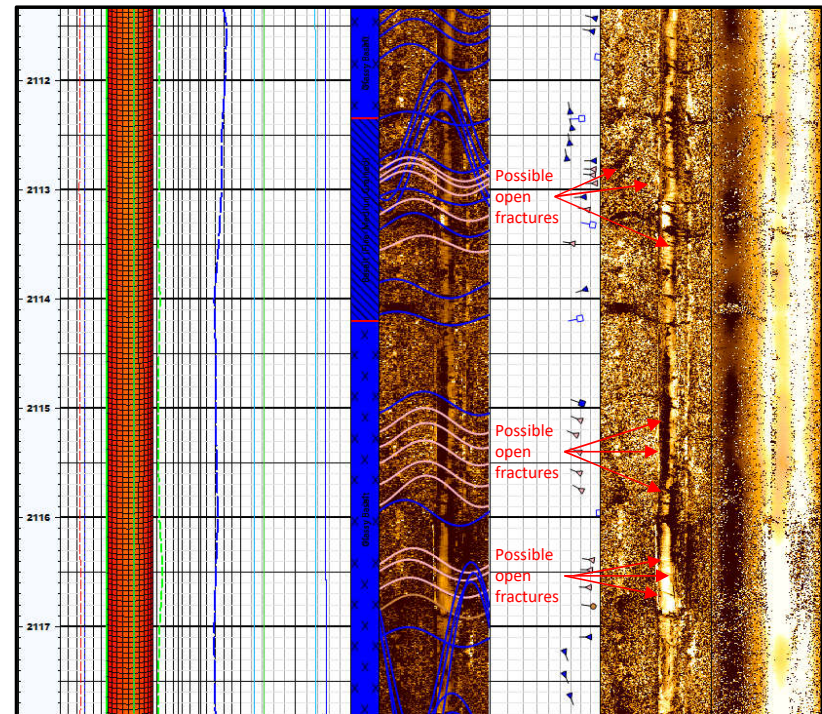
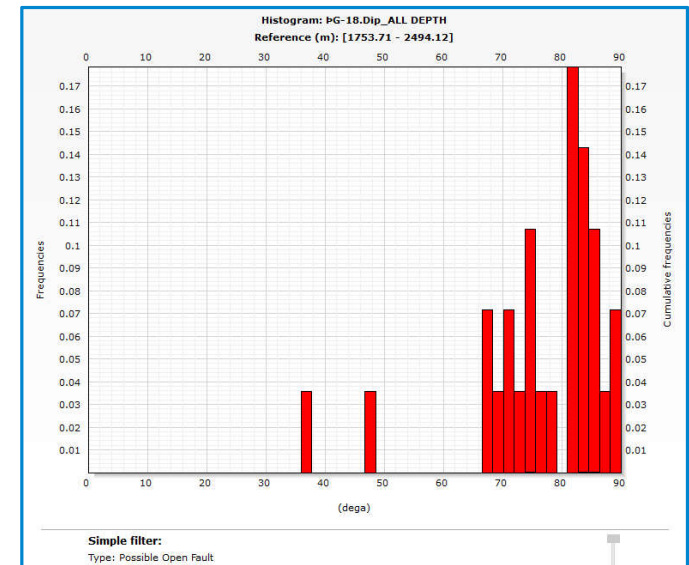
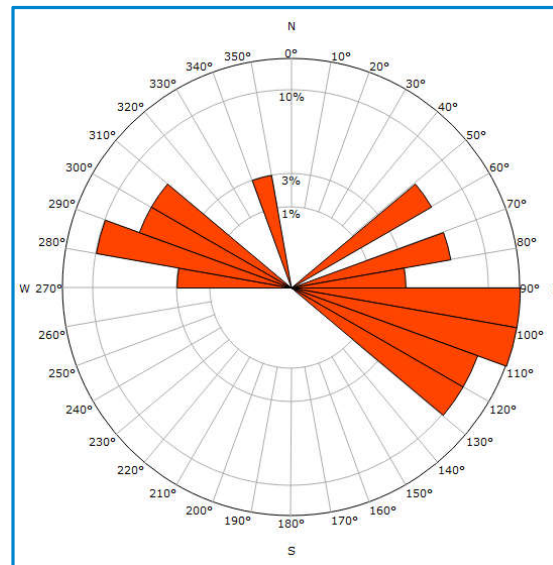
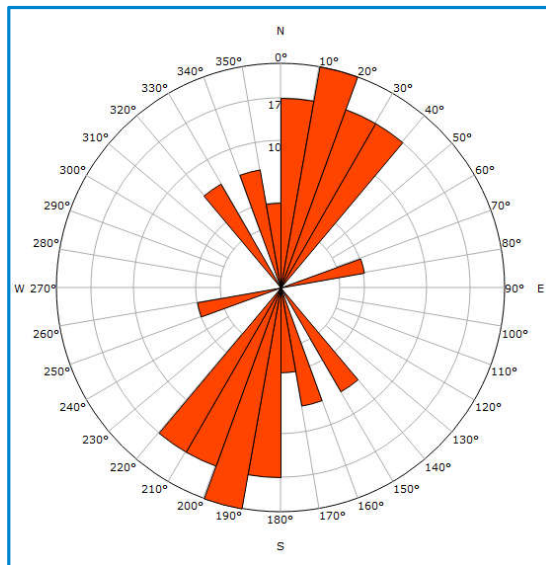


Image example of possible open fractures.

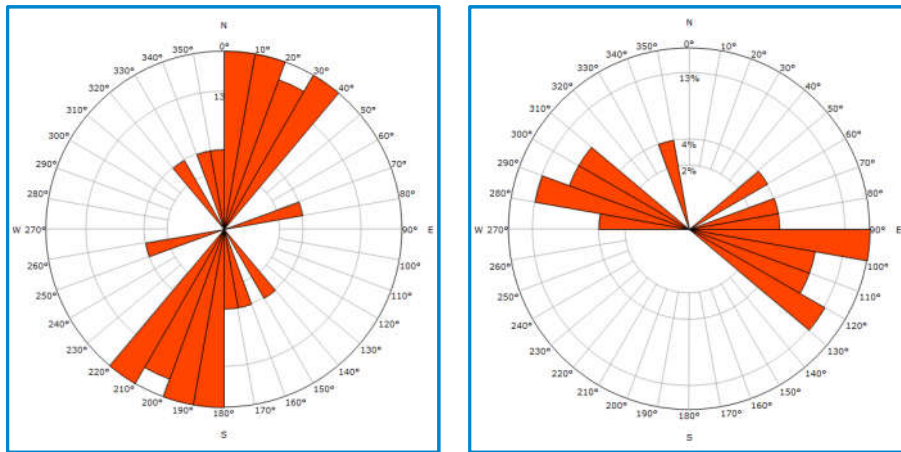
# Dip Statistics: Possible Open Fault



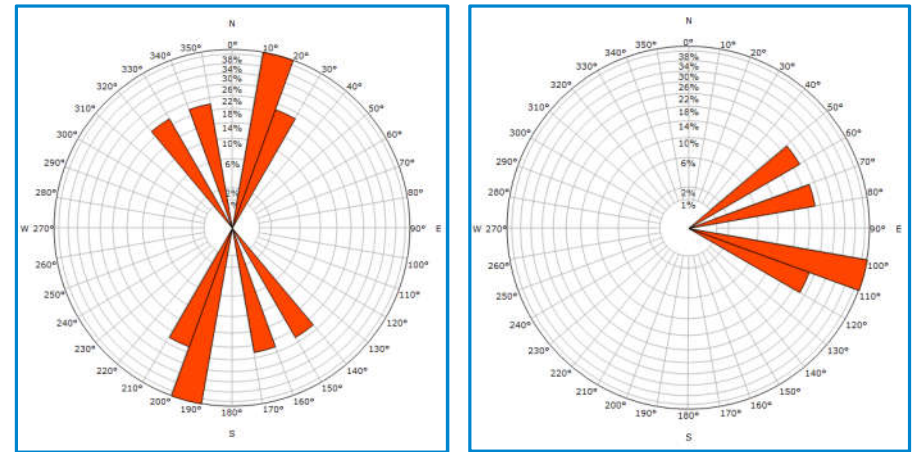
A total of 28 possible open faults were identified in the logged interval. Possible-open-fault dip statistics demonstrate a dominant strike orientation of NNE-SSW, with ESE and WNW azimuths. Dip magnitudes vary from 38° to vertical, but are mainly >70°.

# Dip Statistics: Possible Open Fault

$\geq 70^\circ$  dip magnitudes



$< 70^\circ$  dip magnitudes



Possible open faults with dip magnitudes  $\geq 70^\circ$  show dominant strike orientations of NNE-SSW with ESE and WNW azimuth; those with dip magnitudes  $< 70^\circ$  have dominant strike orientations of NNE-SSW and NNW-SSE with ESE and ENE azimuths.

## Image Examples: Possible Open Fault

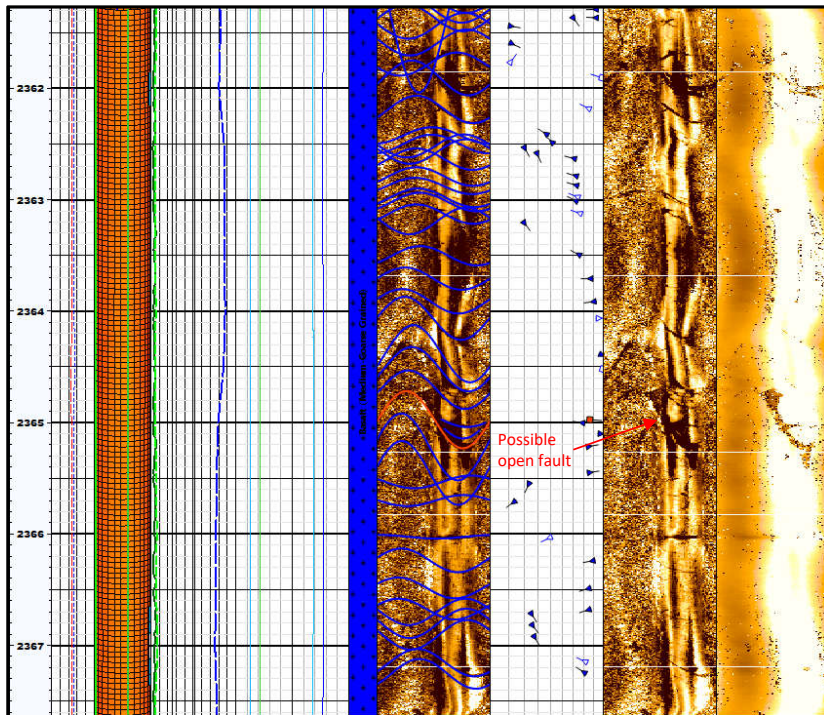


Image example of possible open fault at 2,365 m MD. Continuous, discontinuous, large discontinuous, and large continuous open fractures are well developed near the fault plane. Abrupt terminations of fractures are also observed on the fault's plane.

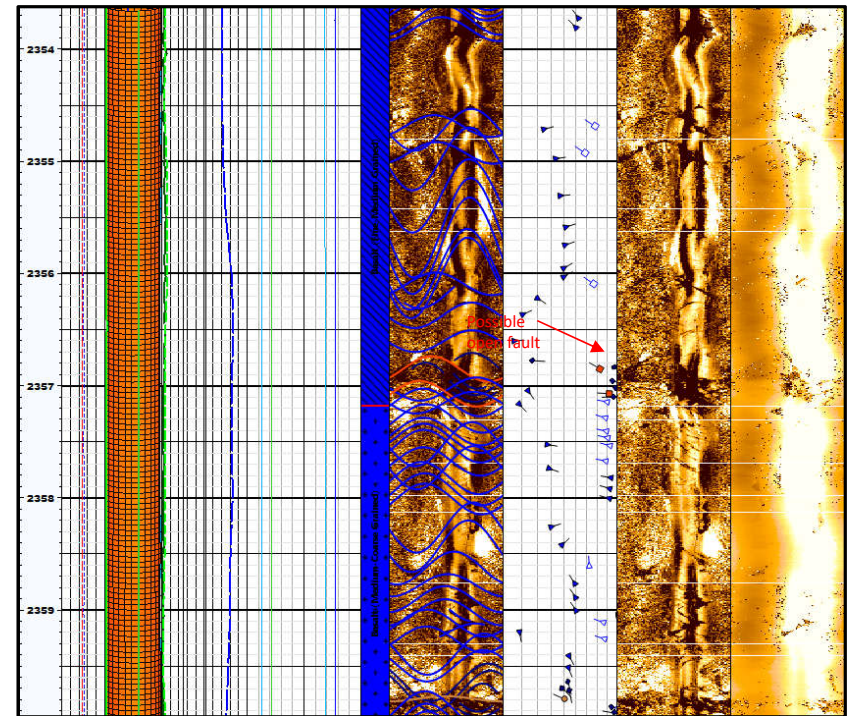


Image example of possible open faults at 2,356.9 m MD and 2,357.1 m MD. Continuous, discontinuous, large discontinuous, and large continuous open fractures are well developed near the fault plane. Large low-amplitude events and abrupt terminations of fractures are also observed on the fault's plane.

# Image Examples: Possible Open Fault

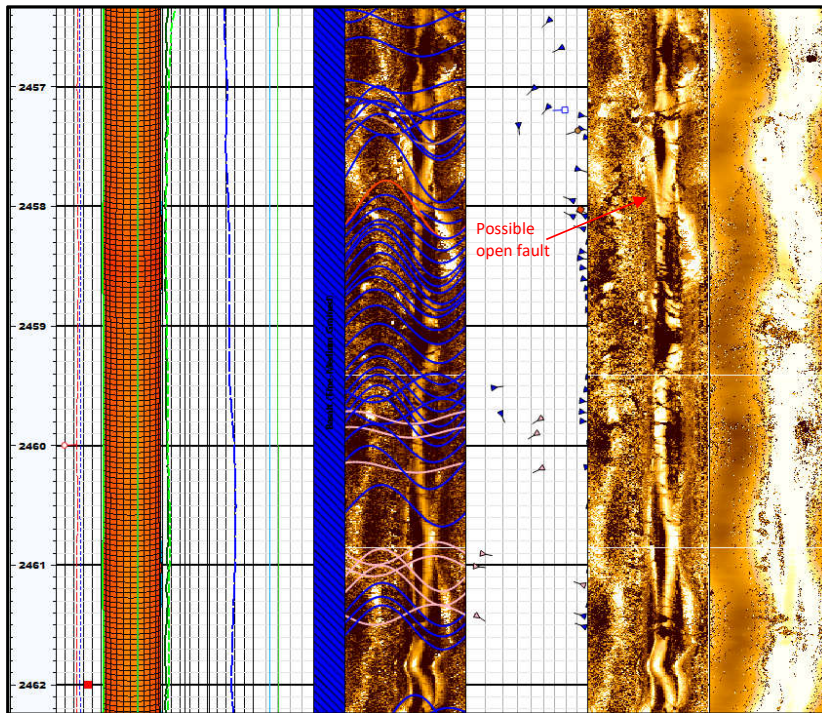


Image example of possible open fault at 2,458 m MD. Continuous, discontinuous, and large continuous open fractures are well developed near the fault plane. Sharp facies change and abrupt terminations of fractures are also observed on the fault's plane.

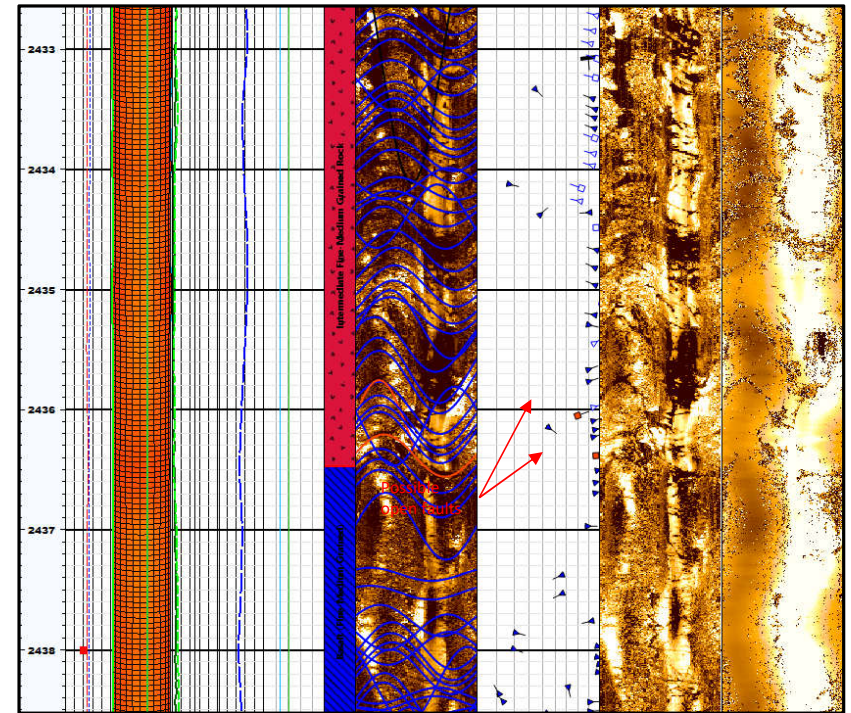
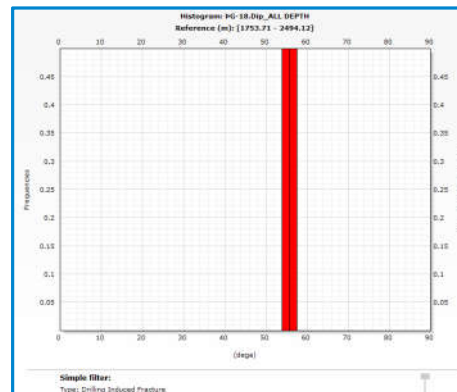
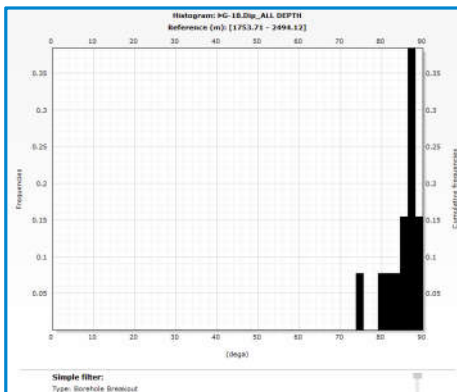
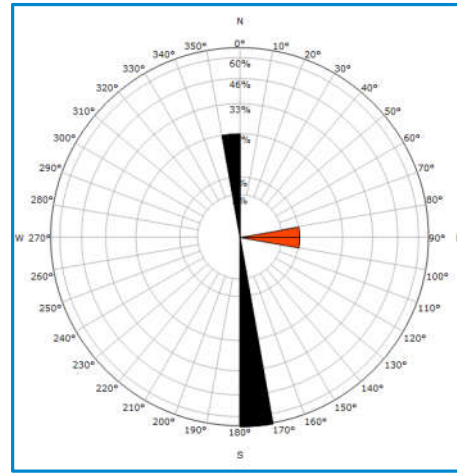
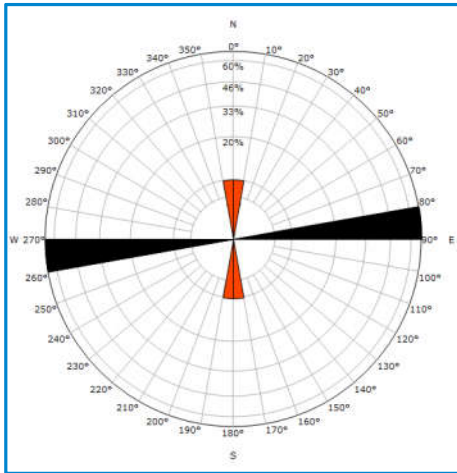


Image example of possible open faults at 2,436 m MD and 2,436.4 m MD. Continuous, discontinuous, large discontinuous, and large continuous open fractures are well developed near the fault plane. Abrupt terminations of fractures and sharp facies change are also observed on the fault's plane.

# Dip Statistics: Drilling Induced Fracture and Borehole Breakouts



A total of 2 drilling-induced fractures were identified, both of the two drilling induced fractures have a strike orientation of N-S. A total of 13 borehole breakouts were identified, with dip statistics showing a dominant strike of E-W/ENE-WSW (perpendicular to the strike orientation of the drilling-induced fractures)

# Image Examples: Drilling Induced Fractures and Borehole Breakouts

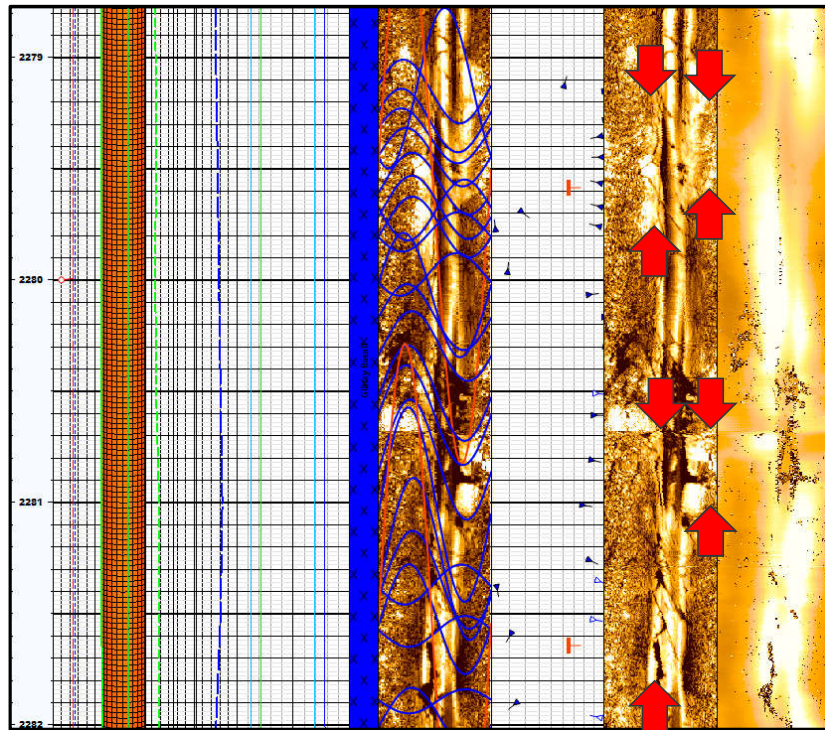


Image example of drilling induced fractures. Fractures were oriented by fitting a sinusoid where these features occur on directly opposite sides of the borehole wall.

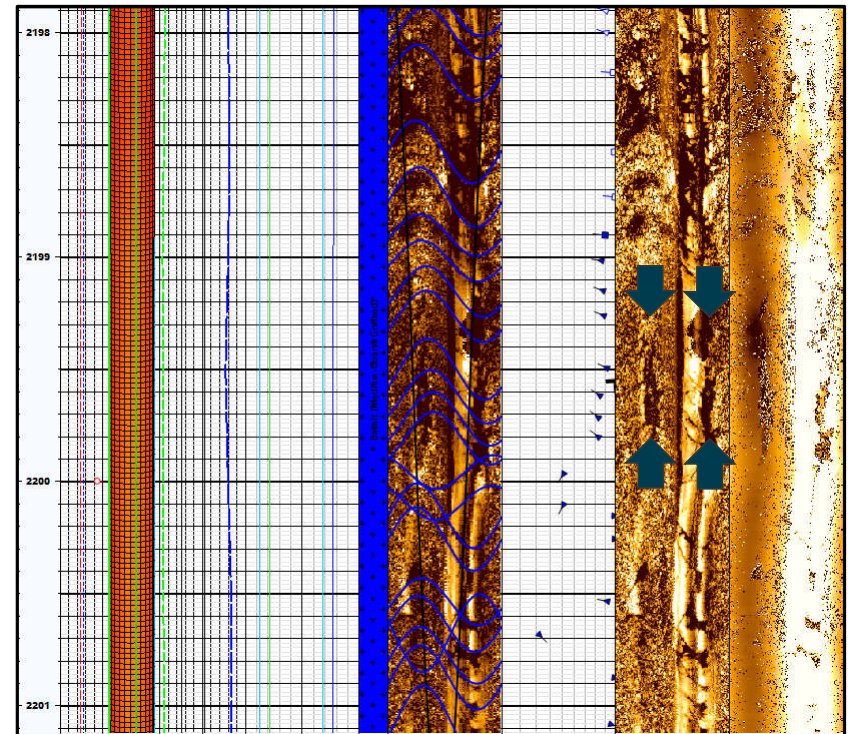
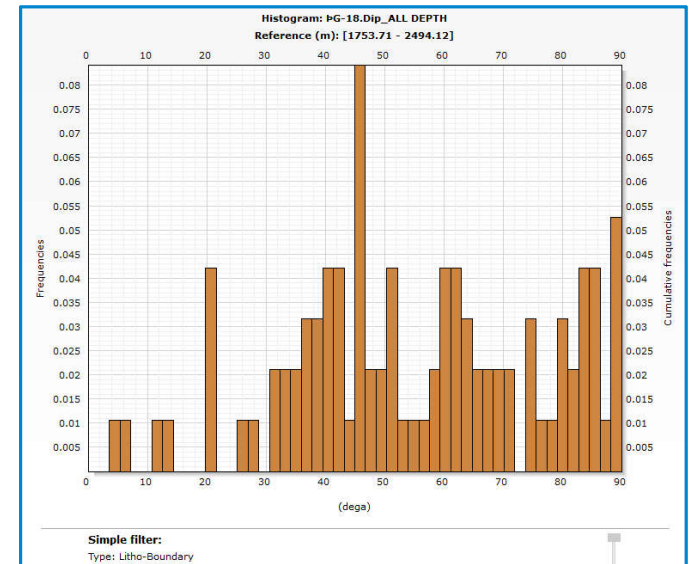
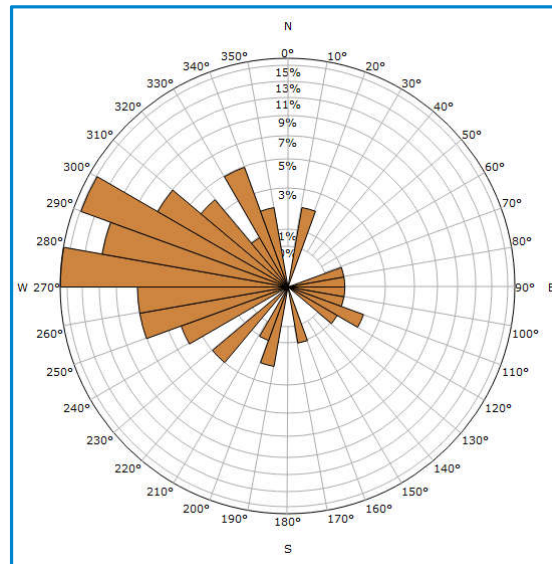
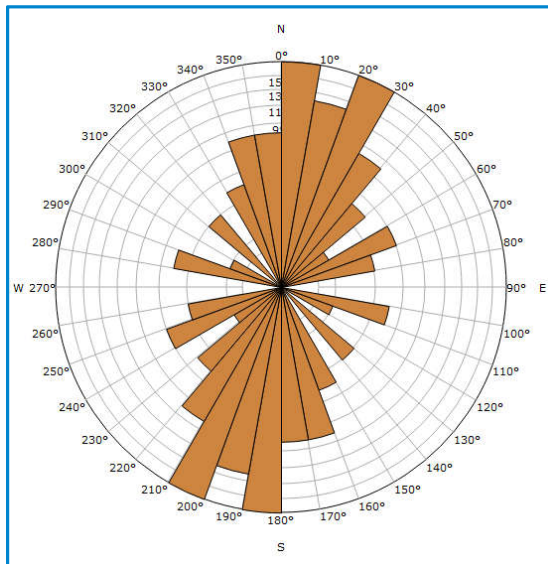


Image example of borehole breakouts. Breakouts were oriented by fitting a sinusoid where these features occur on directly opposite sides of the borehole wall.

# Dip Statistics: Lithological Boundary



Lithologic boundary dip statistics over the interval of 2,494-1,748 m MD. Dip statistics of lithologic boundaries show a dominant azimuth orientation of westerly (WSW, W, WNW). Dip magnitudes are also highly variable, from nearly horizontal to vertical.

# Image Examples: Lithological Boundary

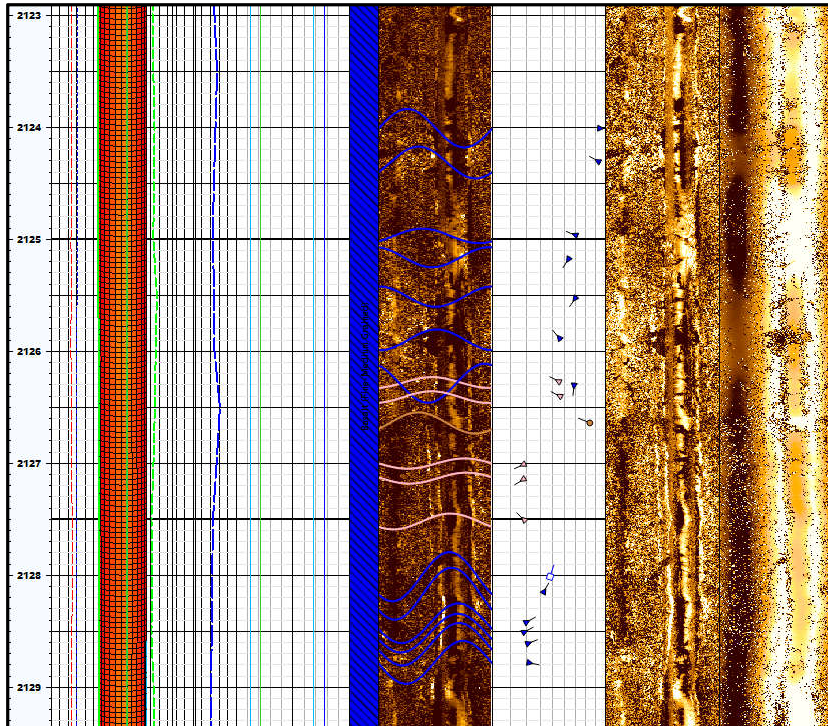


Image example of lithologic boundary.

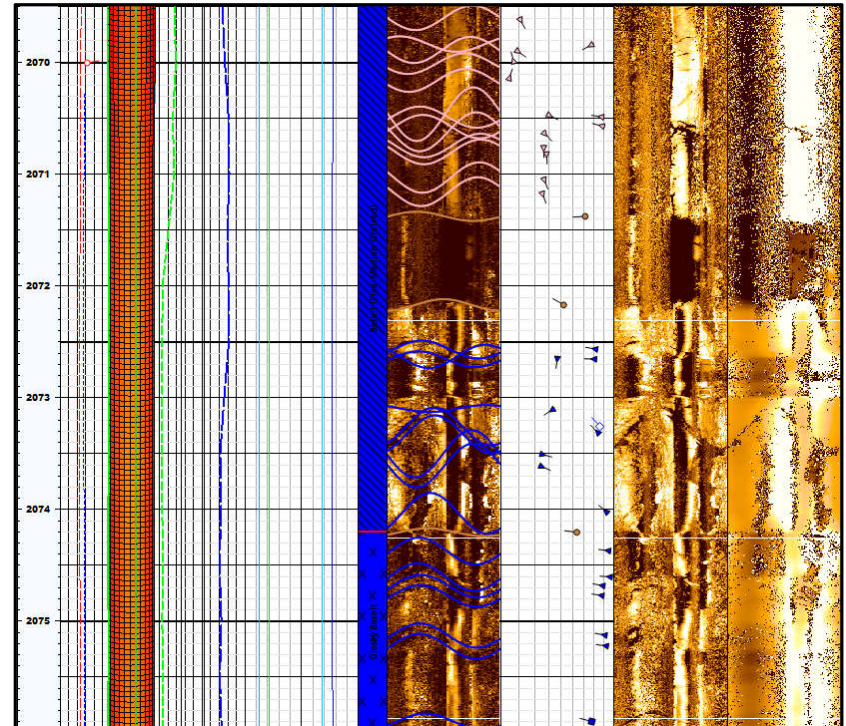
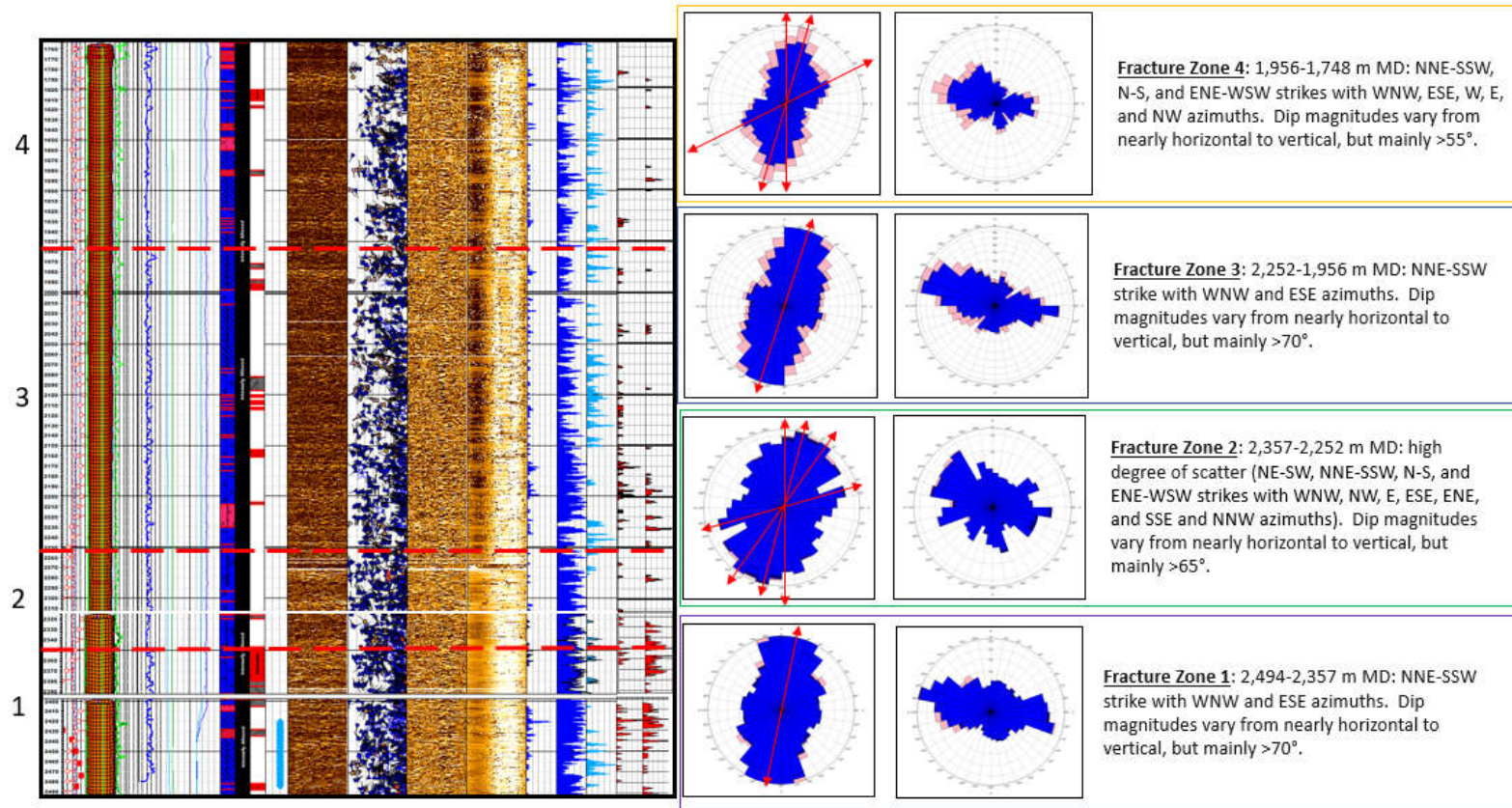


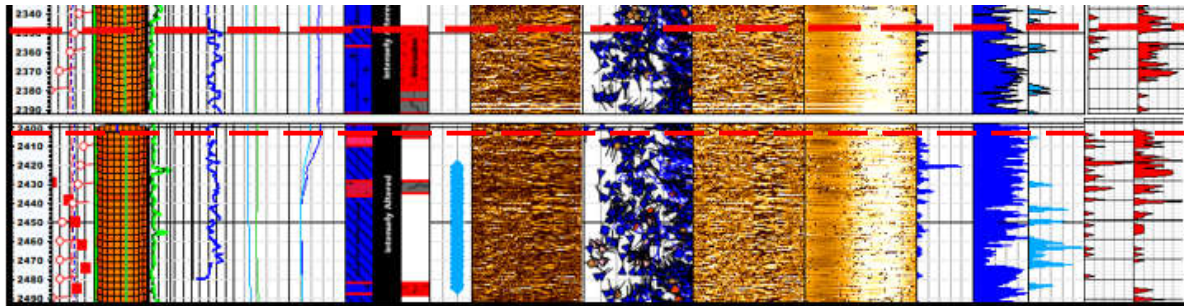
Image example of lithologic boundary.

# ABI Open Fracture Zonation

# Fracture Zonation

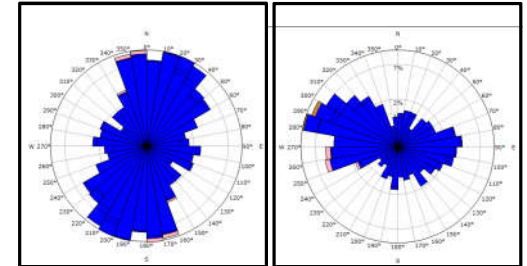


# Fracture Zone 1

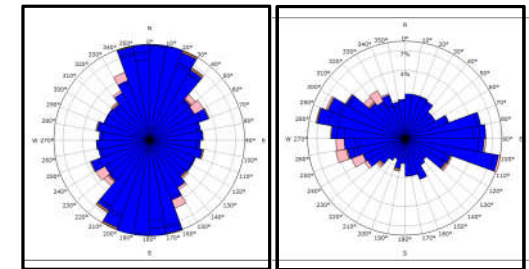


1b  
(2,404-2,357 m MD)

1a  
(2,494-2,404 m MD)

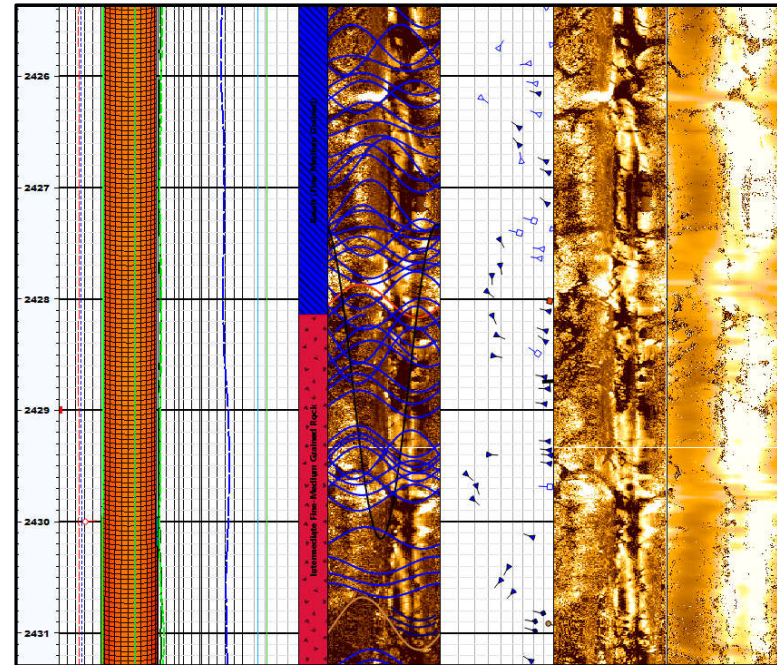
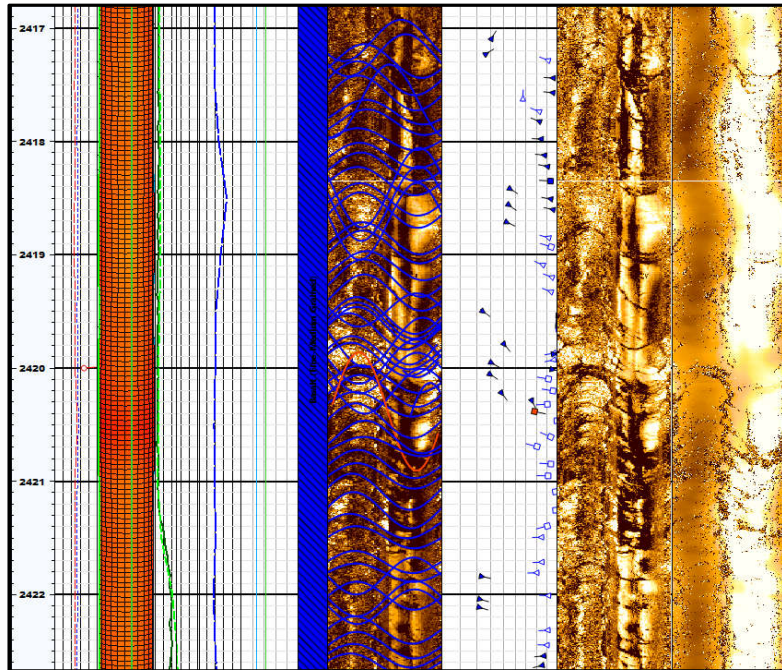


**Fracture Zone 1b:** 2,344-2,404 m MD: Intrusion interval; NNE-SSW, N-S, and NNW-SSE strikes with WNW, WSW, and E azimuths. Dip magnitudes vary from nearly horizontal to vertical, but mainly  $>70^\circ$ .



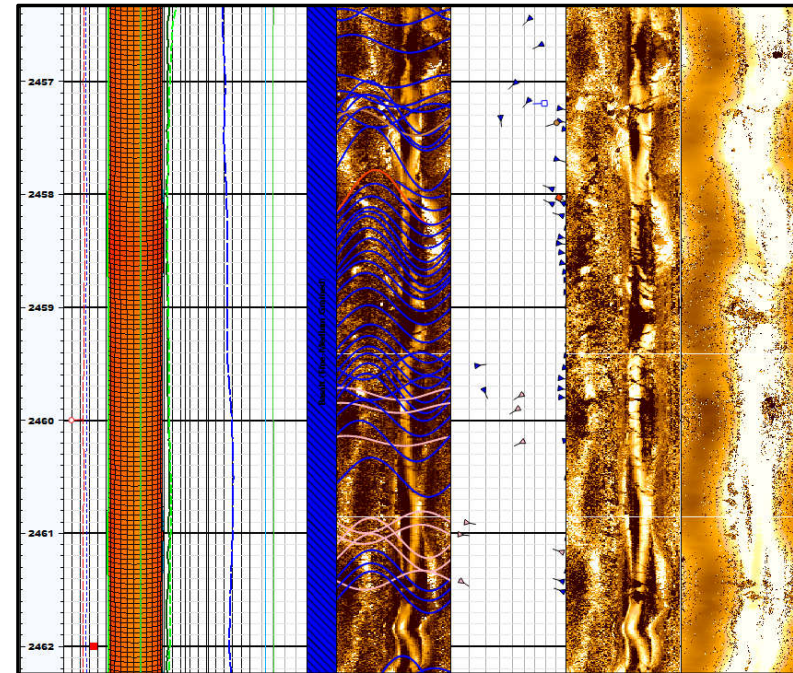
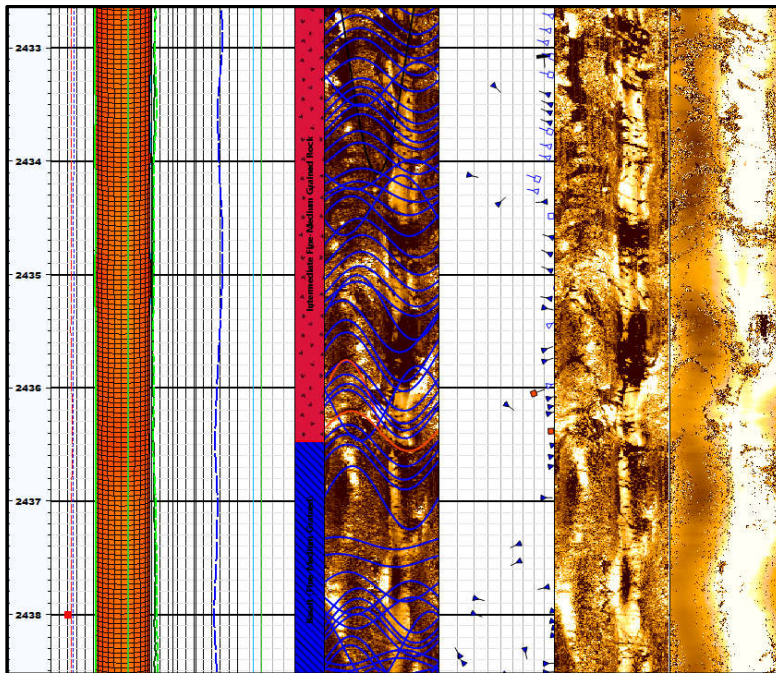
**Fracture Zone 1a:** 2,404-2,494 m MD: NNE-SSW and N-S strikes with WNW, W, E, and ESE azimuths. Dip magnitudes vary from nearly horizontal to vertical, but mainly  $>70^\circ$ .

## Examples of Feed Zones, Fracture Zone 1 (2,494-2,357 m MD)



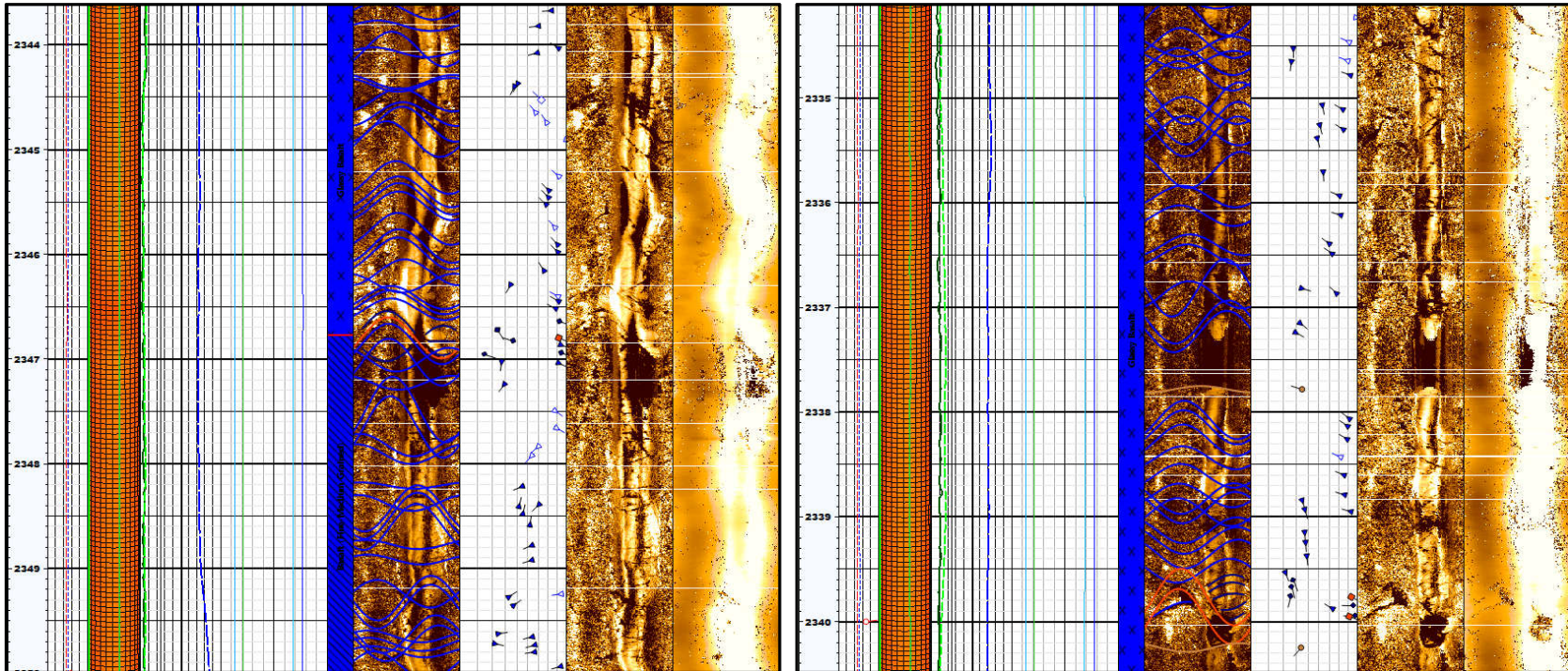
The “size 2” feed zone at 2,420-2,485 m MD is possibly associated with a high angle (68°) NNE-SSW possible open fault at 2,420.4 m MD, a high angle (86°) NNE-SSW possible open fault at 2,428 m MD, a high angle (70°) NNW-SSE possible open fault at 2,436.1 m MD, a high angle (87°) N-S possible open fault at 2,436.4 m MD, a high angle (79°) NNE-SSW possible open fault at 2,443.4 m MD, a lower angle (47°) NW-SE possible open fault at 2,444.8 m MD, a lower angle (37°) NNE-SSW possible open fault at 2,453.2 m MD, a high angle (83°) NNE-SSW possible open fault at 2,458 m MD, a high angle (89°) NNE-SSW possible open fault at 2,485.6 m MD, a high angle (71°) possible open fault at 2,485.8 m MD, and some large continuous and discontinuous open fractures at 2,417-2,491 m MD which demonstrate a dominant strike orientation of NNE-SSW, with WNW azimuth, and dip magnitudes that vary from 20° to vertical but are mainly >70°.

## Examples of Feed Zones, Fracture Zone 1 (2,494-2,357 m MD)



The “size 2” feed zone at 2,420-2,485 m MD is possibly associated with a high angle (68°) NNE-SSW possible open fault at 2,420.4 m MD, a high angle (86°) NNE-SSW possible open fault at 2,428 m MD, a high angle (70°) NNW-SSE possible open fault at 2,436.1 m MD, a high angle (87°) N-S possible open fault at 2,436.4 m MD, a high angle (79°) NNE-SSW possible open fault at 2,443.4 m MD, a lower angle (47°) NW-SE possible open fault at 2,444.8 m MD, a lower angle (37°) NNE-SSW possible open fault at 2,453.2 m MD, a high angle (83°) NNE-SSW possible open fault at 2,458 m MD, a high angle (89°) NNE-SSW possible open fault at 2,485.6 m MD, a high angle (71°) possible open fault at 2,485.8 m MD, and some large continuous and discontinuous open fractures at 2,417-2,491 m MD which demonstrate a dominant strike orientation of NNE-SSW, with WNW azimuth, and dip magnitudes that vary from 20° to vertical but are mainly >70°.

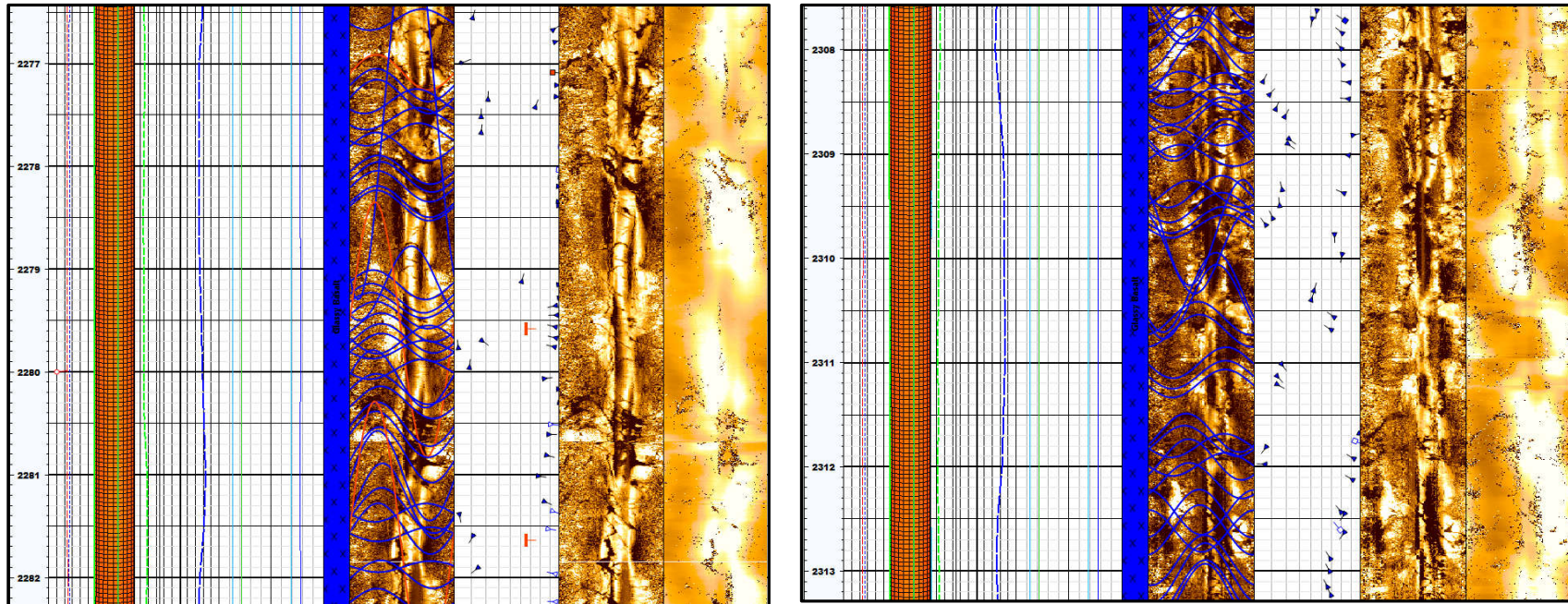
## Examples of Large Open Fractures and Possible Open Fault, Fracture Zone 2 (2,357-2,252 m MD)



Large continuous and discontinuous open fractures in Fracture Zone 2 (2,357-2,252 m MD) are observed at 2,344-2,357 m MD, 2,338-2,340 m MD, 2,311.5-2,313 m MD, 2,277-2,285 m MD, 2,263-2,267 m MD, 2,253-2,255 m MD, 2,333-2,335 m MD, and 2,326-2,330 m MD, which demonstrate a dominant strike orientation of NNE-SSW with WNW and ESE azimuths, and dip magnitudes that vary from approximately  $20^\circ$  to vertical, but are mainly  $>75^\circ$ .

Possible open faults were recognized at 2,357 m MD, 2,356.8 m MD, 2,346.8 m MD, 2,340 m MD, 2,339.7 m MD, 2,319.5 m MD, 2,303.4 m MD, and 2,277.1 m MD, which demonstrate a dominant strike orientation of NNE-SSW with ESE and WNW azimuths, and dip magnitudes range from  $70^\circ$  to nearly vertical ( $85^\circ$ ).

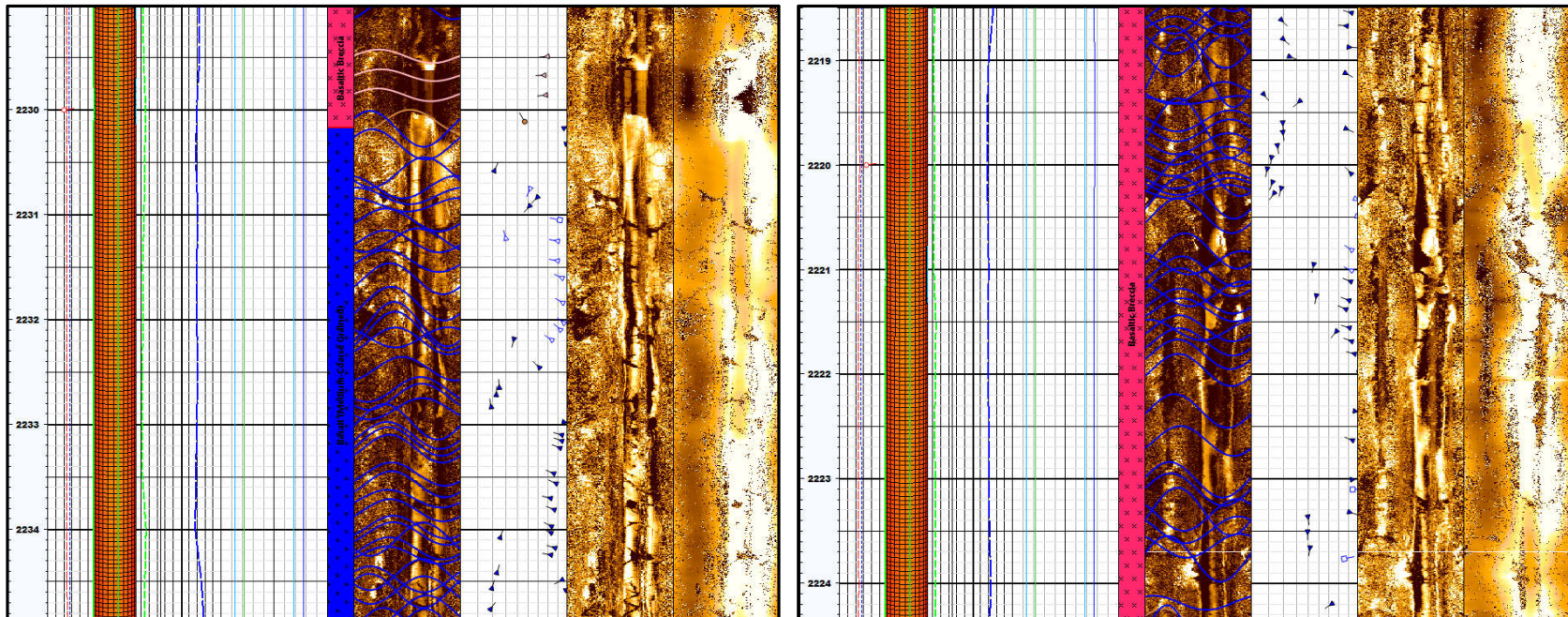
## Examples of Large Open Fractures and Possible Open Fault, Fracture Zone 2 (2,357-2,252 m MD)



Large continuous and discontinuous open fractures in Fracture Zone 2 (2,357-2,252 m MD) are observed at 2,344-2,357 m MD, 2,338-2,340 m MD, 2,311.5-2,313 m MD, 2,277-2,285 m MD, 2,263-2,267 m MD, 2,253-2,255 m MD, 2,333-2,335 m MD, and 2,326-2,330 m MD, which demonstrate a dominant strike orientation of NNE-SSW with WNW and ESE azimuths, and dip magnitudes that vary from approximately  $20^\circ$  to vertical, but are mainly  $>75^\circ$ .

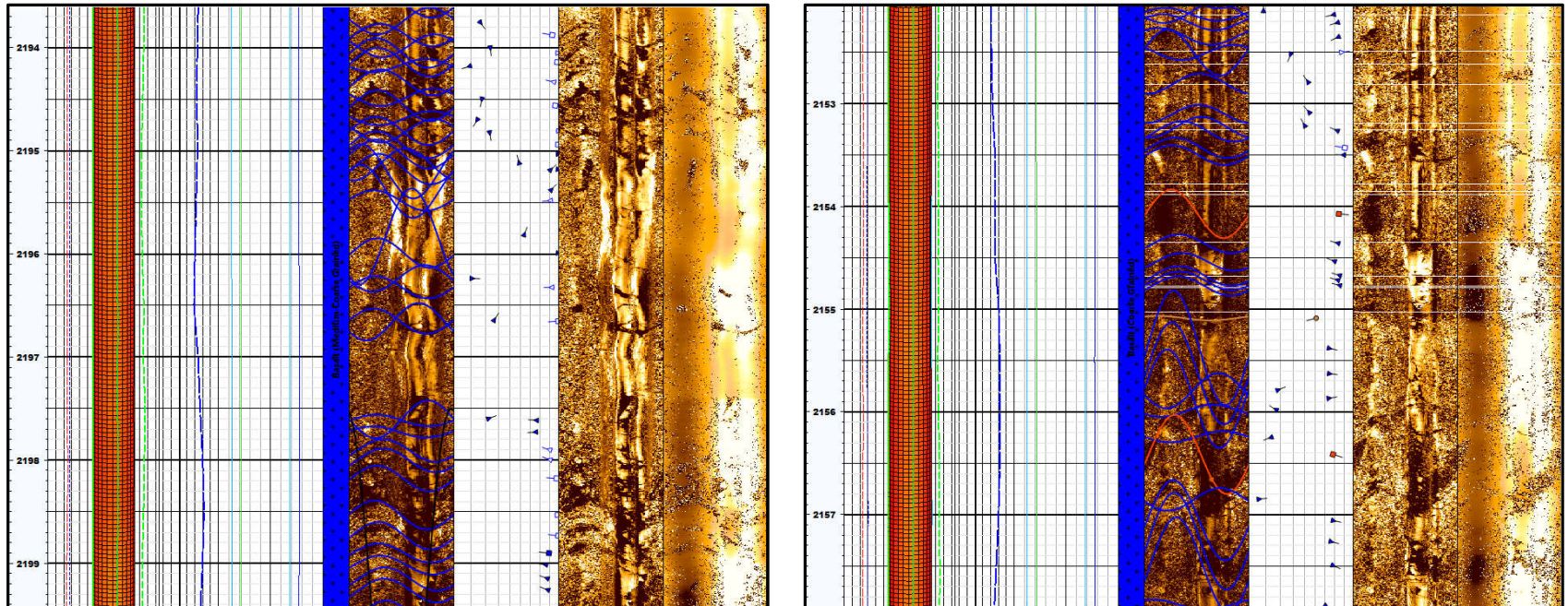
Possible open faults were recognized at 2,357 m MD, 2,356.8 m MD, 2,346.8 m MD, 2,340 m MD, 2,339.7 m MD, 2,319.5 m MD, 2,303.4 m MD, and 2,277.1 m MD, which demonstrate a dominant strike orientation of NNE-SSW with ESE and WNW azimuths, and dip magnitudes range from  $70^\circ$  to nearly vertical ( $85^\circ$ ).

## Examples of Large Open Fractures and Possible Open Fault, Fracture Zone 3 (2,252-1,956 m MD)



Large continuous and discontinuous open fractures in Fracture Zone 3 (2,252-1,956 m MD) are observed at 2,230-2,233 m MD, 2,223-2,224 m MD, 2,220-2,221 m MD, 2,215 m MD, 2,213.7 m MD, 2,205-2,206 m MD, 2,201.8 m MD, 2,197.5-2,199 m MD, 2,193-2,197 m MD, 2,185-2,190 m MD, 2,177-2,179 m MD, 2,170-2,174 m MD, 2,167-2,168 m MD, 2,156.5-2,161 m MD, 2,152-2,154 m MD, 2,139-2,141 m MD, 2,132.5 m MD, 2,128 m MD, 2,116-2,122 m MD, 2,111-2,115 m MD, 2,103 m MD, 2,100 m MD, 2,094-2,096 m MD, 2,087-2,089 m MD, 2,072-2,074 m MD, 2,036-2,043 m MD, 2,033-2,034 m MD, 1,990.5 m MD, and 1,978-1,983 m MD, which demonstrate a dominant strike orientation of NNE-SSW with WNW and ESE azimuths, and dip magnitudes that vary from approximately  $15^\circ$  to vertical, but are mainly  $>80^\circ$ .

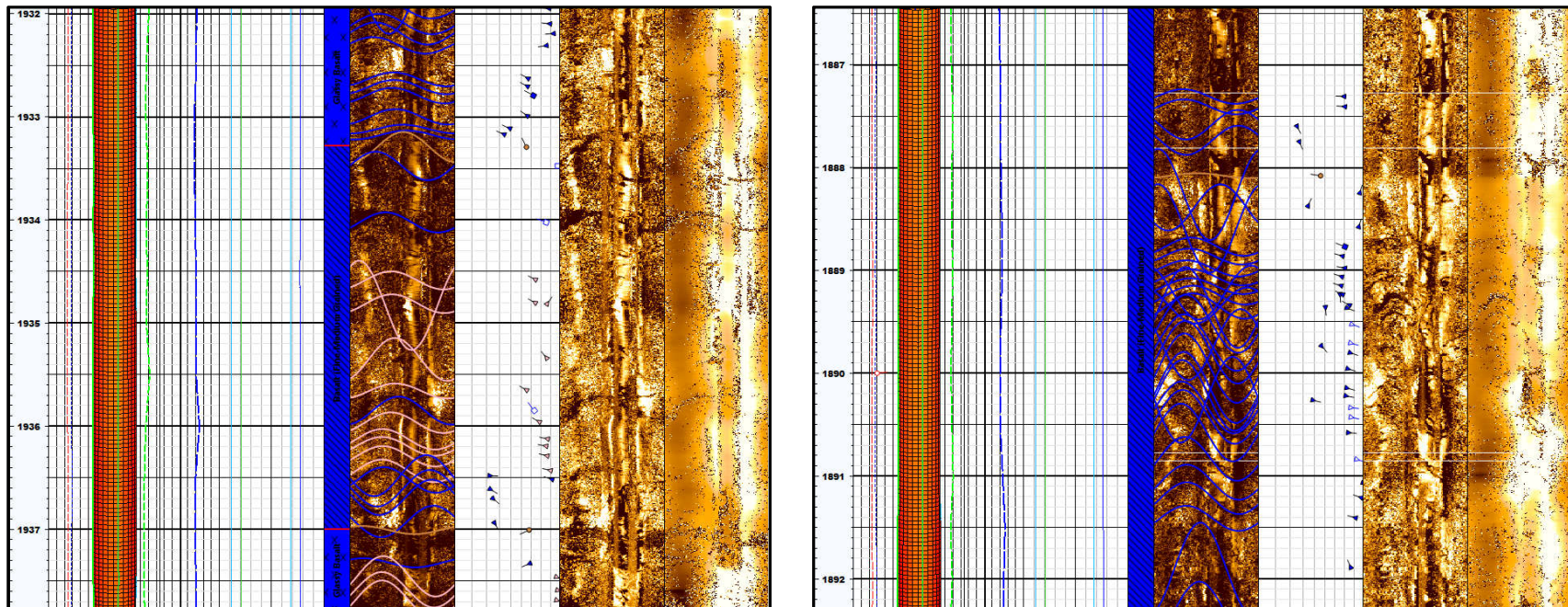
## Examples of Large Open Fractures and Possible Open Fault, Fracture Zone 3 (2,252-1,956 m MD)



Large continuous and discontinuous open fractures in Fracture Zone 3 (2,252-1,956 m MD) are observed at 2,230-2,233 m MD, 2,223-2,224 m MD, 2,220-2,221 m MD, 2,215 m MD, 2,213.7 m MD, 2,205-2,206 m MD, 2,201.8 m MD, 2,197.5-2,199 m MD, 2,193-2,197 m MD, 2,185-2,190 m MD, 2,177-2,179 m MD, 2,170-2,174 m MD, 2,167-2,168 m MD, 2,156.5-2,161 m MD, 2,152-2,154 m MD, 2,139-2,141 m MD, 2,132.5 m MD, 2,128 m MD, 2,116-2,122 m MD, 2,111-2,115 m MD, 2,103 m MD, 2,100 m MD, 2,094-2,096 m MD, 2,087-2,089 m MD, 2,072-2,074 m MD, 2,036-2,043 m MD, 2,033-2,034 m MD, 1,990.5 m MD, and 1,978-1,983 m MD, which demonstrate a dominant strike orientation of NNE-SSW with WNW and ESE azimuths, and dip magnitudes that vary from approximately 15° to vertical, but are mainly >80°.

Possible open faults were recognized at 2,156.5 m MD and 2,154 m MD, which demonstrate a dominant strike orientation of NNE-SSW with ESE azimuth, and dip magnitudes range from 67° to 75°.

## Examples of Large Open Fractures and Possible Open Fault, Fracture Zone 4 (1,956-1,748 m MD)



Large continuous and discontinuous open fractures in Fracture Zone 4 (1,956-1,748 m MD) are observed at 1,928-1,937 m MD, 1,898-1,902 m MD, 1,887-1,891.5 m MD, 1,851-1,855 m MD, 1,819.8 m MD, 1,788-1,797.5 m MD, and 1,784-1,787 m MD, which demonstrate dominant strike orientations of N-S, NNE-SSW, and NNW-SSE with ESE, W, WNW, ENE, and WSW azimuths, and dip magnitudes that vary from approximately  $20^\circ$  to vertical, but are mainly  $>75^\circ$ .

# Fractures, Faults, Drilling Induced Fracture and Breakouts: ÞG-15 vs. ÞG-17 vs. ÞG-12 vs. ÞG-18

Well Name	ÞG-15	ÞG-17	ÞG-12	ÞG-18
Continuous Conductive Fracture	Scatter	<u>N-S, NNW-SSE, and NNE-SSW</u> with easterly and westerly azimuths	<u>NNE-SSW</u> with ESE and WNW azimuths	<u>NNE-SSW</u> , with WNW and ESE azimuths
Continuous Conductive Fracture $\geq 60^\circ$	<u>N-S and WNW-ESE</u> with NNE, E, and W azimuths	<u>NNW-SSE</u> with easterly and westerly dips	<u>NNE-SSW</u> with ESE and WNW azimuths	<u>NNE-SSW</u> with WNW and ESE dips
Continuous Conductive Fracture $<60^\circ$	<u>ENE-WSW</u> with NNW, SSE, and westerly azimuths	<u>NNE-SSW</u> with WNW and ESE azimuths	<u>NE-SW</u> with ESE, SE, WNW, and NW azimuths	<u>NNE-SSW, NE-SW, and E-W</u> with WNW, NW, SW, SSW, SSE, and SW azimuths
Discontinuous Conductive Fracture	Scatter	<u>N-S and NNW-SSE</u> with westerly and easterly azimuths	<u>N-S, NNE-SSW, and NNW-SSE</u> with westerly and easterly azimuths	<u>NNE-SSW</u> , with WNW and ESE azimuths
Discontinuous Conductive Fracture $\geq 60^\circ$	<u>WNW-ESE</u> and E-W with scatter dips	<u>NNW-SSE</u> with easterly and westerly azimuth	<u>NNE-SSW</u> with ESE and WNW dips	<u>NNE-SSW</u> , with WNW and ESE azimuths
Discontinuous Conductive Fracture $<60^\circ$	<u>ENE-WSW</u> with NNW, SSE, and westerly azimuths	<u>NNE-SSW</u> with WNW and ESE azimuths	<u>NE-SW</u> with NW and SE azimuths	<u>ENE-WSW</u> , with NNW and SSE azimuths
Possible Open Fault	Scatter	<u>N-S</u> with westerly and easterly azimuths	<u>NNE-SSW</u> with WNW and SE azimuths	<u>NNW-SSE, NNE-SSW, and NE-SW</u> , with westward (WNW, W, WSW) azimuth
Possible Open Fault $\geq 60^\circ$	<u>E-W and N-S</u> with scatter dips	<u>N-S</u> with easterly and westerly azimuths	<u>N-S and NNE-SSW</u> with easterly and westerly azimuths	<u>NNE-SSW</u> with ESE and WNW azimuth
Possible Open Fault $<60^\circ$	<u>ENE-WSW and NNW-SSE</u> with NW, WSW, and SE azimuths	<u>NNW-SSE and NE-SW</u> with westward azimuths	<u>NE-SW</u> with SE and NW azimuths	<u>NNE-SSW and NNW-SSE</u> with ESE and ENE azimuths
Drilling Induced Fracture	NE-SW	N-S	N-S/NNE-SSW	N-S
Borehole Breakout	NW-SE	-	E-W/ESE-WSW	E-W/ENE-WSW
Lithological Boundary	NE azimuth	NE azimuth	NE azimuth	W

**Thank you!**  
**Terimakasih!**  
**Þakka þér fyrir!**

# GeothermEx

A Schlumberger Company

3260 Blume Drive, Suite 220  
Richmond, California 94806 USA  
Phone: (510) 527-9876  
Fax: (510) 527-8164  
[www.geothermex.com](http://www.geothermex.com)



Landsvirkjun

Háaleitisbraut 68  
103 Reykjavík  
landsvirkjun.is

landsvirkjun@lv.is  
Sími: 515 90 00

